DOE/NASA/0167-11
NASA CR-180818
GARRETT NO. 31-3725(11)

ADVANCED GAS TURBINE (AGT) TECHNOLOGY DEVELOPMENT PROJECT

1986 ANNUAL REPORT

Engineering Staff of
Garrett Turbine Engine Company
A Division of The Garrett Corporation

February 1987

Prepared for

NATIONAL AERONAUTICS AND SPACE ADMINISTRATION
Lewis Research Center
Cleveland, Ohio 44135
Under Contract DEN3-167

for

U.S. DEPARTMENT OF ENERGY
Office of Transportation Systems
Heat Engine Propulsion Division
Washington D.C. 20585

(NASA-CR-180818) ADVANCED GAS TURBINE (AGT) TECHNOLOGY DEVELOPMENT PROJECT Annual Interim Report, 1 Jul. 1985 - 30 Jun. 1986 (Garrett Turbine Engine Co.) 132 p Avail: NTIS HC A07/MF A01 CSCL 13F G3/85 N87-30225 Unclas 0103490

DO E/NASA/0167-11
NASA CR-180818
GARRETT NO. 31-3725(11)

ADVANCED GAS TURBINE (AGT) TECHNOLOGY DEVELOPMENT PROJECT

1986 ANNUAL REPORT

Engineering Staff of
Garrett Turbine Engine Company
A Division of The Garrett Corporation

February 1987

Prepared for

National Aeronautics and Space Administration
Lewis Research Center
Cleveland, Ohio 44135
Under Contract DEN3-167

for
U.S. DEPARTMENT OF ENERGY
Office of Transportation Systems
Heat Engine Propulsion Division
Washington D.C. 20585

TABLE OF CONTENTS

TABLE OF CONTENTS (Contd)

LIST OF FIGURES

LIST OF FIGURES (Contd)

LIST OF FIGURES (Contd)

LIST OF TABLES

1.0 SUMMARY

This report describes progress and work performed by the Garrett Turbine Engine Company/Ford Motor Company Team during July 1985 through June 1986 to develop technology for an Advanced Gas Turbine (AGT) engine for automotive applications. This work was performed for the Department of Energy under NASA Contract DEN3-167. This is the eleventh in a series of technical summary reports and covers a full calendar year of contract activity. Work performed during the periods of the first ten reports (References 1 through 10) initiated design and analysis, ceramic development, component testing, and test bed evaluation.

Project effort conducted under this contract is part of the DOE Gas Turbine Highway Vehicle System Program. This program is oriented to provide the United States automotive industry the high-risk, long-range technology necessary to produce gas turbine engines for automobiles with reduced fuel consumption and reduced environmental impact. Technology resulting from this program is intended to reach the marketplace by the early 1990's.

The advanced automobile gas turbine, when installed in a Ford vehicle (3000 pounds inertia weight), will provide:

- o A combined federal driving cycle (CFDC) fuel economy of 42.8 miles per gallon based on Environmental Protection Agency (EPA) test procedures using diesel No. 2 (DF-2) fuel. The AGT-powered vehicle will substantially give the same overall vehicle driveability and performance as a comparable production vehicle powered by a conventional spark-ignition powertrain system
- o Emissions less than Federal standards
- o Ability to use a variety of fuels

1.1 Power Section Development

Initially, three AGT101 engines (S/Ns 001 through 003) were assigned to support the development program. In January 1985, S/N 003, a metallic configured engine, was diverted from the AGT101 program to support another government program under DOE/NASA Contract DEN3-181 (Brayton Cycle Solarized Advanced Gas Turbine -- SAGT-1A). A fourth AGT101 engine, S/N 004, was assembled as a replacement, to maintain the minimum level required for the development program. In addition to being identified by serial numbers, AGT101 engines essentially constructed with ceramic componentry are further identified by the suffix C appended to the serial number, e.g., S/N 004C.

During this reporting period, Engine S/N 001 was operated to measure the heat transfer coefficients in the engine flowpath. It was also used as a proof test bed for ceramic turbine rotors, and to determine strain levels in a rotor under simulated operating conditions. S/N 002C was tested primarily to evaluate the regenerator drive system, and so better control regenerator torque. Information was also gained regarding rotor integrity during the course of this testing.

Engine S/N 004C was built in the all-ceramic configuration (including ceramic rotor and combustor), and successfully tested to 2000F and 70 percent speed. This test is considered the most significant accomplishment of this report period. At the close of the period, preparations were underway for the build of an all-ceramic engine for durability testing.

1.2 Combustion Rig Activity

Combustor rig usage during the reporting period included extensive testing of the ceramic combustor using fuel nozzles of a

Garrett design and a Garrett-based Delavan design. Testing examined the potential for fuel nozzle coking and fouling as well as evaluation of nozzle modifications to improve combustion, light-off, and component life. The rig was also used to thermally screen ceramic combustor hardware to be used in for engine tests.

1.3 Regenerator Development

Seals work during this report period was concentrated on developing the Phase VI seal design that features equal length retainers and symmetrical peripheral diaphragms. This phase represents the final configuration of the evolutionary design and development technique that is projected to satisfy the program objectives for leakage and temperature capability.

The first set (hot and cold) of Phase VI-A seals demonstrated the anticipated characteristics of leakage being nearly independent of the seal working range.

Additional seals work concentrated on further improvements to the seal cooling design to meet increased temperature projections.

A total of five cold and eight hot Phase VI seals have been built and have met leakage test specifications.

Core development included the funding of Corning to prepare samples of extruded aluminum silicate (AS) matrix (approximately 1100 cells/in^2). Also, over 500 hours of testing were accumulated on NGK's magnesium aluminum silicate (MAS) material, both in the standard version and an improved low-porosity version. The low-porosity MAS demonstrated better thermal stability than the standard, and two full-size cores were received at the end of this report period.

An extensive sequence of tests was completed in Ford's regenerator rig to isolate system leakage sources, their relative magnitude and corrective actions. This testing also provided the background for follow-on tests with all ceramic hot flow path components planned for the next report period.

Garrett's hot ceramic structures rig was run to determine dynamic leakage using the helium detection system. The rig was modified to incorporate five different stations for injecting helium, providing for segregation of regenerator system, flipper seal and piston ring leakages. Examination of the limited leakage data revealed inconsistencies, which indicated that the helium injection procedure did not provide satisfactory homogeneous mixing.

Regenerator development for this period also included analysis and initial hardware preparation relative to replacement of the hot side seal with a non-diaphragm (face seal) configuration, and an investigation into the wear characteristics of regenerator support components.

1.4 Ceramic Development

Testing continued in the ceramic component rigs to qualify hardware for engine testing. Design iterations centered around improving the ability to seal the flowpath through the ceramic structures, and on incorporating ceramic materials into the combustor design. Also, an alternative design to the existing flow separator housing was initiated, which may eventually allow the hot side regenerator seal to be replaced with a non-diaphragm (face seal) configuration, as mentioned above.

Twenty-six hours of testing at 2500F were accumulated during this reporting period. This testing revealed some of the effects of high temperatures on ceramic component assemblies.

Significant progress was made in rotor development during this period, including the initial operation of an all-ceramic engine, as referred to above. Three suppliers contributed to the effort: Ford supplied three wheels of their RM-20 material, NGK-Locke supplied four wheels of silicon nitride, and Kyocera supplied 13 turbine wheels, also of silicon nitride.

2.0 INTRODUCTION

This report is the eleventh in a series of Technical Summary Reports for the Advanced Gas Turbine (AGT) Technology Development Project, authorized under NASA Contract DEN3-167 and sponsored by the DOE. This report has been prepared by the Garrett Turbine Engine Company (hereinafter referred to as Garrett), a Division of the Garrett Corporation, and includes information provided by the Ford Motor Company (hereinafter referred to as Ford), Sohio Engineered Materials Company/Carborundum, and AiResearch Casting Company (ACC). The project was administered by Mr. Thomas Strom, Project Manager, NASA-Lewis Research Center, Cleveland, Ohio. This report presents plans and progress from July 1985 through June 1986.

Project effort conducted under this contract is part of the DOE Gas Turbine Highway Vehicle System Program. This program is oriented at providing the United States automotive industry the high-risk, long-range technology necessary to produce gas turbine engines for automobiles that will have reduced fuel consumption and reduced environmental impact. The intent is that technology resulting from this program be capable of reaching the marketplace by the early 1990s.

The advanced gas turbine, when installed in a Ford vehicle (3000 pounds inertia weight) would provide:

- o A CFDC fuel economy of 42.8 miles per gallon based on EPA test procedures and DF-2. The AGT-powered vehicle shall give substantially the same overall vehicle driveability and performance as a comparable production vehicle powered by a conventional spark-ignition powertrain system
- o Emissions less than federal standards
- o Ability to use a variety of fuels

The Garrett/Ford advanced gas turbine has been designated the AGT101.

The program is oriented toward developing advanced gas turbine long-range, high-risk technology such that the automotive industry can carry forward to production in the 1990s. Emphasis on ceramics, gas bearings, low emission combustion, and improved component performance shall continue. The AGT101 is being used as a test bed in which to develop these technologies.

The program schedule is depicted in Figure 1. The program continues technology work through FY86, culminating in 100-hour operation of an all-ceramic engine, and demonstration of combustor performance with alternate fuels. In addition, the viability of ceramics will have been demonstrated in the AGT101 test beds, and the potential of economically producing the ceramic parts in automotive production quantities will have been assessed. When these goals are achieved, Ford will be in a position to proceed, without Government support, through the typical preproduction tasks that could then lead to production in the 1990s.

Development and production of high performance ceramic components continues to be

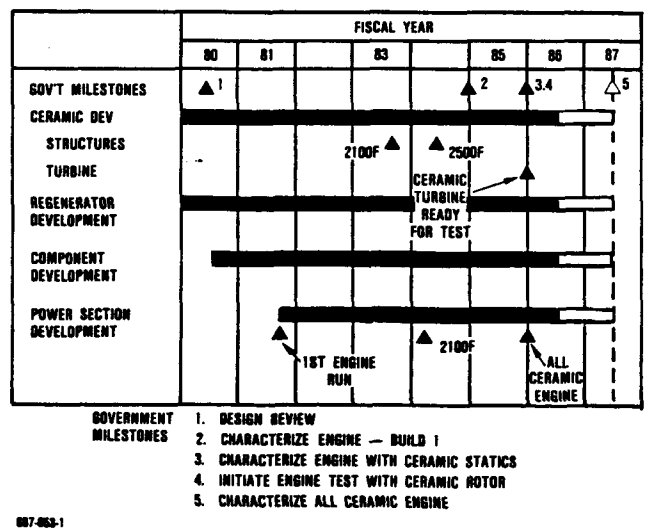

Figure 1. AGT101 Program Schedule.

a primary challenge in the program. The AGT101 nominally is a 100 shp engine, capable of speeds to 100,000 rpm and operating at turbine inlet temperatures (TIT) to 2500F with a specific fuel consumption level of 0.3 pounds/horsepower/hour over much of the operating range.

This report reviews the power section (metal and ceramic) effort conducted to date, followed by a review of the components/ceramic technology development. Appendices include reports of progress from Ford, ACC, and Standard Oil (formerly reported as Carborundum).

3.0 POWER SECTION DEVELOPMENT

AGT101 power section development for this reporting period supported the assembly and operation of an all-ceramic engine. The test of the all-ceramic engine was the most significant accomplishment of the period. This engine test was performed on engine S/N 004C during the last part of January 1986. Also significant in this year's work were efforts to understand the regenerator high drive loads experienced by high temperature engines and ceramic turbine rotor testing. This work is reported in more detail below.

3.1 S/N 001 Engine

S/N 001 engine has made major contributions toward ceramic engine development. This engine is characteristically similar to the ceramic engines, in that it uses the same engine control system, the same test facilities and hookups, and to the extent that its metallic components allow, the same internal flowpath. This characteristic allows this engine to be used as a preliminary test bed for new test procedures, rotating group design modifications, and to collect data on engine flowpath thermal characteristics. This work can be accomplished with minimum risk because of the durability of its metallic components.

S/N 001 engine, in Builds 34 through 41, was used to perform the following work during this reporting period.

- o Flow path heat transfer coefficient determination
- o Ceramic turbine rotor pretesting and qualification
- o Ceramic rotor shaft motion measurement
- o Rotor dynamic development

3.1.1 Build 34: Engine Flowpath Heat Transfer Parameter Determination

The purpose of Build 34 was to help fill an analytical modeling gap that hampered the design of certain ceramic engine components. Up to this time, the film coefficients along the ceramic flow separator housing and through the turbine stators were assumed based on experience and expertise. However, the need for more accurate models with high confidence in the component stress and distortion levels prompted this effort to empirically determine these important parameters.

As shown in Figures 2 and 3 the metallic flow separator housing and turbine stators were extensively instrumented with thermocouples along the flow path and within the component walls. These parts were then assembled into the engine and run through a predetermined series of start transients each with a peak turbine inlet temperature of 1600F.

These data for the stator and flow separator housing were then compared with the output of the computer model using the assumed heat transfer coefficients to determine the accuracy of the existing models. Figures 4 and 5 show typical comparisons of the thermal transients between the test data and the computer model of the flow separator housing. These curves show that the tested components came up to temperature much faster than predicted, indicating that the heat transfer assumptions in the model were inaccurate. This disparity persisted even when the heat transfer coefficients were increased beyond reasonable limits. Thermal radiation was determined to have a larger influence than originally assumed. Thermal radiation was a significant factor in the transient thermal behaviour of the gas path components, not only thermal radiation from the combustor and other adjacent components, but also from other surfaces of the same component.

Work to update these models is continuing on a priority basis. The stator model is being updated first. The flow separator housing model may be updated in the future depending on need.

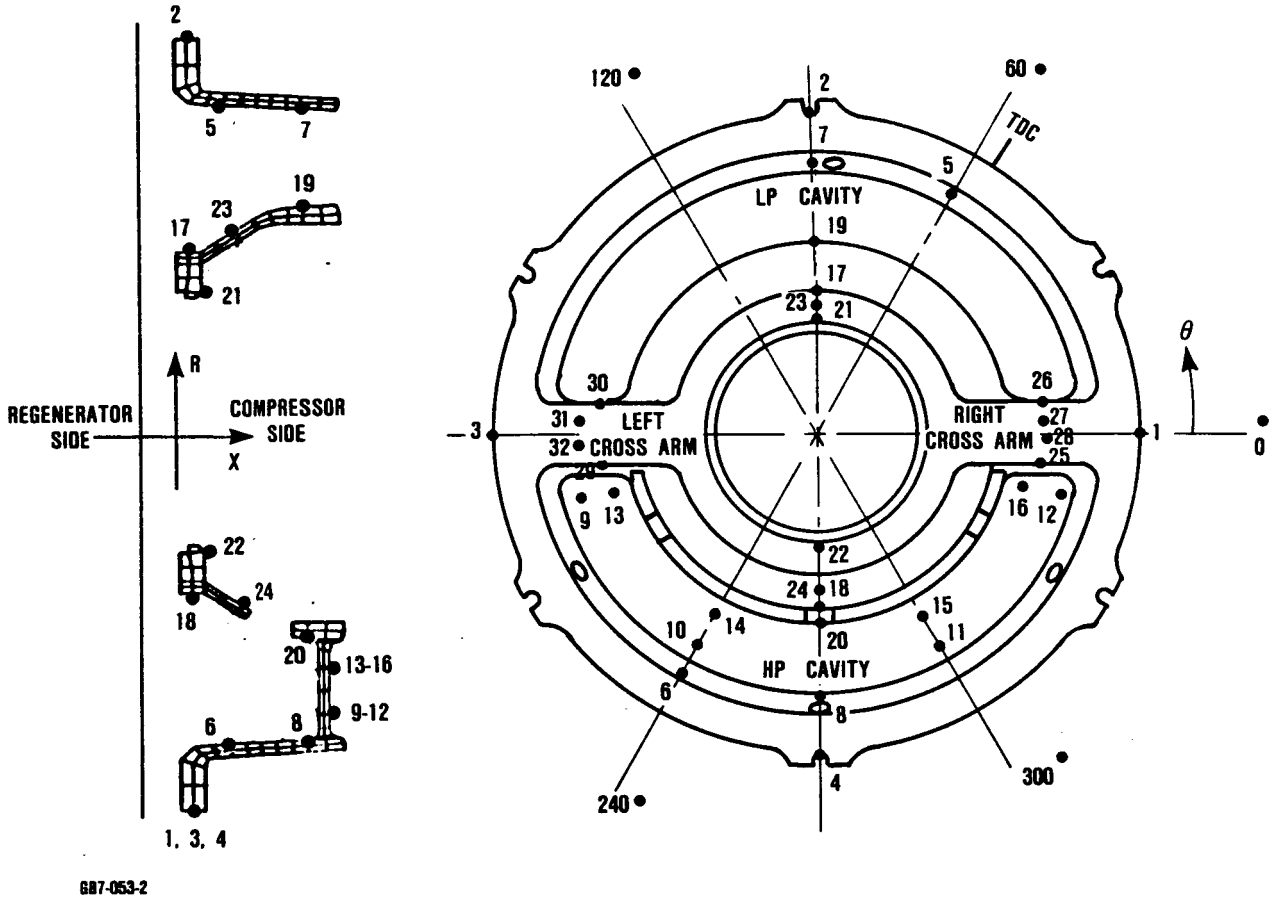

Figure 2. Flow Separator Housing Thermocouple Locations.

3.1.2 Builds 35 Through 39: Ceramic Turbine Rotor Testing

As noted above, the metal structured engine was used to evaluate features and concepts under 1600F engine operating conditions before testing in ceramic structured engines. By this approach, if there was a design problem or a fabrication defect in the test hardware, it would surface in the metal engine, thus risking damage only to metallic hardware which are more easily repaired than ceramic components.

In this way S/N 001 engine was used to evaluate the operation of a ceramic turbine rotor with a high temperature foil bearing before these rotors were used in ceramic structured engines. The first two tests of this type were reported previously in the last summary report as Builds 25 and 26. During this reporting period Builds 35, 36, 37, 38, and 39 were used for this purpose. These engine builds successfully qualified four Kyocera hollow shaft SN 220M turbine rotors for ceramic engine use at various speeds up to 88,000 rpm. Table 1 summarizes the parameters of these engine tests.

The objective of these tests was to operate the engine with the ceramic turbine rotor through a range of engine speeds that excite

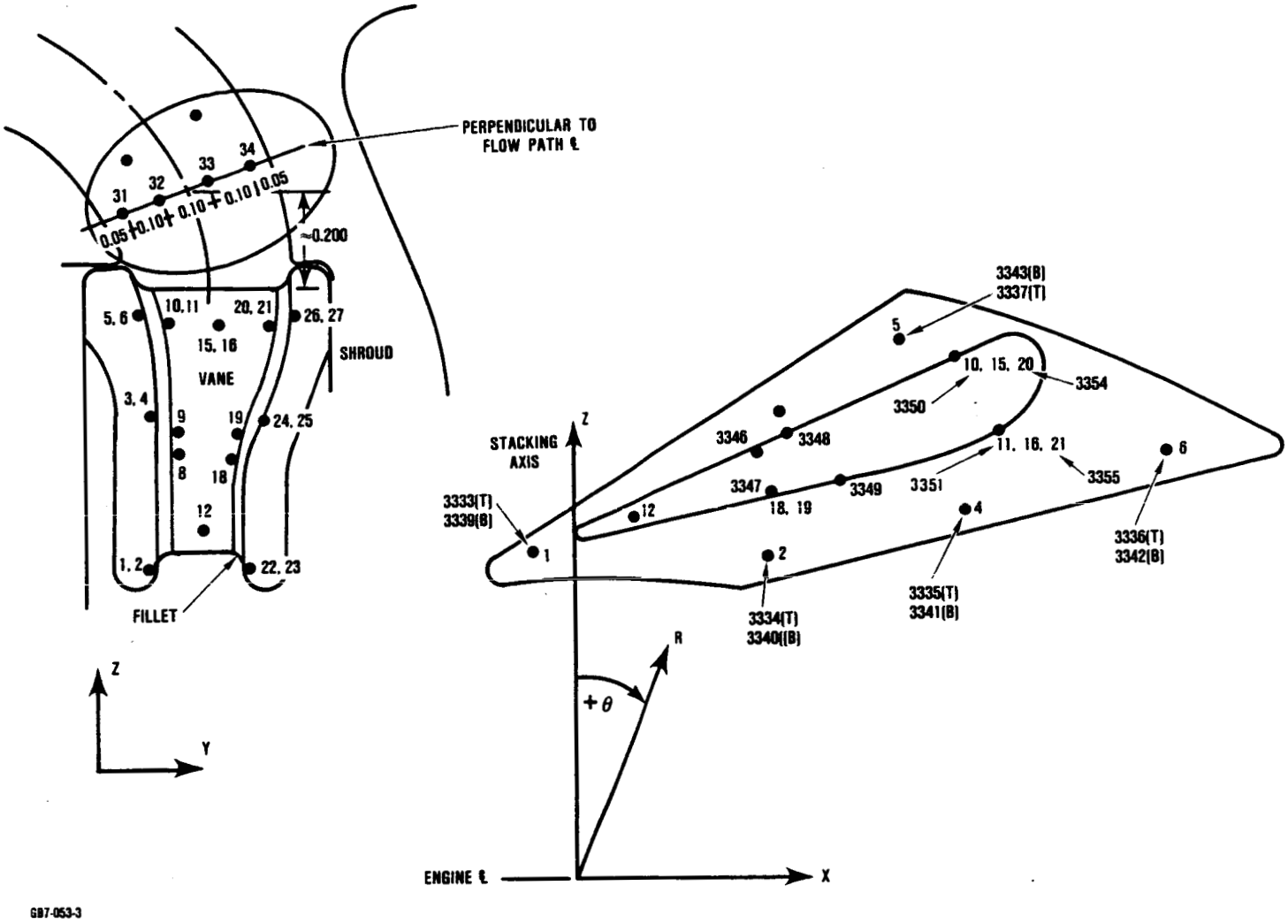

Figure 3. Stator Instrumentation.

the turbine blades into resonance. With the Kyocera SN 220M rotors, this speed range was between 50,000 and 65,000 rpm. Since it was blade resonance that caused the ceramic rotors in Builds 25 and 26 to fail, these tests reduced the probability of rotor failure during testing in engines with ceramic structures.

Each of these engine tests completed the speed transient through the speed range without rotor failure. Some tests were shortened due to other test considerations, however, all the ceramic rotors survived with no difficulty. During the course of this testing, a number of other engine test features were evaluated. These features are summarized below.

High Temperature Foil Bearing

To provide low wear and low friction support of the rotating group hot end with the capability for operation at temperatures up to 1200F, a new gas foil bearing was developed. This bearing featured similar geometry to the polyimide coated bearing used with the metallic rotors, however a hardened gold alloy coating was used on the foils. Rig testing had shown that this coating was compatible with the sintered silicon nitride shaft journal over the desired temperature range and showed little wear after 2000 rig start cycles.

This bearing was used in each of the engine builds with the hollow shaft ceramic rotor.

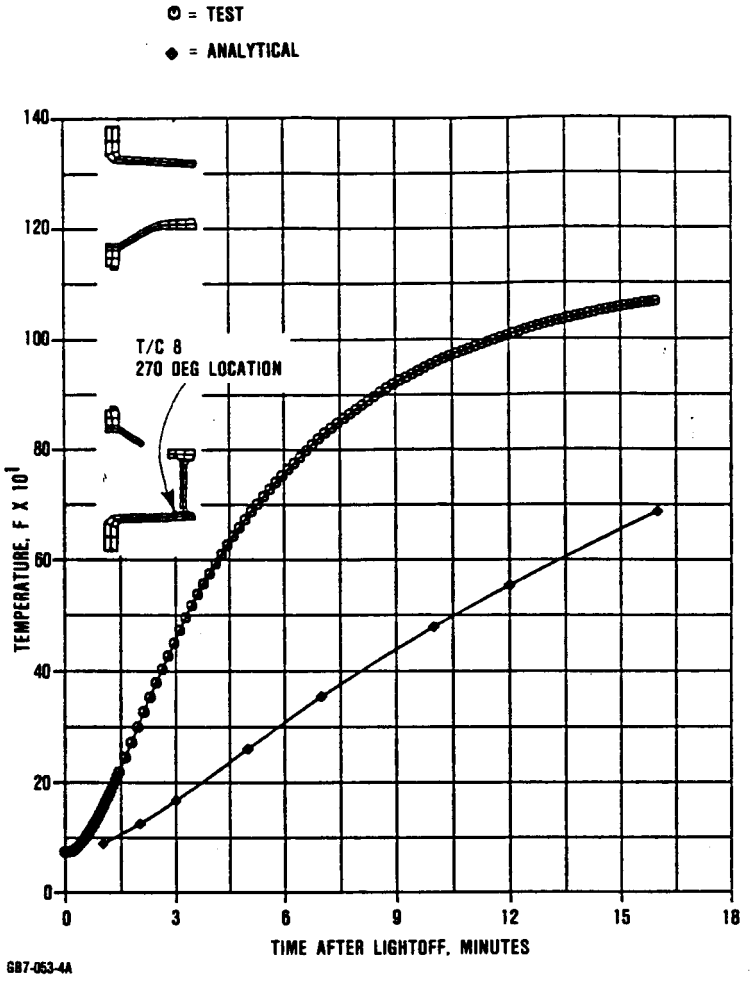

Figure 4. Comparison of Thermal Transients (Test versus Computer Model).

Throughout this series of tests the foil bearing performed admirably. Not only did the bearing provide reliable operation during start and shutdown, it survived rotor excursions of 3 mils without distress. This is particularly significant because the old polyimide coated foils used with a metallic shaft consistently failed due to overload when shaft motion exceeded 1.5 mils. The photo in Figure 6 shows a set of high temperature foils after an engine test in which 3 mils synchronous shaft motion was experienced.

Rectangular Wayne-Kerr Probes

Metallic turbine shaft motion was measured on previous engines with Wayne-Kerr probes mounted to the foil bearing shield as shown in Figure 7. When the ceramic turbine rotor was installed in the engine, these probes were recalibrated against the ceramic target in a static calibration rig. During engine testing however, the output signal from these probes was erratic and unreliable. The reason for the erratic behaviour of the vibration probes was traced to a combination of poor grounding of the ceramic target, and incompatibility of the probe signal conditioning with the ceramic target.

Shaft vibration measurement was regained when the probe was redesigned and repositioned to read motion at the titanium curvic ring which is mounted on the compressor end of the turbine shaft as shown on Figure 8. The

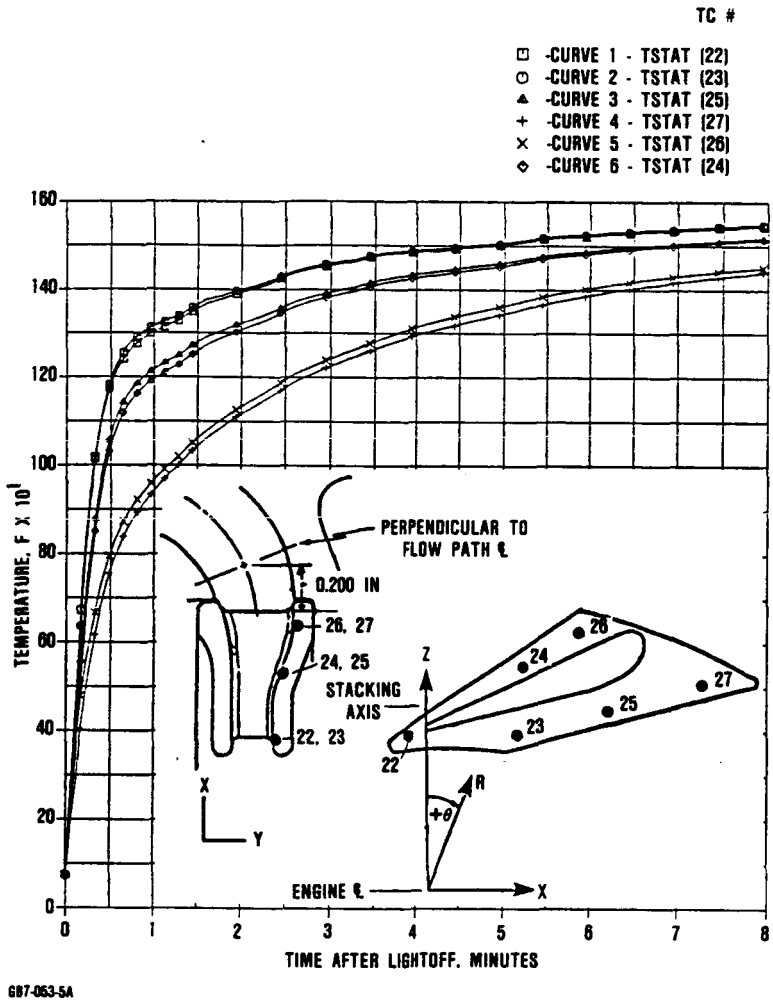

Figure 5. Stator Instrumentation.

Table 1. S/N 001 Engine Test Summary.

Build	Starts	Max Temp., F	Max Speed, krpm	Run Time, hours
35	3	1400	66.9	0.1
36	3	1600	70.5	0.5
37	1	1600	70.0	0.01
38	1	1600	88.0	0.93
39	2	1600	73.5	0.28

rectangular probes are shown installed in S/N 001 engine in the photograph in Figure 9.

Turbine Curvic Alignment

During check balance of the engine rotating groups for Builds 37, 39, and 41 unacceptably high imbalances were recorded. The cause of the high imbalance was traced to faulty curvics on the turbine rotor that misaligned the turbine with respect to the rest of the rotating group components.

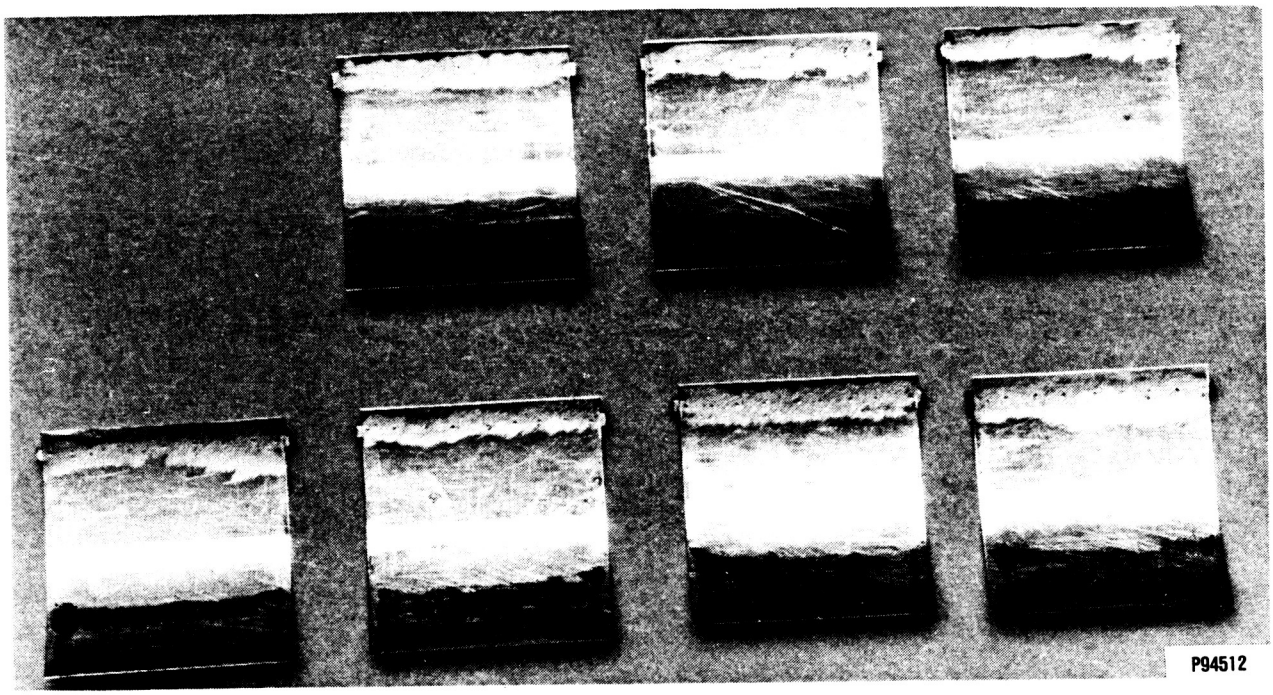

Figure 6. Bearing Foils Show Little Evidence of Unusual Rotor Motion.

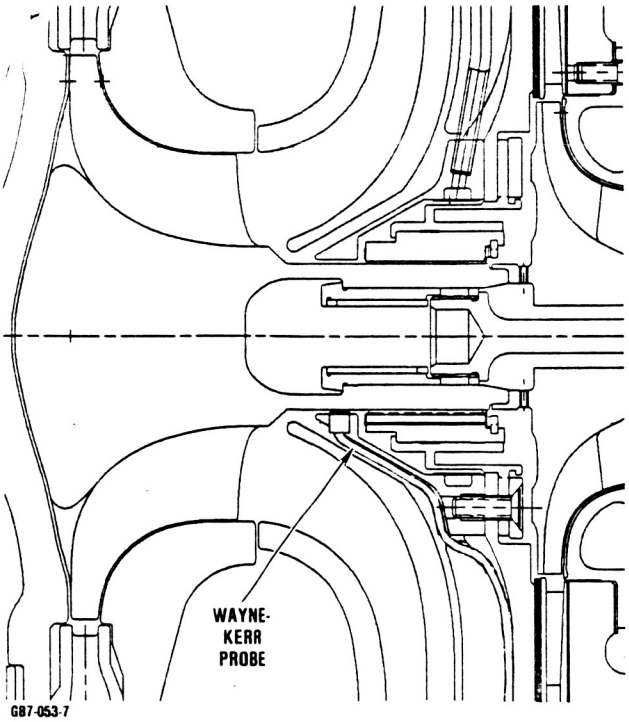

Figure 7. Wayne-Kerr Probes Mounted on the Foil Bearing Shield.

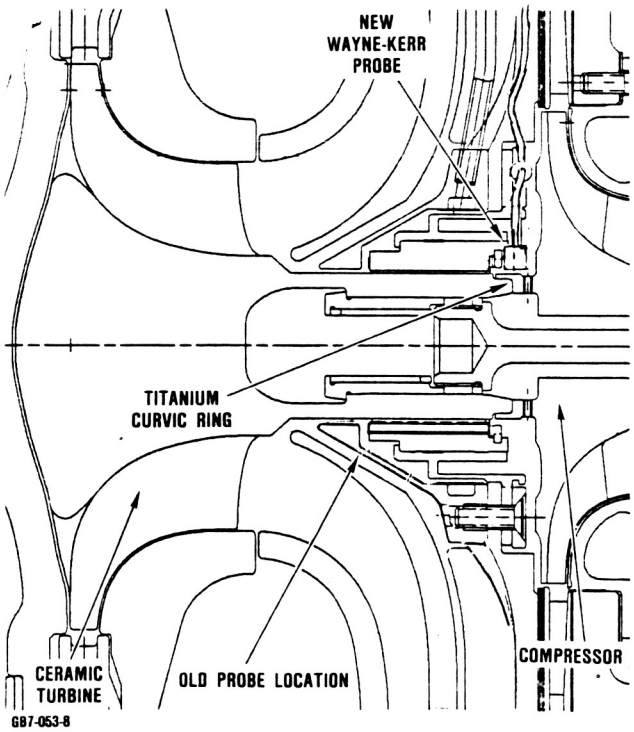

Figure 8. Relocation of Wayne-Kerr Probes.

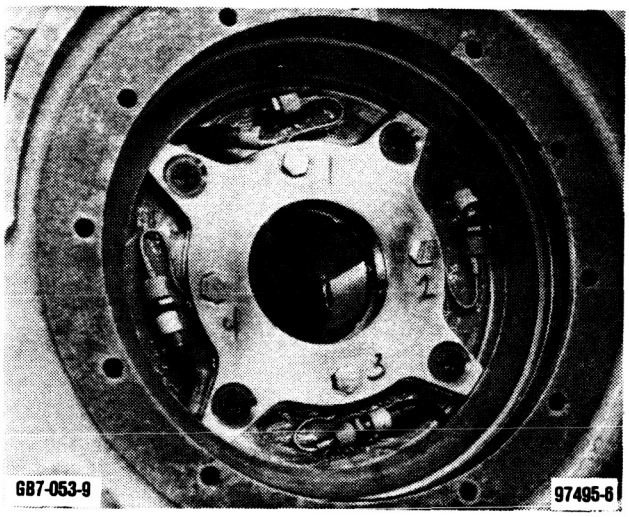

Figure 9. View Showing Rectangular Wayne-Kerr Probes.

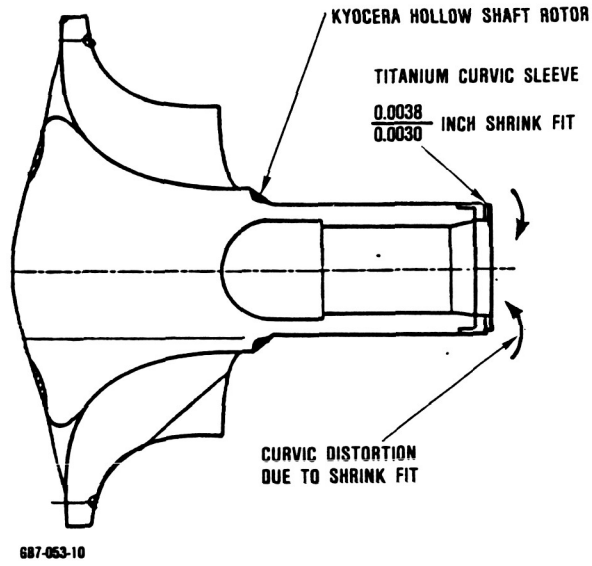

Figure 10. Titanium Curvic Sleeve Distorts Due to Shrink Fit.

Figure 10 shows the turbine rotor/curvic assembly. A titanium curvic ring is shrunk on to the rotor shaft with an interference fit of 0.003 to 0.004 inch. This interference causes a dish-like (concave) distortion of the curvic end of the ring. The distortion of the curvics reduces the curvic contact area and inhibits seating of the ring on the rotor, causing an inadequate bearing pattern and misalignment.

Experiments showed that proper turbine alignment could be achieved by reprocessing the rotor/sleeve assembly. This process consisted of compressively loading the curvic sleeve to the rotor with a 5000 lb load while simultaneously running the assembly through a heat cycle to 800F. Rotor assemblies that were inspected initially and found with perpendicular curvic misalignment to the rotor shaft of 0.001 to 0.008 inch were reprocessed, seating the curvic ring to the rotor shaft and reducing the curvic misalignment to less than 0.0005 inch.

Engine Gearbox Spline Coupling

During testing of Build 37 and 38, problems were experienced with alignment of the quill shaft coupling between the engine output shaft and slave gearbox.

As a result of repeated installation and removal of the quill shaft from engine rotating groups, the pilot diameter on the matching splined spacer wore until its interference fit with the quill shaft was not sufficient to retain the quill shaft in alignment with the engine shaft during engine operation. This resulted in high rotor vibration that caused the early shutdown of Build 37.

The rotor assembly was redesigned to eliminate the separate quill shaft. This design is shown in Figure 11. By changing the design such that the tiebolt piloted the components of the rotor assembly and integrating the spline with the tiebolt, the problems associated with the quill shaft were eliminated.

This new design features a splined extension which is held in alignment to the rotating group by the tiebolt. Distortion in the tiebolt which could misalign the spline is minimized by divorcing the splined extension from the tiebolt thread with an undercut. To economize on hardware the new design used existing

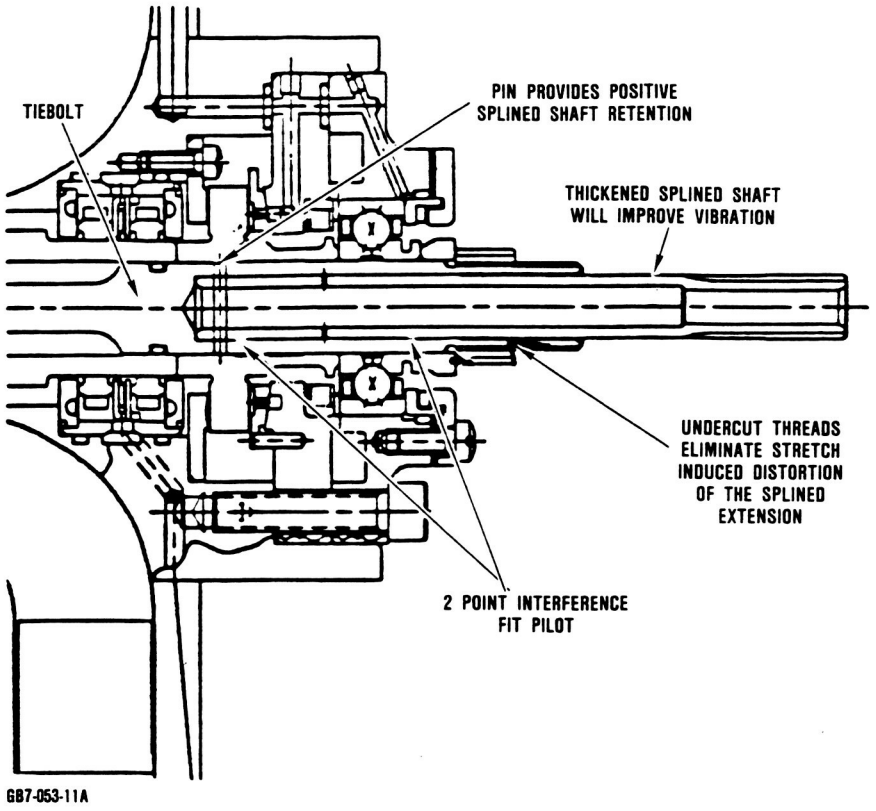

Figure 11. Splined Tiebolt Features Several Improvements.

components from a previously obsolete design with only the tiebolt modified. Testing of this new configuration will begin during the next reporting period.

3.1.3 Build 40: Strain Gaged Turbine Rotor Test

To provide confidence in the ability of the newer ceramic turbine rotors to operate in and through the blade resonance speed range, a series of tests were performed. These tests included blade strain measurement during motoring, bench tests, and hot (1600F) testing in a metal structures engine.

An NGK turbine rotor meeting blueprint requirements, was instrumented with strain gages in locations of peak stress on selected inducer and exducer blades as shown in Figure 12. This rotor was installed in S/N 001 Build 40 engine. This engine, shown in Figure 13 was modified for operation with ambient temperature air ducted directly to the turbine. Peak blade strain amplitude was measured as the engine was motored through the resonant speed range. Blade response is shown in Figure 14. The relative amplitudes of the inducer and the exducer blade resonance indicates that exducer resonance was not significant.

The turbine blades are excited into resonance as the blade inducer passes through the pressure pulse field at the stator exit. The relationship between a cold engine motored at the blade resonant speed and a hot engine running at the same physical speed is based on

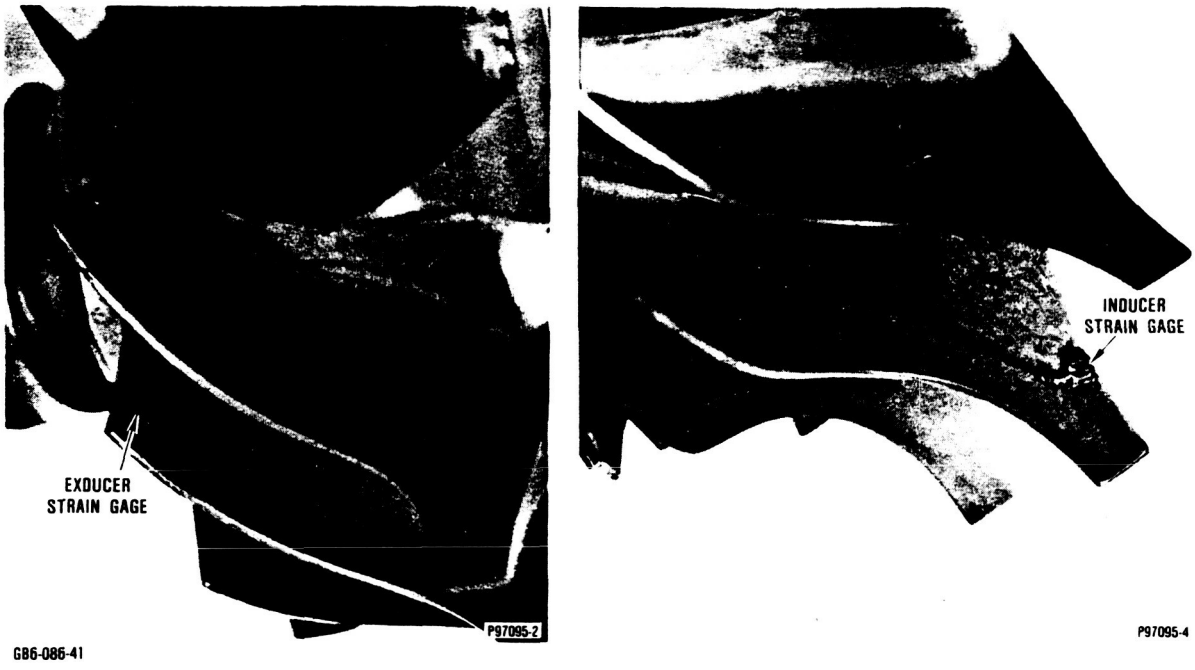

Figure 12. Strain Gaged Ceramic Turbine Rotor.

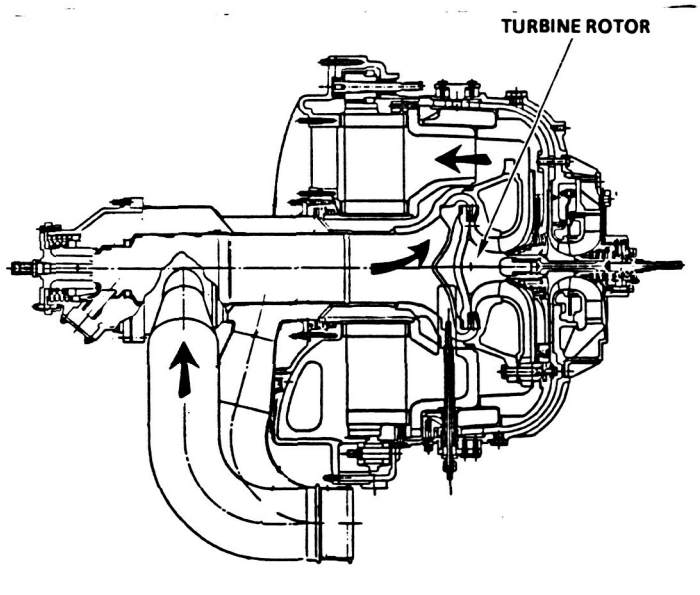

Figure 13. Ceramic Rotor Motoring Test Configuration.

a comparison of the stator wakes in both cases. An off-design turbine aerodynamic model was used to match cycle data collected during the motoring test and generates pressure distribution across the stator wake. The same analysis was used on cycle data generated by the RPD performance model at a similar physical speed. The results of this analysis, shown on Figure 15 indicate that the cold motoring condition is actually much more severe than the hot operating condition.

The equivalent hot operating engine blade strain was estimated by multiplying the cold engine blade strains by the ratio of the hot-to-cold pressure rise of the stator wake. The blade stresses indicate a low hot operational cumulative stress which adds the vibratory peak-to-peak stress to the centrifugal and thermal stresses in the blade.

A complementary test was performed in which a similarly instrumented rotor was vibrated on a magnetostrictive shaker at the

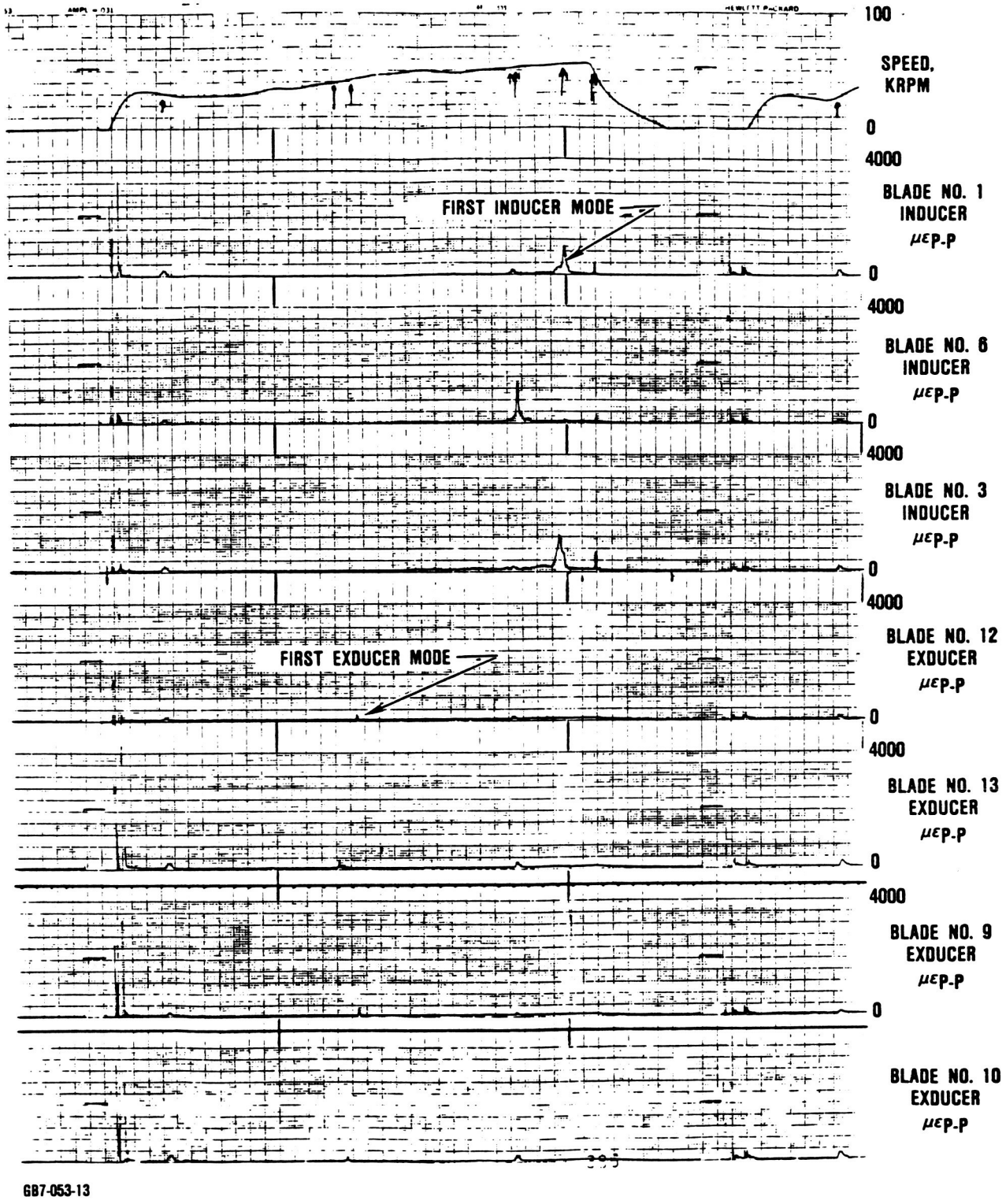

Figure 14. Peak-to-Peak Blade Vibration Acceleration Run S/N 001, Build 40.

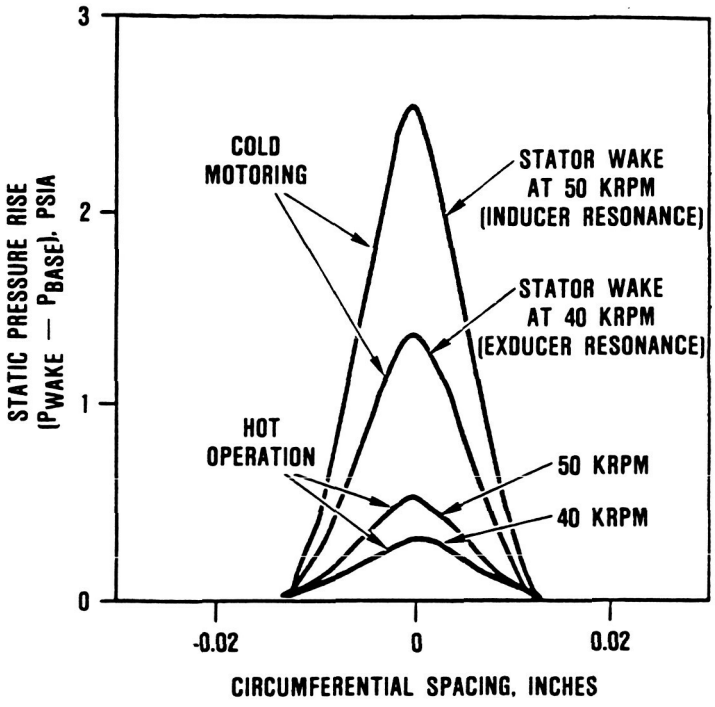

GB6-086-7

Figure 15. Analysis Shows Cold Motoring Test More Severe Than Hot Operational Condition.

blade resonant frequency until blade fracture occurred. The strain level in the inducer blade at the time of fracture was 2280 μin/in. This strain calculates to be a 90 ksi (peak-to-peak) stress level. These data indicate a large margin over the maximum cumulative stress (19 ksi) expected in hot operation. This test analysis indicates that the new turbine rotors are unlikely to fail due to resonance under engine operating conditions.

This conclusion is supported by engine tests of Kyocera ceramic turbine rotors made of SN 220M and SN 250M materials. These tests in metal and ceramic engines covered a 1600-2200F turbine inlet temperature range and 60,000 to 100,000 rpm speed range. A total of 8 ceramic rotors experienced over 72 speed transients through the blade resonant frequencies at various acceleration rates. Many of the passing rates were very slow. During these tests at the blade resonant speeds, none of the rotors failed.

3.2 Engine S/N 002C

S/N 002C engine was used to evaluate exhaust housing distortion and its effect on regenerator drive torque. Subordinate to this primary objective, testing of this engine during this reporting period resulted in significant discoveries regarding dual alloy turbine rotor integrity, downstream fuel burning during engine starts, and structural integrity of the strutted flow separator housings.

3.2.1 Builds 14A, 15, 16, 16A: Regenerator Drive Evaluation

These engines were assembled in the 2100F configuration. The purpose of these tests was to evaluate the regenerator core drive problems that have occurred during high temperature engine operation. The test plan was developed around the conditions found to produce high regenerator drive loads in previous high temperature ceramic engine testing. This testing evaluated the effect of both the metallic and ceramic combustor configurations on exhaust housing heating, the ceramic configuration is shown during assembly in Figure 16. The effect of external cooling on distortion of the exhaust housing was also evaluated.

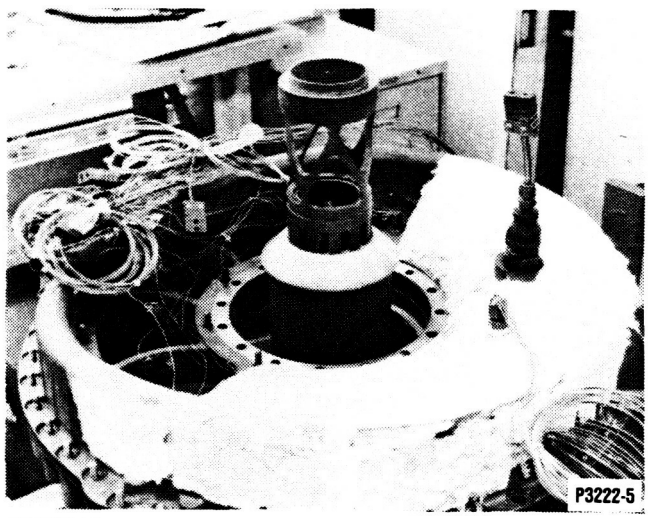

GB7-053-14

Figure 16. Assembly of First Ceramic Combustor into 2100F Engine.

A series of starts were to be made from a relatively "cool" thermal state. In each successive transient, the end condition would be more severe than the last, until eventually a regenerator seizure occurs. Thermocouple instrumentation installed on the exhaust housing and combustor cap would provide the information needed to model the housing thermally and predict housing distortion, and linear displacement transducers mounted on the exhaust housing would provide a check for the distortion analysis. The engine turbine inlet temperatures would be controlled between 1600 and 2000F, and the engine speed would be varied from 60,000 to 90,000 rpm.

The results of this testing indicated that the exhaust housing did distort under the effects of temperature and pressure to increase the regenerator drive loads. However, the magnitude of this increase was not sufficient to cause a regenerator drive seizure. An analysis of the combined thermal influences which establish the regenerator pocket indicated that the maximum closure of the pocket was 0.013 inch and occurs approximately 13 minutes after light-off. Build studies of the regenerator system indicate that this amount of closure was not sufficient to seize the regenerator given the initial regenerator assembly build dimensions.

However, evidence showed that regenerator drive loads could be reduced by decreasing the radial thermal gradient in the exhaust housing. This could be accomplished by cooling the bore of the exhaust housing and by more effectively insulating the exhaust housing and combustor spacer from the heat of the combustor.

Further work is in process at Ford and Garrett to resolve this problem. Ford is investigating regenerator drive characteristics at high temperatures in their regenerator rig and characterizing seal coating friction as a function of temperature. At Garrett, the laboratory regenerator drive is being redesigned to incorporate a torque meter with a pneumatic drive.

During the course of this testing the failure of a dual alloy turbine rotor, a ceramic turbine rotor, and a flow separator housing occurred. These events are discussed below.

Dual Alloy Turbine Rotor

During the test of Build 14A, a dual alloy turbine rotor failed while operating at 67,000 rpm engine speed and 2000F turbine inlet temperature. The dual alloy turbine rotor failed in the bond joint between the astroloy hub and the MAR-M 247 blade ring.

The cause of the failure was traced to a large unbonded area between the blade ring and the hub. This defect would have been difficult to detect using ultrasonic inspection techniques due to the geometry of the rotor, and did not surface during the 115,000 rpm overspeed proof test which qualified the rotor. Since the dual alloy rotor was only an intermediate step in the ceramic engine development and ceramic turbine rotors were soon to be available, further development of the dual alloy rotor was unwarranted. The use of dual alloy rotors in AGT engine testing was discontinued.

Ceramic Rotor Blade Failure

A ceramic turbine rotor made of Kyocera SN 220M material was installed in Build 15 engine. This rotor had passed a 115,000 rpm overspeed test at Kyocera, a 105,000 spin test at Garrett to check the shaft integrity after final machining, and a short test in S/N 001 engine to 90,000 rpm prior to this test. Two minutes after light-off an inducer blade failed on the turbine rotor while operating at 76,000 rpm.

The cause of the failure was traced to a flaw in a blade of the turbine rotor as shown in Figure 17. This flaw was oriented in such a manner that the overspeed test did not stress the flaw. The fact that this flaw went undetected and that the existing qualifying test did not screen this part indicate that improved NDE technique for in-process and final inspection are required in addition to more effective proof testing.

Figure 17. Fractured Inducer Blade on Ceramic Turbine Rotor.

Strutted Flow Separator Housing Failure

During the test of Build 16, a strutted flow separator housing failed in a benign manner, such that no damage was done to adjacent ceramic parts and the only impact was an increase in engine leakage. The failure was not detected until the lower compressor discharge pressure was noted after a subsequent cycle was started.

Disassembly revealed that the flow separator was fractured about its outer periphery. Inspection of the flow separator housing revealed that the part apparently failed due to contact stress generated between the flow separator housing and the ring support housing. On future builds of the ceramic engine with the strutted flow separator configuration the ring support housing and the flow separator flanges were to be treated with a Boron Nitride lubricant to reduce the potential for contact stress failure.

The turbine rotor was also damaged from this test. The rotor blades were apparently burned off during the test. Analysis indicated that the rotor tips were heavily oxidized and the material showed incipient melting, as if overheated.

The strip chart in Figure 18 mshows the turbine inlet and discharge during the third start of the engine. Note that for a short period during the start sequence, the turbine discharge temperature was higher than the turbine inlet temperature, indicating that combustion was still taking place in the turbine cavity.

This can be explained by the broken flow separator. Because of the broken flow separator housing, some compressed air was allowed to bypass the combustor and dump into the turbine discharge passage, the remaining air which passed through the combustor and turbine was consequently very fuel rich during the start causing the prolonged burning phase.

3.3 S/N 004C Engine

S/N 004C engine was the second ceramic structured engine in the AGT101 program. The purpose of this engine was to evaluate ceramic engine performance and high temperature durability. Initial testing was performed using a dual alloy turbine rotor and metallic diffusion flame combustor. Later engine builds incorporated a ceramic turbine rotor and a ceramic lean burn combustor.

Significant testing of this engine was performed in Builds 2, 4, and 5. In Build 2, this engine was assembled with a dual alloy turbine rotor and operated up to 100 percent speed. Build 4 was the first build of an all ceramic engine. Assembly of Build 5, in process at the completion of this reporting period, was in preparation for a 100-hour endurance test at 2200F.

3.3.1 Build 2: High Speed Ceramic Engine Testing

This engine was assembled to evaluate AGT101 ceramic engine operation at high

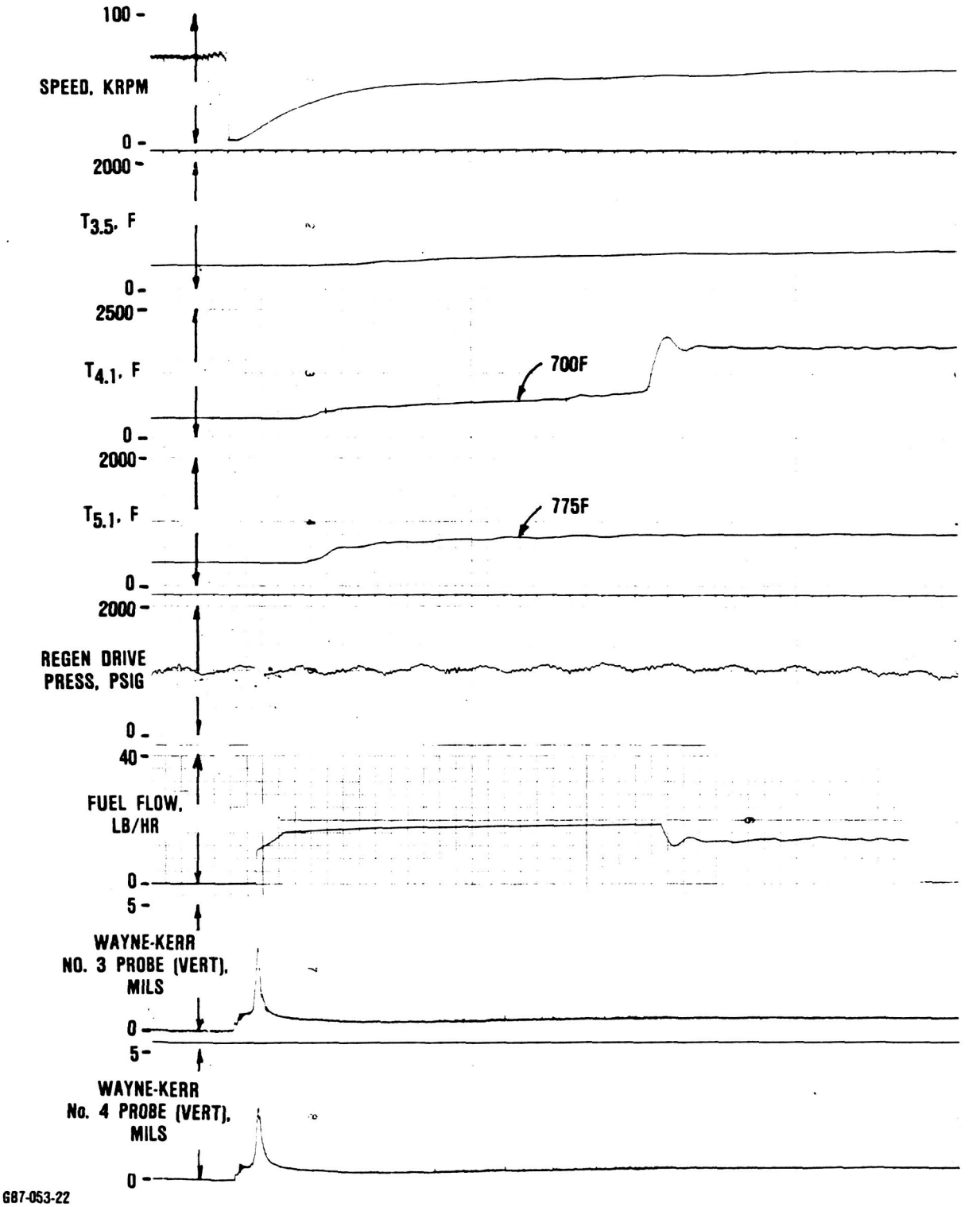

Figure 18. Chart Recording Shows $T_{5.1}$ Higher Than $T_{4.1}$ During Start Transient, S/N 002C, Build 16A.

speeds and turbine inlet temperatures up to 2100F. It incorporated ceramic static structures qualified to normal start conditions and configured for 2100F operation. The purpose of this test was to place the highest developmental pressure-induced stresses on the ceramic components and to check engine performance over the engine speed range.

During this test, a total of 25 starts were made, of which at least 8 were "hard" starts. Hard starts were accomplished by initiating a manual start, then immediately after the combustor was ignited and the 15-second turbine inlet temperature transient ramped to 1600F, the engine was loaded to 1800 to 1900F.

This engine was operated over the entire engine design speed range, including several dwell periods at 100,000 rpm with turbine inlet temperatures at 2100F. At those conditions, the pressure loading on the ceramic structure interfaces are at the greatest levels.

Performance evaluations indicated an inconsistency from day to day, with no identifiable trend. One-hundred percent power would vary from zero on the first day, to 17 hp on the next. On the third day maximum power would peak at 12 hp. This variation was believed to be due to foreign material generated within the engine, fouling the turbine shroud seal. This could possibly cause one or both of these ring seals to jam due to the close clearance with the bore of the flow separator housing. In order to seal properly, these seals must float to compensate for thermal movement of the ceramic structures.

On the third day of testing, the dual alloy turbine rotor failed at 95,000 rpm. The cause of the failure was traced to premature stress rupture failure of the MAR-M 247 cast blade ring. This rotor failure, in concert with the dual alloy turbine rotor failure in S/N 002C Build 15, contributed to the decision to discontinue engine testing with dual alloy turbine rotors at high temperatures in the AGT101 ceramic engines. As much as possible, future engine testing will be conducted with ceramic turbine rotors.

3.3.2 Build 3: Aborted Exhaust Housing Testing

Testing of this engine build was aborted when high subsynchronous rotor motion was experienced during the first cold motoring run. The cause was traced to misalignment of the quill shaft.

3.3.3 Build 4: All Ceramic Engine Testing

This engine was assembled with a completely ceramic hot power section. In addition to the ceramic hot section static structures, the combustor and turbine rotor were ceramic. The purpose of this test was to demonstrate the operation of this engine at cruise speeds and elevated turbine inlet temperatures.

The diagram in Figure 19 shows the sources and materials for each of the major ceramic components used in this build. These materials were chosen based on the temperature, stress and compatibility with adjacent materials, in addition to the shape making capability of the suppliers. Half of the ceramic components used in this first all ceramic gas turbine engine were from domestic suppliers such as AiResearch Casting Company, Carborundum, and Corning. Of the foreign supplied ceramic components, the most significant suppliers were NGK and Kyocera.

The turbine rotor was made of Kyocera's SN 220M sintered silicon nitride material. The rotor configuration featured an integral foil bearing journal with a hollowed shaft to accommodate the turbine attachment collet. Due to stress rupture limitations of the SN 220M material, the test was limited to 2000F maximum turbine inlet temperature and 70,000 rpm.

Three hours and forty-three minutes of operation were accumulated on this engine build. Maximum turbine inlet temperature was 1850F and the maximum speed was 70,000 rpm. The turbine inlet temperature was limited by an extremely sensitive regenerator drive system. As the turbine inlet temperature was increased, the regenerator drive

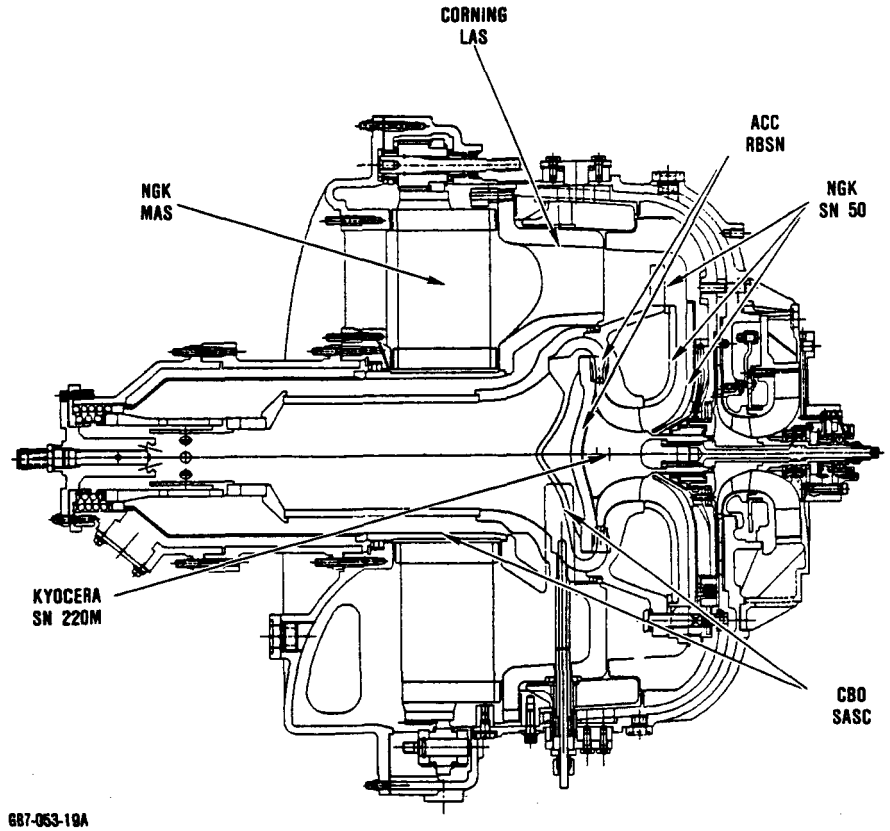

Figure 19. All Ceramic Engine Ceramic Component Sources.

pressure also increased. At 1850F turbine inlet temperature, the regenerator drive pressure was at its maximum limit.

This test was terminated due to a failure in the regenerator drive system. Shown in Figure 20, the hot regenerator seal diaphragm locating tab was not seated in its locating slot in the engine assembly. Locally, this caused a reduction in seal clearance needed to compensate for thermal variations in the regenerator stack. The load distribution in regenerator drive system was also changed, overloading the fixed roller regenerator support and causing the graphite busing to prematurely wear. The excessive wear in the bushing caused the regenerator core to translate radially and interfere with the internal ceramic structures, causing them to fail.

Corrective action was taken to ensure that the seal tabs on future engines are properly located. In addition, a proximity probe was installed to monitor fixed roller bushing wear. Should the fixed roller bushing wear excessively, the probe will activate an alarm at the test console. The probe installation is shown in Figure 21.

3.3.4 Build 5: 2200F Endurance Engine Assembly

At the close of this reporting period, effort was underway to prepare the hardware for the next build of this engine. Build 5 will be used to demonstrate engine durability over 100 hours of continuous operation at 2200F. Since this engine will be used to evaluate engine durability at 2200F turbine inlet temperature,

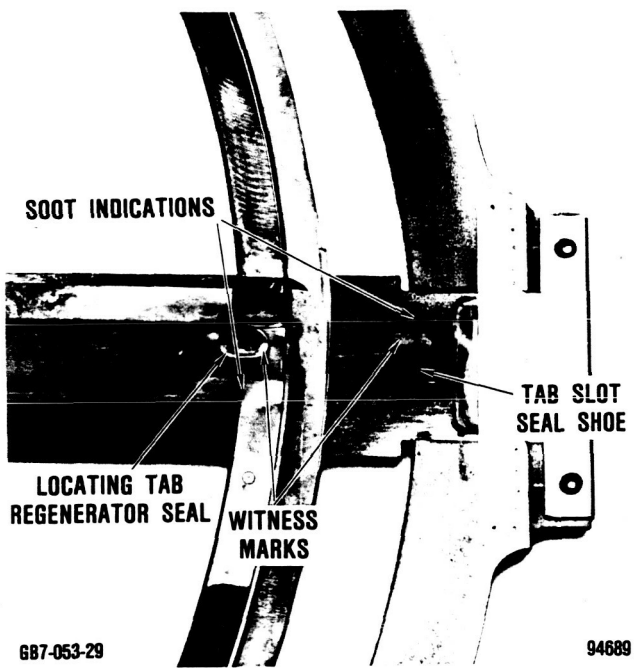

Figure 20. Seal Tab Witness Marks.

it will utilize the latest improvements in ceramic component and seal design. Some of the features of this engine are listed below:

- o Kyocera SN 250M sintered silicon nitride hollow shaft turbine rotor
- o Kyocera SN 250M hot section structural components, i.e., turbine shroud, turbine backshroud, turbine stators, combustor baffle, and transition duct
- o Dual ring turbine shroud seals
- o Ceramic spring loaded regenerator shield seal
- o Dual baffle foil bearing seal
- o Increased loading on the regenerator shield spring

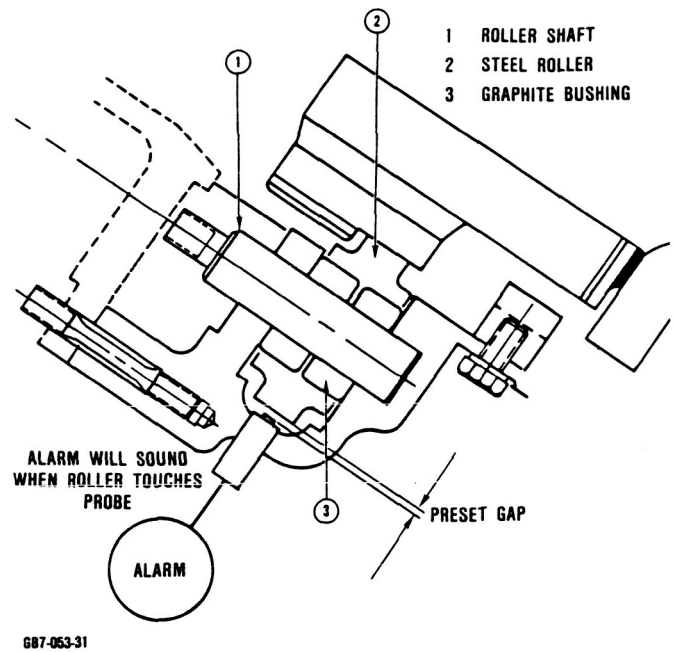

Figure 21. Diagram of Regenerator Fixed Roller Wear Limit Probe Installation.

- o External combustor cap and exhaust cover cooling
- o Ford Phase VI-B regenerator seals

The temperature capability of this engine was increased over that of Build 4 by virtue of the new Kyocera SN 250M material. Preliminary stress rupture testing of this material indicates a substantial improvement over the SN 220M material. Data from four-point flexure testing of test bars show that at 2000F and 50 ksi stress, the SN 220M test bars fractured on loading. This equates to an operating condition of 2200F turbine inlet temperature. The SN 250M test bars did not fail, even after 1000 hours of testing.

Analysis is in process to determine the stress rupture life of the rotors made of the SN 250M material for this planned 2200F endurance test, though it is expected that this

value is much more than the 100 hours planned for the test. The utilization of this material for the other hot section components with significant stresses will also increase their probability of survival.

The dual ring turbine shroud seal, discussed more thoroughly in Section 4.5.5, was incorporated in this engine configuration to reduce the leakage in this area and to reduce the effect of internal thermal growth and foreign matter on seating of the seal.

External combustor cap cooling was added to improve combustor load spring life. This spring, made of Inco X750, may see gas temperatures as high as 1700F. By preventing hot gas flow through the spring cavity and cooling the combustor cap walls, the spring temperatures can be kept below 1200F and the spring loads can be maintained. In addition the combustor cap and exhaust housing cooling will reduce regenerator drive loads as demonstrated during testing of S/N 002C engine and discussed in Section 3.2.

4.0 COMPONENT/SUBSYSTEM DEVELOPMENT

Component/subsystem development activities during this reporting period concentrated on supporting AGT101 2100F testing, improved engine sealing capabilities, and combustor development. Figure 22 shows the performance rating stations for the AGT101 engine and components.

The following sections discuss major efforts and accomplishments during this reporting period for the component subsystems.

4.1 Compressor Development

No activity during this reporting period.

4.2 Turbine Development

No activity during this reporting period.

4.3 Combustion System (Rig Activity)

Combustor rig usage during the reporting period included extensive testing of the ceramic combustor using fuel nozzles of a Garrett design and a Garrett-based Delavan design. Testing examined the potential for fuel nozzle coking and fouling as well as evaluation of nozzle modifications to improve combustion, light-off characteristics, and component life. The rig was also used to thermally screen ceramic combustor parts to be used in the engine.

Fuel Nozzle Development

Testing of the Garrett nozzle, which was designed and fabricated at the end of the prior reporting period, demonstrated its acceptable performance with a spark ignitor. Testing of the torch ignitor ended with the successful demonstration of the spark ignitor. Delavan designed and fabricated a nozzle which was based on the Garrett design. The nozzle performed unacceptably in rig testing due to Delavan's use of a geometry which helped to simplify fabrication. The next Delavan effort, S/N 002, was a revised configuration more similar to the Garrett design while maintaining simple construction features. Light-off, stability, lean blow-out, and temperature rise tests were conducted using the S/N 002 nozzle, and will be discussed in the combustion section of this report.

A second Delavan nozzle, S/N 003, was instrumented with 20 thermocouples and two pressure probes to measure atomizing and cooling air pressures (see Figure 23). This nozzle was used to assess potential of coking and fouling problems by measuring the fuel and metal temperatures at critical points. This nozzle and all subsequent Delavan nozzles were also modified to route part of the atomizing air to the cooling air ports in order to enhance fuel cooling. Testing with the instrumented nozzle was done at idle engine speed since it imposed the most severe conditions with regard to coking and fouling. Average fuel temperature versus cooling air pressure is shown in Figure 24. The chart indicates that at cooling air pressures above 5 psid the average fuel temperature is essentially independent of the cooling air flow. Nozzle face temperatures are shown in Figure 25. Both temperatures are in the acceptable range for cooling air pressures near 5 psi above combustor pressure. Further testing at combustor inlet temperatures over 1600F and discharge temperatures over 2200F has shown the nozzle face to be self-cleaning in the operating range.

Combustor Development

The ceramic combustor components were successfully tested for structural integrity in a combustion environment with a series of combustor temperature rise tests. Combustor discharge temperature was ramped to 1800F while maintaining ambient inlet temperatures.

Combustor performance was tested in the rig with a number of simulated engine starts

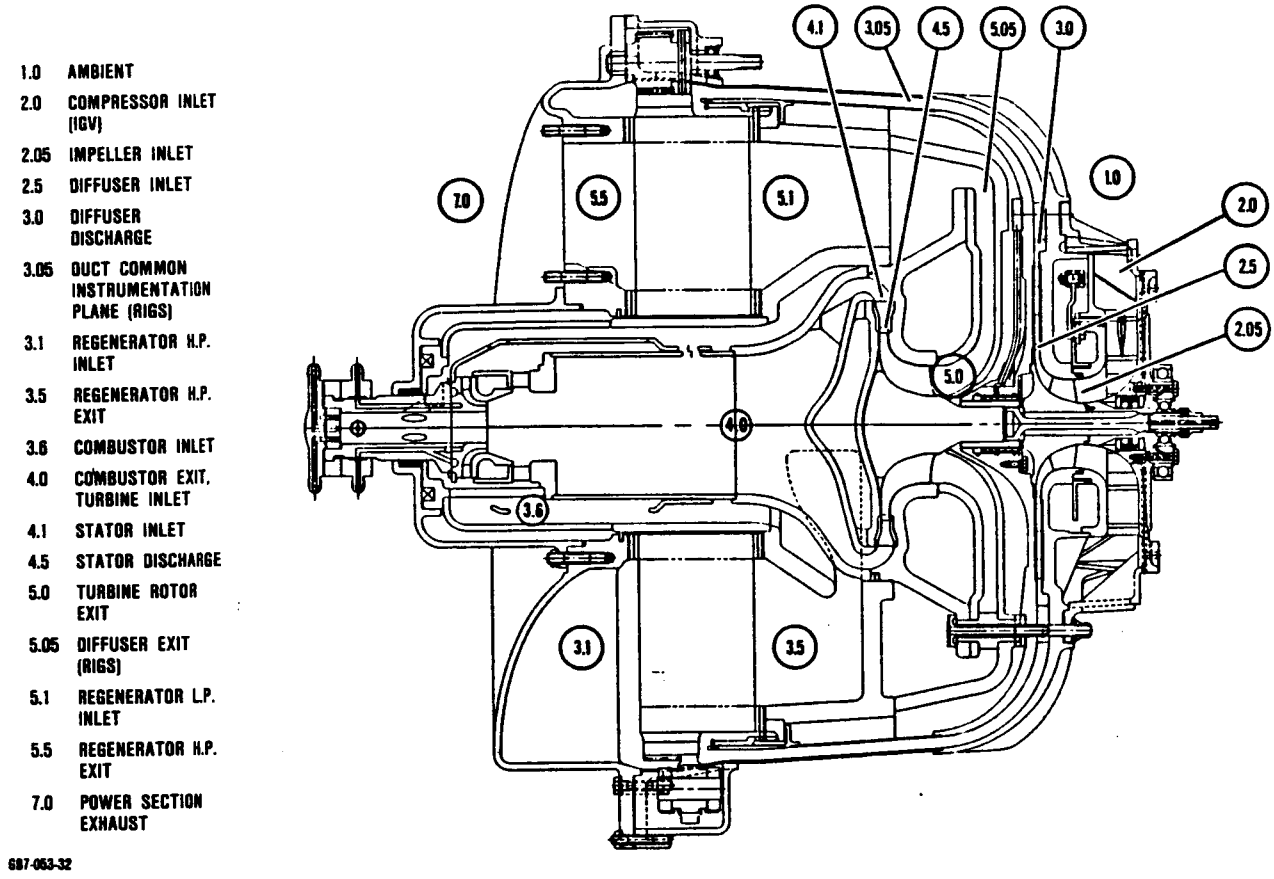

Figure 22. Performance Rating Stations.

using the Garrett and Delavan nozzles. Consistent light-offs for ambient inlet temperatures at 35-45 percent speed conditions were obtained using JP-4 fuel. The inlet air temperature was ramped to 1800F to simulate regenerator warm-up and combustor discharge temperatures ranged from 2000-2500F. Inlet air was heated with an indirect-fired burner to reach 1200F and direct-fired heater to achieve 1800F.

Ignition testing established an envelope of air assist and cooling air pressures for combustor light-off with atomizing air being the more substantial effect. The combustor would not light for atomizing air pressures less than 2 psid and experienced light off and blow out at higher pressures. Further efforts will be directed at broadening the light-off envelope.

Lean blow-out data obtained for the combustion system utilized non-vitiated air to 900F and vitiated air to 1600F. The lean blow-out fuel air ratio was appreciably lower than the engine idle fuel air ratio. The data as correlated for an atomizing air pressure of 4-6 psid is shown in Figure 26 as a function of fuel air ratio versus $V_{Ref}\ \theta.\delta$.

Combustion System Design Improvement

An initial configuration of the ceramic combustor incorporated a metal preburner

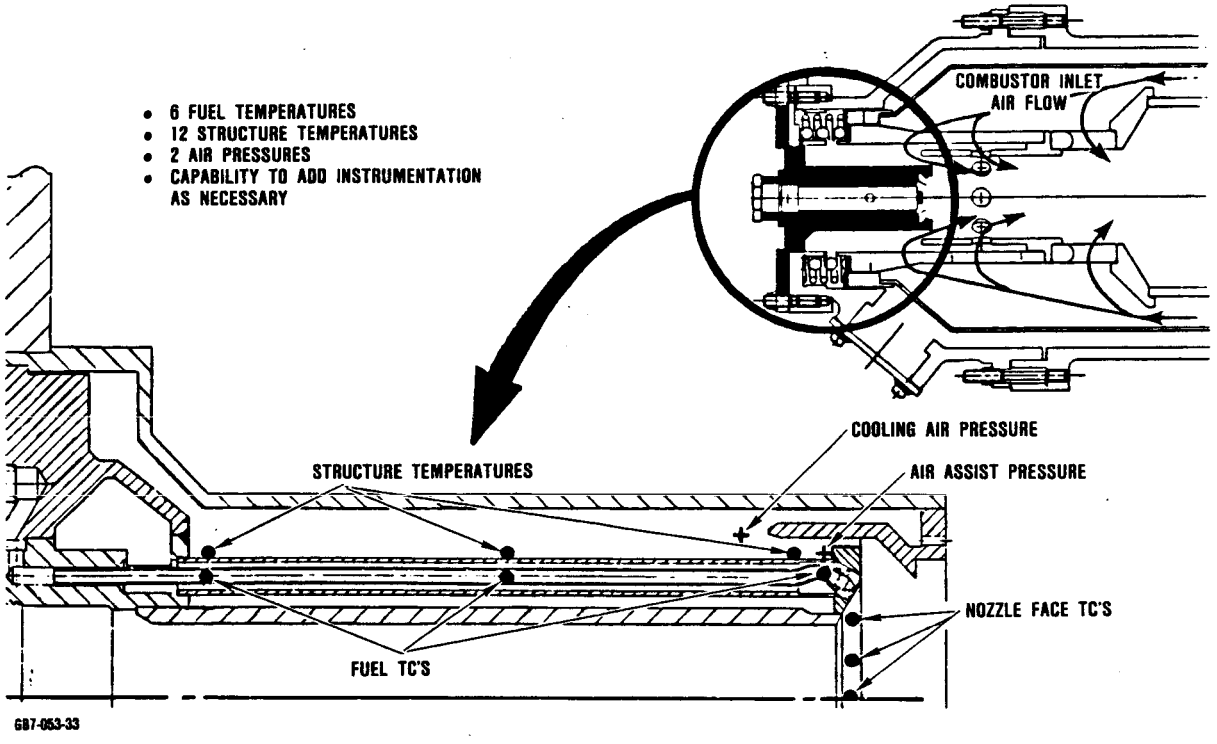

Figure 23. Instrumented Fuel Nozzle Testing in Process.

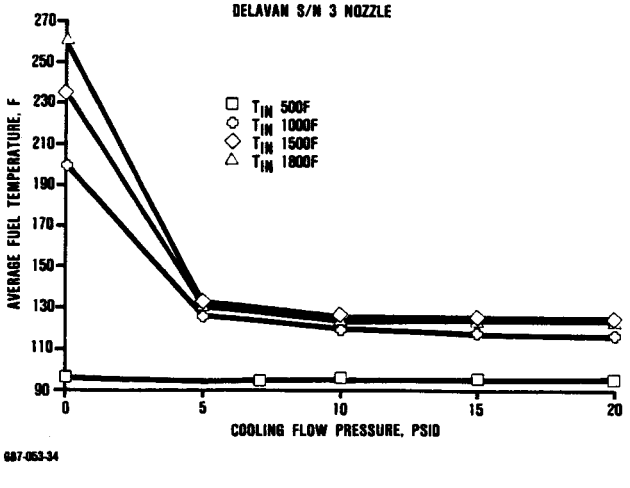

Figure 24. Average Fuel Temperature versus Cooling Pressure.

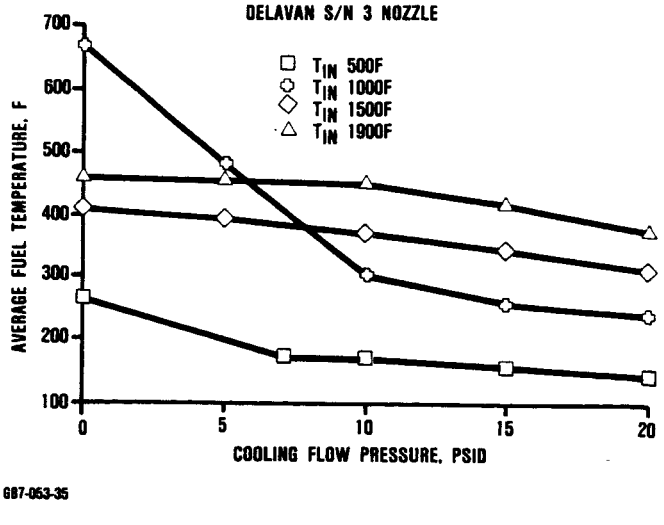

Figure 25. Nozzle Face Temperature versus Cooling Air Pressure.

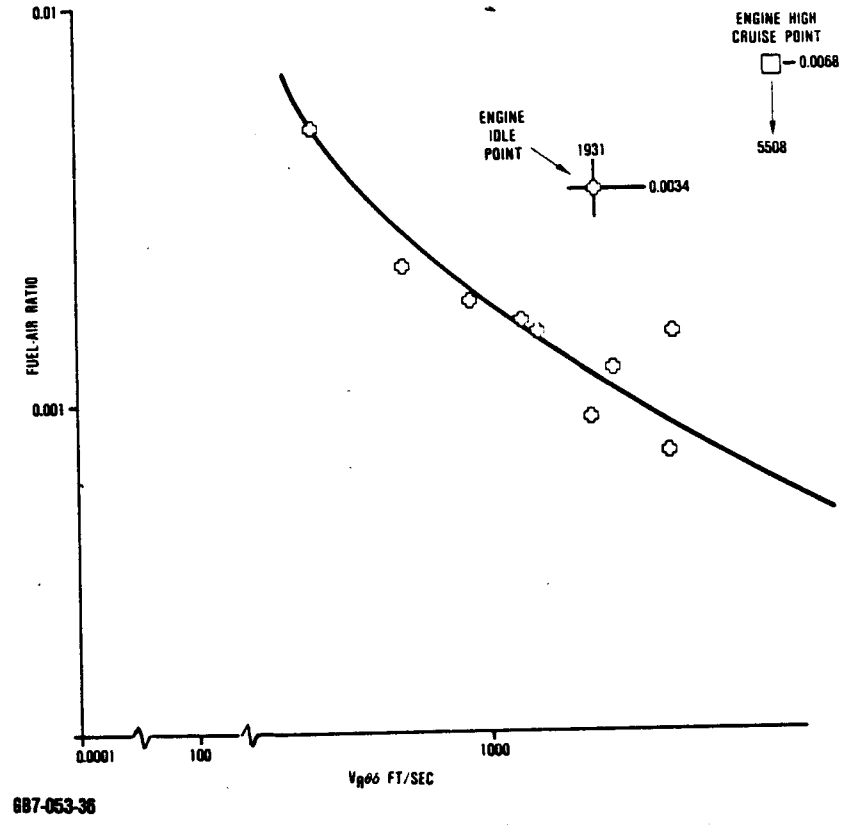

Figure 26. Rig Measured Combustor Stability (50-70 Percent Speed).

welded to the fuel nozzle. Instrumented fuel nozzle testing indicated that temperature levels on the preburner reached 1830F at a combustor inlet temperature of 1600F and air exit temperature of 2200F. The combustor was upgraded to incorporate a ceramic preburner to replace the metal as shown in Figure 27. Performance testing indicated no discernible changes for light-off or steady-state conditions.

In an effort to achieve rapid cold start engine acceleration to 70,000 rpm, an enlarged pilot combustor and integral swirler were designed for improved stability. The initial configuration, shown in Figure 27, is being fabricated of metal for proof of concept testing. Future combustor testing will examine methods of obtaining better light-off consistency and stability to support engine testing.

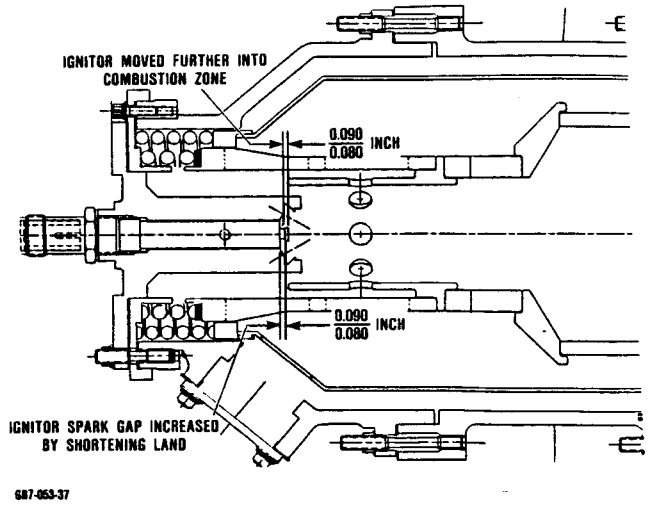

Figure 27. Modifications to Nozzle Assembly Required for Engine Operation on DF-2 Fuel.

4.4 Regenerator System

4.4.1 Regenerator System Development - Ford

4.4.1.1 Regenerator Seals

The primary effort at Ford during this report period was to refine the Phase VI seal design until the leakage objective of 3.6 percent is satisfied.

An interim quality control standard was established for the static seal leakage rig to ensure that low leakage seals would be sent to Garrett for engine and test rig evaluation. A 12 cfm static leak test requirement per seal (inboard or outboard) at 0.276 inch seal working height, which is based on the best seals evaluated previously in the engines and rig tests at Garrett, was established.

This limit (24 cfm) is believed to be equivalent to 5.5 percent regenerator seal system leakage in an engine based on helium leakage measurements at Garrett.

The Phase V-A (Figure 28) seal design developed in the previous report period featured overlapping ends on the crossarm and peripheral diaphragms for reduced leakage. Seven Phase V-A seal sets were delivered to Garrett, which satisfied the delivery requirements for calendar year 1985. Each of these seals met the static leak test requirements.

Four previously used crossarms that were reprocessed and delivered in December 1985, were found to have distortions which seriously affected leakage when assembled and tested in the seal leakage rig. Unlike the circular and cold crossarms, which are blanchard ground to remove coatings, the hot crossarm has a nonmagnetic substrate and also has serrations in the coating surface. This requires the coating in the hot crossarm to be removed by grit-blasting, which produces significant stresses in the crossarm substrate. On previously used crossarms, the normal stress-relief treatment apparently does not restore the substrate to a flat condition. A full anneal heat treatment, with the substrate loaded on a flat ceramic plate, was introduced after stripping to restore the part to a flat condition before coating. Subsequent crossarms have met the 0.010 inch flatness requirement after coating using this procedure.

An investigation into the effect of seal shoe flatness on leakage was completed. Three sets of hot seal shoes with different degrees of flatness were evaluated in the static seal rig using the same Phase VI diaphragm system. The results showed the leakage was reduced from 15 to 8 cfm at 0.285 inch nominal build clearance when flatness was reduced from 0.010 to 0.004 inch.

Work during this report period was concentrated on developing the Phase VI (Figure 28) seal design, which features equal length retainers and symmetrical peripheral diaphragms. Based on anticipated availability of the various dies that are required, Phase VI is being developed in two stages as illustrated in Figure 28. This phase represents the final configuration of the evolutionary design and development technique that is projected to satisfy the program objectives for leakage and temperature capability.

The first set (hot and cold) of Phase VI-A seals, featuring equal length retainer legs and symmetrical peripheral diaphragm combined with Phase V-A crossarm diaphragms, were built and tested on available shoes. They demonstrated the anticipated characteristics of leakage being nearly independent of the seal working range.

Two Phase VI-B cold seals were assembled. The crossarm has a dual coating, I-112 on the inner periphery to accommodate venting the exhaust gas and I-85 on the crossarm extensions. The inner periphery exhaust section has pressure relief grooves resulting from masking during the spraying process. Both of these cold seals had less than 12 cfm leakage at 0.276 inch seal working height. One of the cold seals had a leakage of 8 cfm at 0.276 inch seal working height and it is believed that this

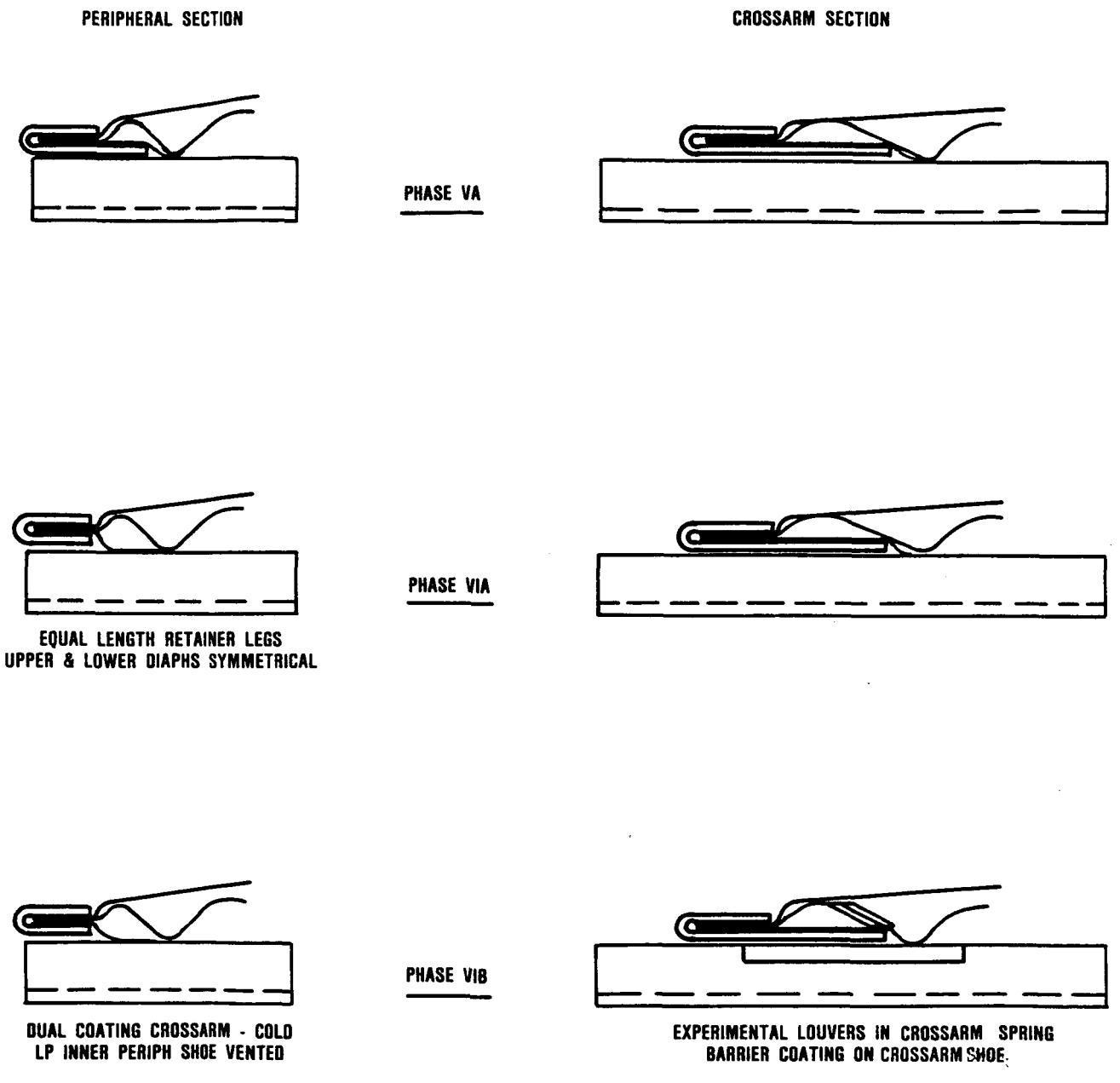

Figure 28. Proposed Variations in Phase VI Regenerator Seal Development.

seal will meet the program objective of 3.6 percent leakage. This leakage is equal to the lowest leakage ever measured on a Phase V-A seal. Both of the Phase VI-B seals were assembled with reprocessed shoes having the full anneal heat treatment after stripping. Even so, these shoes were not as flat as completely new shoes; further leakage reductions can be anticipated when new shoes are used together with the Phase VI-B diaphragm system.

Two Phase VI-B hot seals were assembled. The crossarm has a barrier coating (stabilized zirconium oxide) plasma sprayed in a recess 0.050 inch deep on the diaphragm side of the shoe. Both seals qualified with less than 12 cfm leakage at 0.276 inch seal working height. Both of these hot seals were also made with reprocessed, used shoes.

To date a total of five cold and eight hot Phase VI seals have been built and met leak test specifications. The Garrett 1986 calendar year requirement is eight cold and twelve hot seals. The majority of the thirteen seals assembled have not been shipped because they are not currently needed to support testing and more feedback from engine tests is desired to update these seals into more advanced configurations.

In order to accommodate the 2000F regenerator system operating temperature associated with the all ceramic engine, the regenerator inboard (hot) seal crossarm will require diaphragm cooling. This design (Figure 29) has a funnel incorporated into the crossarm end diaphragm, which allows cooling air to flow between the upper and lower diaphragms. A transfer tube at the corner allows the air to continue through the HP side of the inner periphery. The amount of cooling air flow is dependent on the pressure differential that exists in the channel. Pressure differential (less than 0.25 psid) establishes the minimum rate of cooling air flow. For maximum cooling, holes in the retainer (Figure 29) allow the air to discharge into the center hole cavity, which is vented to the exhaust duct.

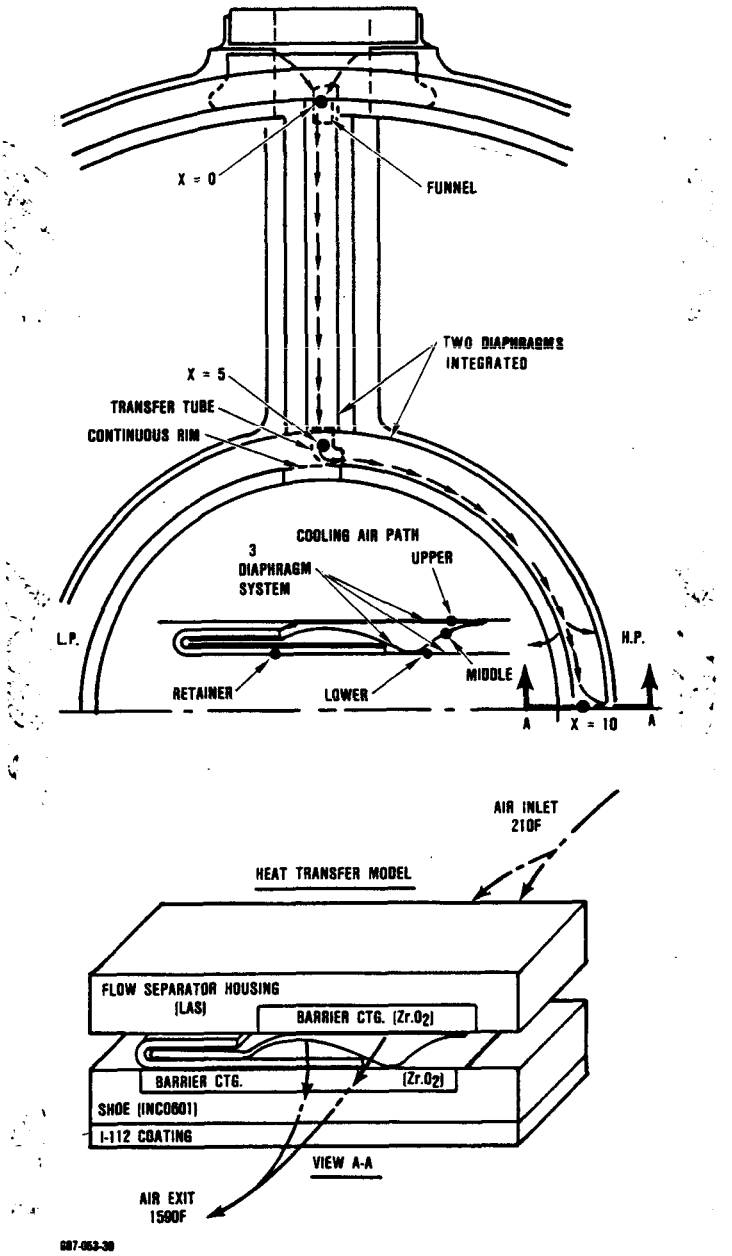

Figure 29. Inboard Seal Crossarm Diaphragm Cooling Schematic.

During the previous report period, minimum cooling air for three design concepts was evaluated for MOD II engine flow conditions at 60 percent engine speed with the flow separator housing varying from 1400 to 1700F (Figure 30). The results indicate the middle diaphragm will operate at an acceptable temperature level of 1650F with cooling flow on both sides (Design 3) and a 0.050 inch barrier coating on the diaphragm side of the metal rubbing shoe.

Because of recent interest in fabricating a flow separator housing (FSH) with reaction bonded silicon-nitride (RBSN) instead of lithium-aluminum-silicate (LAS), a detailed finite-element model of the FSH was completed. The initial heat transfer analysis was conducted at simulated steady-state cruise operating conditions to evaluate thermal distortion of the FSH fabricated with LAS or RBSN materials. Based on this analysis, the temperature level at the inner circular portion of the RBSN or LAS FSH will be 1900 to 1950F for a gas inlet temperature of 2000F.

Since the recent temperature predictions for the FSH are significantly higher than the 1400 to 1700F from the previous analysis, the cooling requirements for the Design 3 concept were re-evaluated with an additional barrier coating applied to the circular portion of the FSH. For this analysis, the inner circular portion and the straight section temperatures of the crossarm were 1900 to 1950F for a gas inlet temperature of 2000F.

In addition, the higher operating temperature required an investigation of the current Phase VI seal design. Initial diaphragm stress levels were based on the Phase IV seal design. Since the Phase VI diaphragm design has a significantly lower lift angle (Figure 31) compared to the Phase IV configuration, the diaphragm stress levels will be reduced from 75 to 65 ksi. Consequently, the design temperature objective for the middle diaphragm can be increased from 1650 to 1700F. The Waspaloy material will have adequate strength at this temperature for the Phase VI diaphragm stress levels.

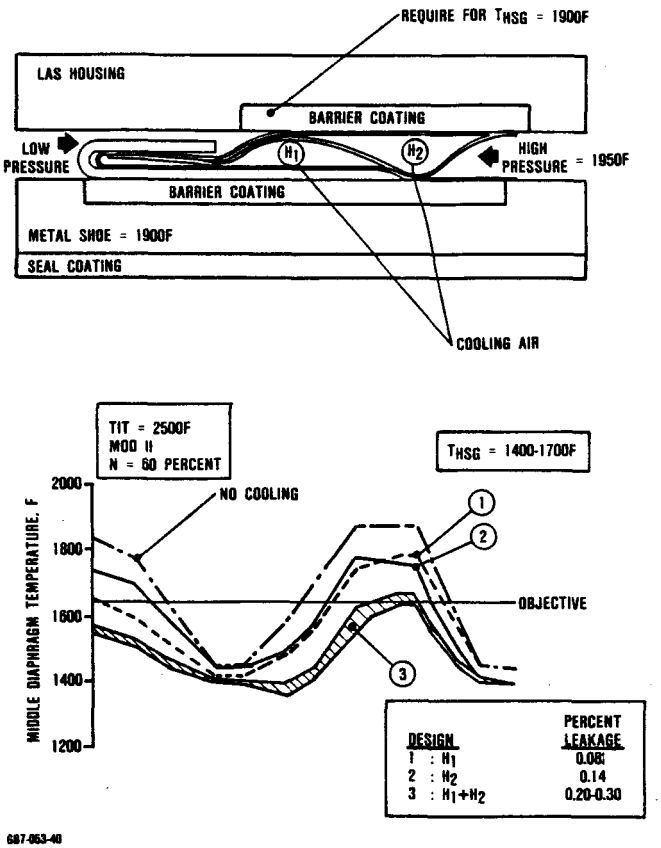

Figure 30. Crossarm Diaphragm Cooling Analysis.

The Design 3 concept was re-evaluated for cooling flows varying from 0.053 to 0.180 lb/min, which corresponds to 0.25 (minimum) and 0.85 percent leakage, respectively. For each cooling flow the convection heat transfer coefficient was increased 20 percent to simulate interrupting the flow by incorporating an appropriate spacing of openings in the axial direction of the middle diaphragm. For cooling flows greater than 0.25 percent, the air will be discharged through holes in the retainer into the regenerator center hole cavity, which is vented to the exhaust housing duct. This will require incorporating a restriction at the crossarm end diaphragm to throttle the cooling flow required.

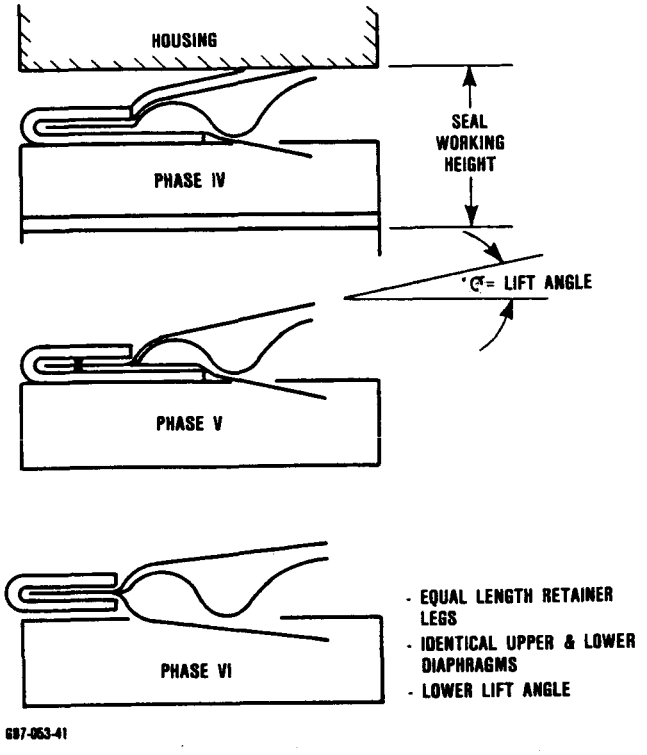

Figure 31. Seal Diaphragm Comparison.

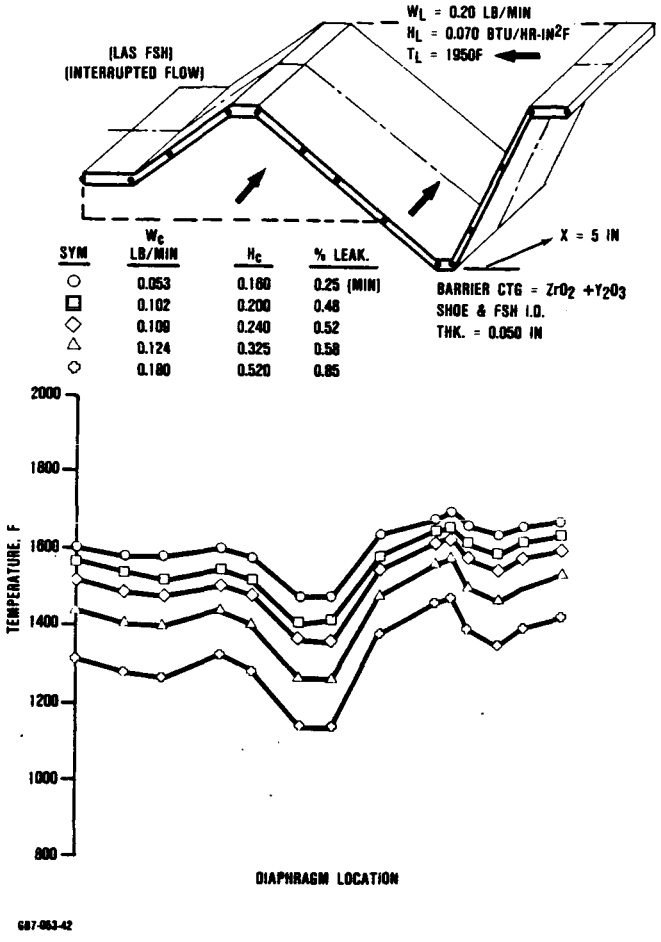

Figure 32. Effect of Cooling Rate on Temperature Distribution.

The middle diaphragm temperature distribution for axial locations of 5 and 10 inches as a function of cooling flow are illustrated on Figures 32 and 33, respectively. these locations correspond to the transfer tube from straight to circular and cooling flow exit at the center of the inner circular portion of the crossarm (Figure 29). the barrier coating thickness for the seal substrate and FSH inner circular section are both 0.050 inch. The minimum cooling flow (0.25 percent) is sufficient to keep the middle diaphragm temperature below 1700F for the straight portion of the crossarm (x = 0 to 5 inch) as shown in Figure 32. In order to cool the circular portion of the crossarm (x = 5 to 10 inch) to the design temperature level the cooling flow requirement is 0.85 percent, as illustrated on Figure 33. Since 0.25 percent cooling was included in the original leakage objective (3.6 percent), the additional 0.60 percent cooling requirement (0.85 percent total) will increase total regenerator system leakage to 4.2 percent.

Seal Coatings - Two Phase VI hot seal crossarms have been received from APS Materials, Inc. for evaluation at Garrett and the Ford development rig. These crossarms had a 0.050 inch thick barrier coating (stabilized zirconia oxide) plasma sprayed into a recess on the back side of the shoe.

LAS samples were plasma sprayed in-house with zirconium-oxide to evaluate a barrier coating on the flow separator housing. Zirconium-oxide (ZrO_2) without pre-treatment of

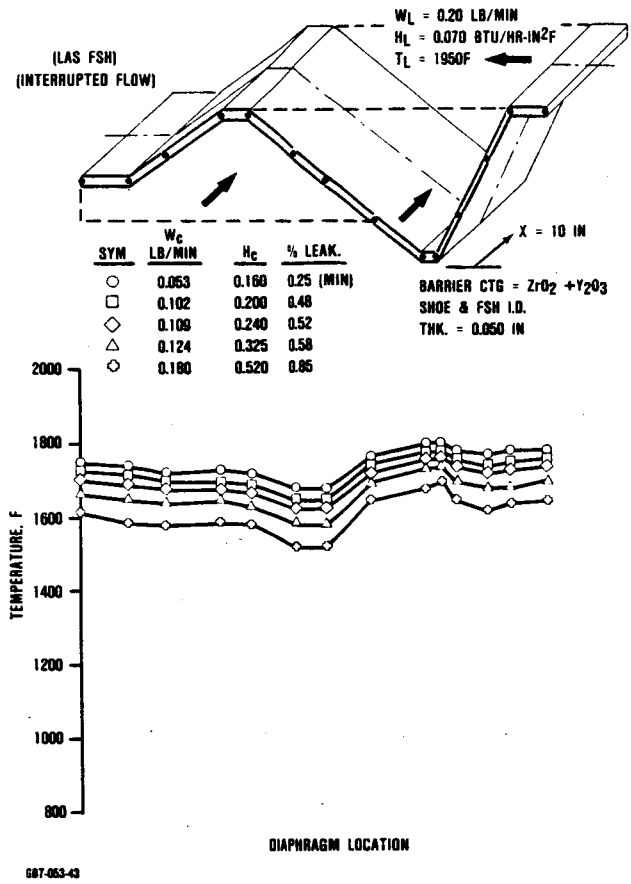

Figure 33. Effect of Cooling Rate on Temperature Distribution.

the LAS could be pried off with a screwdriver. Another sample, with the LAS chemically treated, demonstrated improved bonding. Pretreated LAS samples have been sent to APS for plasma spraying their APS-1411 barrier coating (80 percent ZrO_2, 20 percent Y_2O_3).

4.4.1.2 Regenerator Core and Drive System

The design performance objectives for the AGT regenerator are 92.9 percent effectiveness with less than 7.5 percent pressure drop at 100 percent engine speed. To meet the 3.6 percent leakage objective, the through wall porosity leakage must be less than 0.5 percent. The current Corning aluminum-silicate (AS) wrapped sinusoidal matrix (900 cells/in^2) satisfies the pressure drop objective but is 1 percent low in effectiveness (91.9 percent). Corning has been funded to fabricate samples of an extruded AS matrix with a rectangular cell shape and density of approximately 1100 cells/in^2 required to meet the AGT101 regenerator effectiveness and pressure drop objectives. The samples are expected in the third quarter of 1986.

Corning has fabricated new extrusion dies and has successfully extruded samples with LAS material, which is easily extruded. The next step will be to evaluate the more complex LAS material extrusions with these dies prior to leaching.

NGK has developed a matrix fin geometry (C0.7) with an isosceles triangular shape with a density of approximately 1500 cells/in^2 that will satisfy the effectiveness and pressure drop objectives (Table 2). They have also demonstrated significant improvements in modifying their standard magnesium-aluminum-silicate (MAS) material in order to achieve the porosity leakage objective. The improved MAS material, which incorporates increased shrinkage during firing, has reduced wall porosity from 38 to 27 percent. Based on leakage data from NGK, the full-size core leakage is estimated to be 0.6 percent, which is slightly above the 0.5 percent objective. In addition, the matrix wall thickness is reduced from 0.0047 to 0.0043 inch, with a corresponding increase in cell density from 1100 to 1200 cells/in^2.

The performance of the new improved MAS material was estimated utilizing parametric curves for effectiveness and pressure drop. The rectangular matrix parameters (C0.9) with increased shrinkage are listed on Table 2 (marked with an asterisk). Effectiveness and pressure drop increase 0.7 and 0.5 percent respectively, at 100 percent engine speed, which are both slightly higher than the Corning thin-wall matrix.

Matrix examples from the new MAS-A material, as well as the standard MAS mate-

Table 2. Regenerator Core Performance.

OBJECTIVES: (N = 100 PERCENT)

EFFECTIVENESS	=	92.9 PERCENT MINIMUM
PRESSURE DROP	=	7.5 PERCENT MAXIMUM
POROSITY LEAKAGE	=	0.5 PERCENT MAXIMUM

	Fin No.	Wall Thickness (in)	Cell Density Openings in^2	ε (%)	ΔP/P (%)	Leakage (%)
Corning (AS) Wrapped Sinusoidal	T14.20	0.0025	1310	91.9	7.3	0.20
NGK (MAS) Extrusion Isosceles	C0.3	0.0055	920	90.1	6.0	0.30
Isosceles	C0.7	0.0030	1510	93.6	7.3	1.7
Rectangle	C0.9	0.0047 0.0043*	1115 1225*	91.4 92.1*	7.2 7.7*	0.80 0.60*
Rectangle	C.8	0.0043	1390	93.3	9.2	1.0 (Est)

NOTE: NGK leakage based on Ge-Cordierite coating and impregnation.

*MAS-A material which has increased shrinkage without GE-cordierite coating and impregnation.

rial, were received for thermal stability testing at 1832 and 2012F. Both materials have been tested for a total of 504 hours of exposure at each temperature.

After this limited testing the measurements show the new MAS-A material to be more stable at 1832F (Figure 34) and 2012F (Figure 35) than the original material, which previous tests had shown to have acceptable stability. Three additional 168-hour test increments are scheduled for a total of 1008 hours.

Two full-size cores fabricated with the new MAS-A material were received from NGK at the end of this report period. Ring gears will be assembled to them for engine and test rig evaluation during the next report period.

4.4.1.3 Regenerator Development Rig

During this report period, an extensive sequence of tests were completed in an attempt to isolate system leakage sources, their relative magnitude and corrective actions.

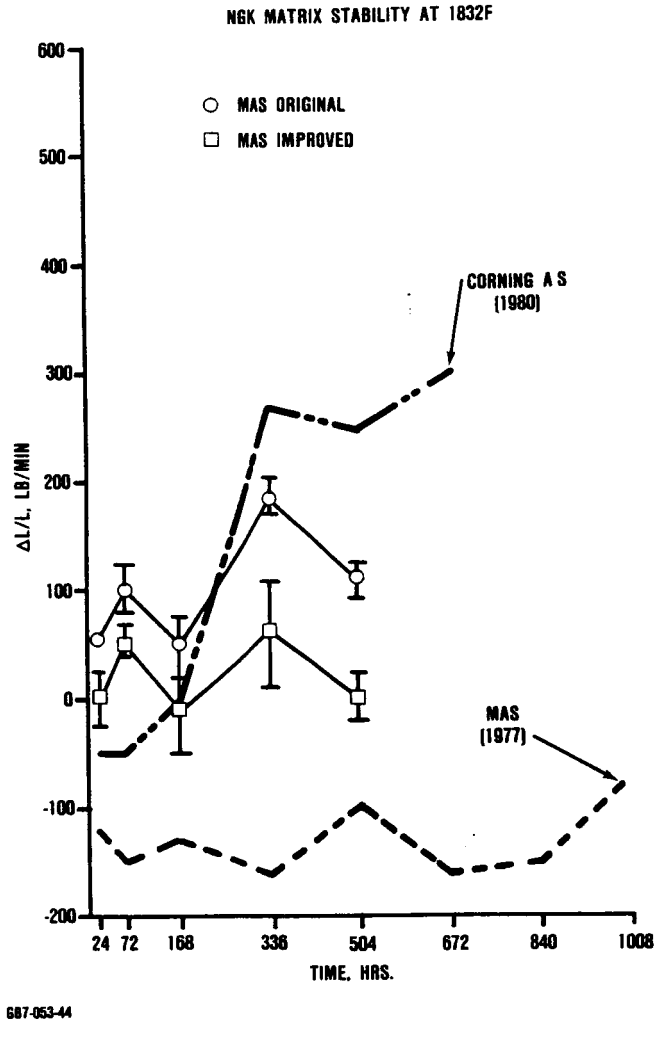

Figure 34. NGK Matrix Stability at 1832F.

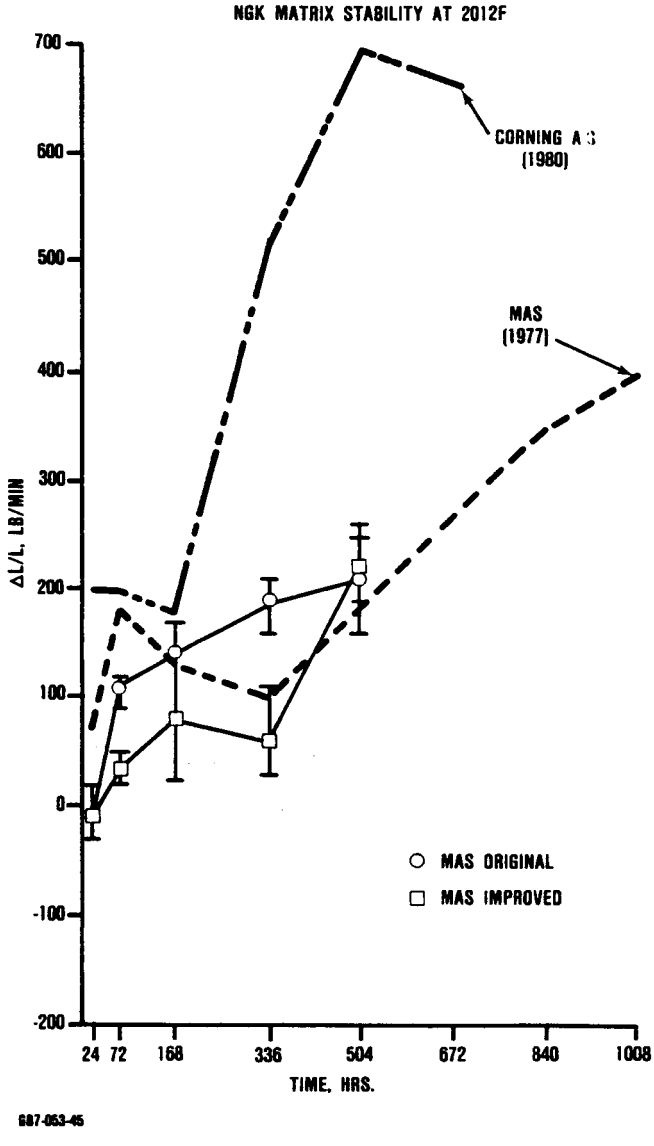

Figure 35. NGK Matrix Stability at 2012F.

The Ford regenerator development rig features a cross-over duct (Figure 36) to provide an exit orifice on the HP side in addition to the inlet orifice. A tapered disc with an internal variable throttle drive in place of a stationary rotor simulates turbine pressure drop. With this arrangement dynamic total leakage can be measured by flowing air through the rig. Static leakage can be measured by inserting a blanking plate at the exhaust housing together with a plug at the regenerator core inside diameter as illustrated on Figure 36.

The rig became operational in the second quarter of 1985. After initial de-bugging three major builds were conducted during this report period. The first build represented the baseline and the second and third represented an effort to correct the regenerator cover distortion. This distortion is believed to be a major contributor to the total regenerator seal system leakage.

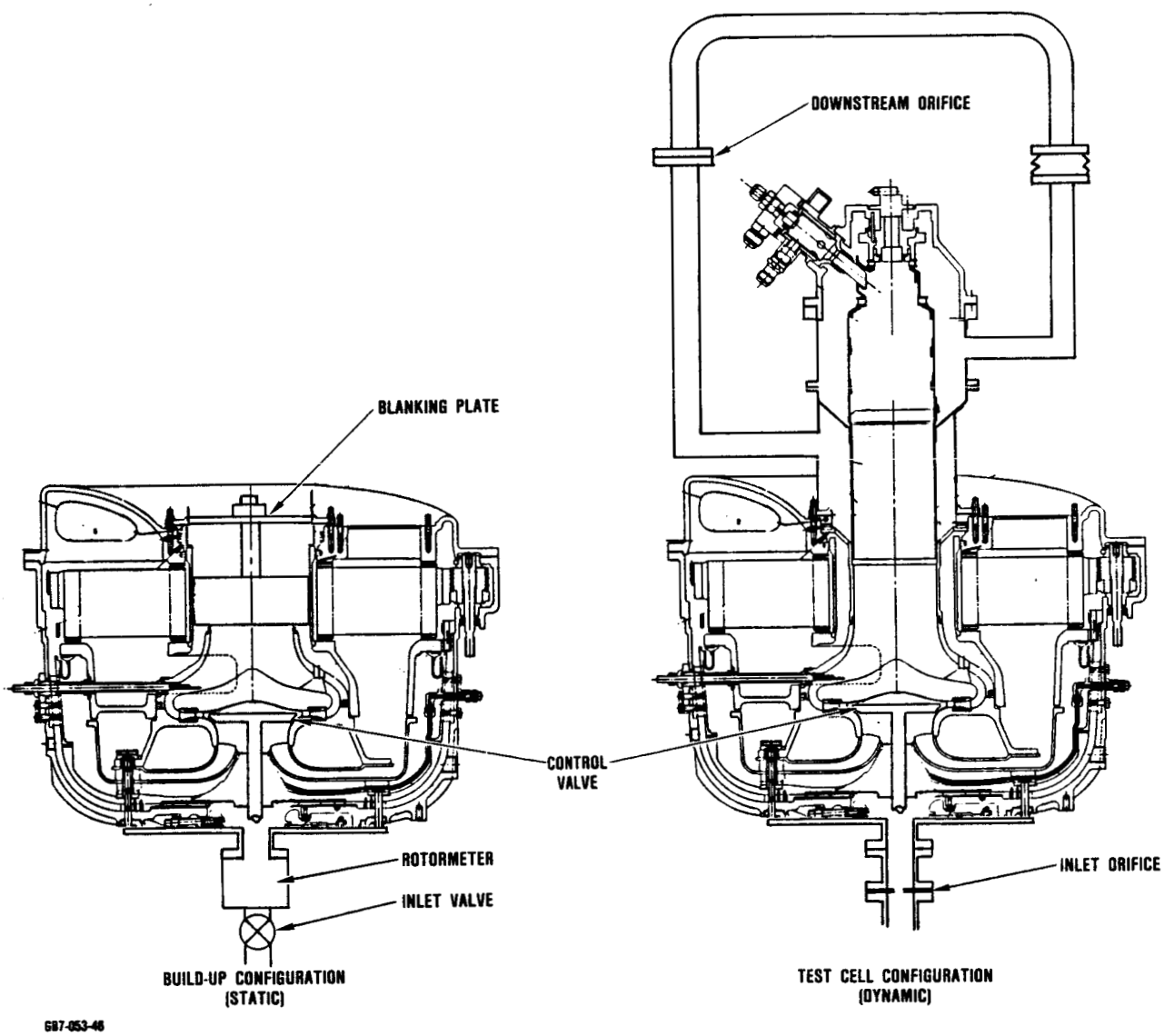

Figure 36. Test Rig Arrangements.

Figure 37 summarizes a sequence of eleven static tests conducted in build-up for the first build prior to installing the rig in the test cell. Special adaptors and sealants were used to isolate the various leakage locations. For safety reasons, full pressure could not be applied to these adaptors, so the tests in build-up were limited to a maximum pressure of 80 in.Hg absolute. The leakage locations are shown in Figure 38. The leakage increase with the NGK core was due to cracks and internal porosity present in this core.

Because of a hardware shortage, the same NGK core and seals were used in both the first and second builds. The sum of these individually measured leakages is about 13.1 percent (valve open with the NGK core). Tests results

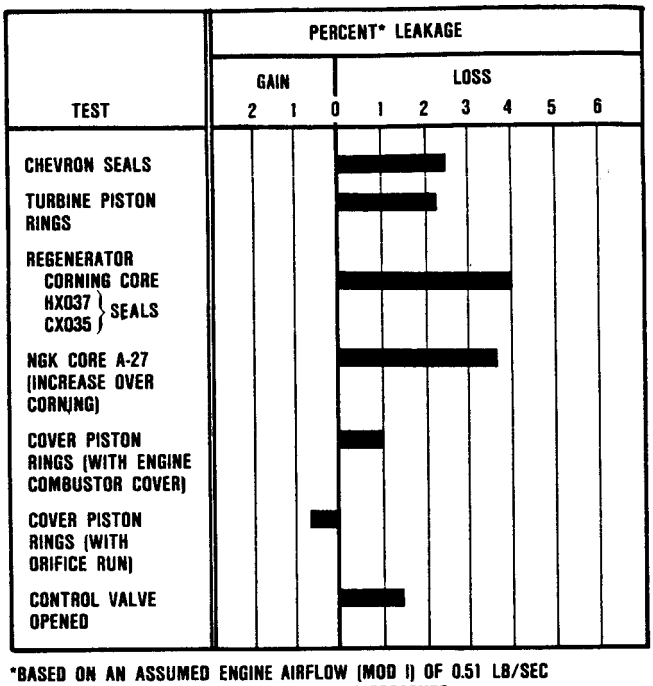

*BASED ON AN ASSUMED ENGINE AIRFLOW (MOD I) OF 0.51 LB/SEC AT 80 IN HG ABS COMPRESSOR DISCHARGE PRESSURE.

687-053-47

Figure 37. Build No. 1 - Static Tests in Build-Up.

for the assembled rig indicated a leakage of 13.9 percent at 80 in. Hg Abs. The agreement appears adequate. Leakage of the chevron seals combined with the piston rings exceeded that of the regenerator system with the Corning core (5.5 versus 4.1 percent).

By adjusting the control valve, the pressure level of the engine can be simulated. It should be noted that opening the control valve introduces a leakage from the compressor discharge region to the turbine inlet region (Figure 38). The pressure difference causing this leak was generated by the drop through the downstream orifice. This large pressure drop and this leak would not be present in an engine, where compressor discharge and turbine inlet pressures are almost equal.

The rig was then installed in the test cell for a sequence of hot and cold dynamic tests. There was good agreement for cold dynamic leakage in the cell and static leakage in build-up even though the measurement techniques are different. The primary inconsistency was the increase in cold leakage after a hot test (Figure 39), which suggests that one of the components in the rig did not return to its original position due to temperature or vibration.

Temperature measurements made on the regenerator cover indicated the highest temperatures occur near the inside diameter with the outer regions running much cooler. At the the inside diameter, the highest temperatures occur near the vent holes on the exhaust side. These metal temperatures are 300F higher than compressor discharge air and 200F higher than exhaust gas discharge air, which normally flows over this regenerator cover. These temperatures are believed to have caused a thermal distortion of the cover which contributes to uneven seal loads and additional seal system leakage. These data suggest that hot gas escaping through vent holes in the regenerator cover, which are used to bleed seal leakage that collects in the center hole region, caused the cover to distort under thermal loads.

These vent holes were plugged in Build No. 2. Grooves were machined on the low pressure circular half of the outboard (cold) seal crossarm to allow the hot gases to escape between the seal and regenerator core (Figure 40). This modification would theoretically reduce the amount of heat introduced locally into the cover. Linear displacement transducers were mounted on the cover to measure regenerator cover deflection during transient operation of the rig for both builds.

The same increase in leakage after a hot run was present in the second build (Figure 39). This time the leakage levels were considerably higher. The leakage obtained in build-up with the valve closed for the second build is equivalent to that obtained with the first build, yet the first run in the test cell showed the second build to have almost 50 percent higher leakage. This was further

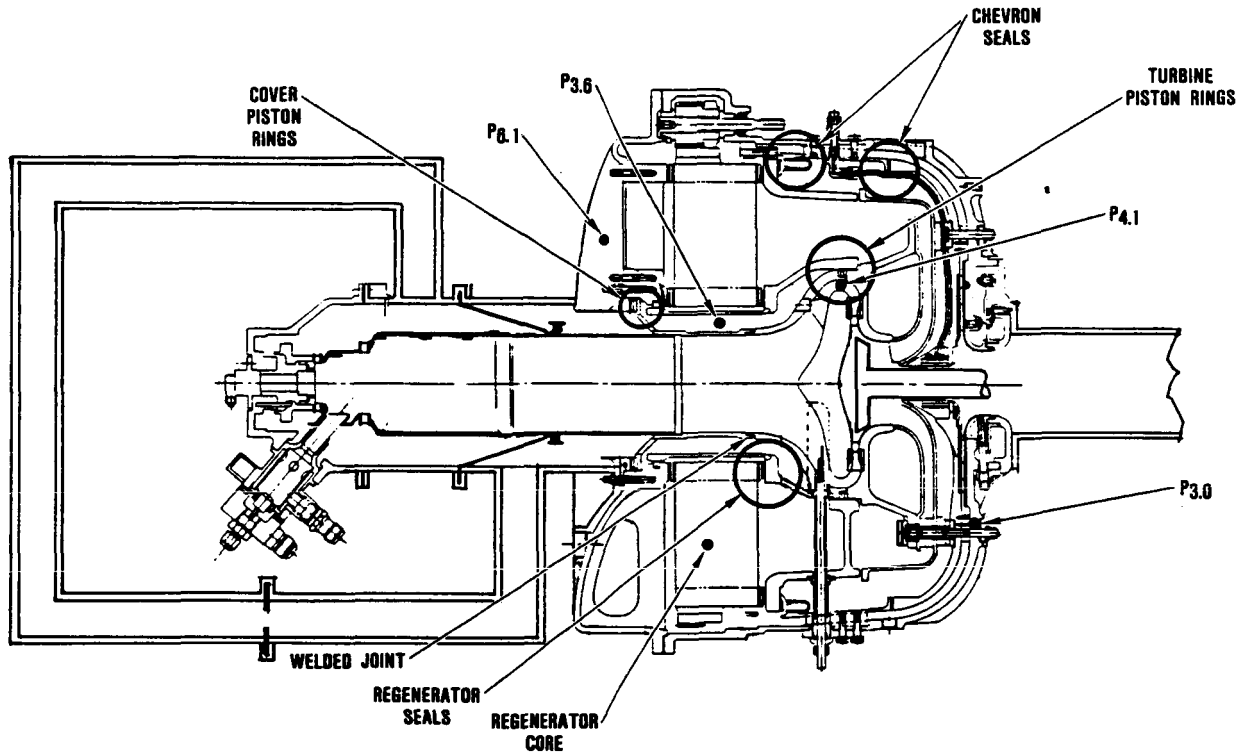

Figure 38. Leak Paths and Pressure Notation.

evidence that the assembly is structurally unstable, causing one or more sealing elements to have restrictive movement. The vibration imposed on the rig during transportation and installation in the cell probably unseated one of the chevron and/or piston ring seals.

Both builds showed that the leakage increased significantly when the control valve, which simulates turbine pressure drop, was opened. This permitted a leak from the compressor discharge, P3.0, to the turbine inlet, P4.1. To examine this leak in greater detail, data was taken with the valve in four different positions during the second build (Figure 41).

Figure 42 compares the first and second builds at a constant temperature and core speed but with varying pressures. Within accuracy of the data the drive torques are the same for both builds. The deflection and temperature plots show that a major improvement was achieved with the second build at low pressure levels. In addition the temperature and deflection of the second build were influenced by pressure.

As a result of the first two major builds of the test rig during this report period, the following conclusions can be summarized:

a) Static tests showed that leakage of the chevron seals and piston rings exceeded that of the regenerator system with a Corning core (5.5 percent versus 4.1 percent).

b) Build-up cold static leakage measurement with a rotometer agree well with test cell cold leakage measurements using two orifices with simulated engine air flow.

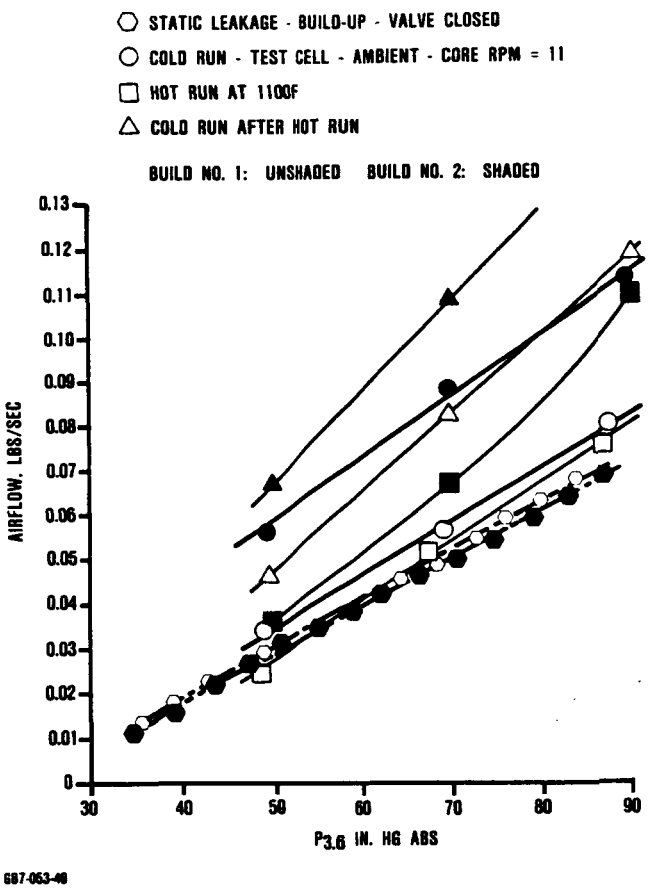

Figure 39. Leakage Comparison Build No. 1 Versus Build No. 2.

c) Leakage can be changed if the rig is thermally cycled, vibrated or impacted, indicating the metal rig is unstable. In the second build, measurements suggest that a large increase in compressor discharge to turbine inlet leakage occurred after the rig left build-up.

d) In the second build the compressor discharge to turbine inlet (P3.0 - P4.1) leak was the same magnitude as the sum of all the other leaks together. This leak is not present in an engine. Suspicions are that this leak was caused by the nozzle piston rings sticking.

e) Regenerator cover temperatures are highest at the hub on the exhaust side and are 200F hotter than the exhaust gas temperature at a 1100F TIT. As a result, regenerator cover deflection is primarily caused by thermal distortion.

f) Venting the regenerator bore through a seal shoe rather than the exhaust cover reduced the cover temperatures and deflections at low compressor discharge pressure levels.

In the testing described above, data showed that compressor discharge ($P_{3.0}$) to turbine inlet ($P_{4.1}$) leakage (which is not present in an engine) was significant. In an effort to reduce this leakage, three additional wave springs were installed behind the turbine nozzle piston rings (Figure 38) during the third build. In addition, the old cracked, leaky NGK core was replaced with a new, unused, low-leakage NGK core. Other than the new core and additional springs, this build was identical to the second build described above.

The valve-closed static leakage of the third build was approximately 15 percent lower than the previous builds, which is attributed to the new, low leakage NGK core or the extra springs behind the nozzle piston rings.

The leakage increase after a hot run was similar in magnitude to that experienced previously. This build showed a 0.035 lb/sec leakage increase (at 80 in.Hg) compared to a 0.025 - 0.080 lb/sec leakage increase after a hot run experienced in the previous two builds.

The overall performance of all three builds are compared in Figure 42. Due to an operational error, the third build data was taken at 950F rather than the conventional 1100F. Based on past experience, increasing temperature from 950 to 1100F would increase deflection by about 10 mils and raise the cover temperature by 50F. It would have little effect on torque and leakage. The third build demonstrated significantly lower cover deflections, temperatures and drive torque compared to the previous builds. As a result, Garrett

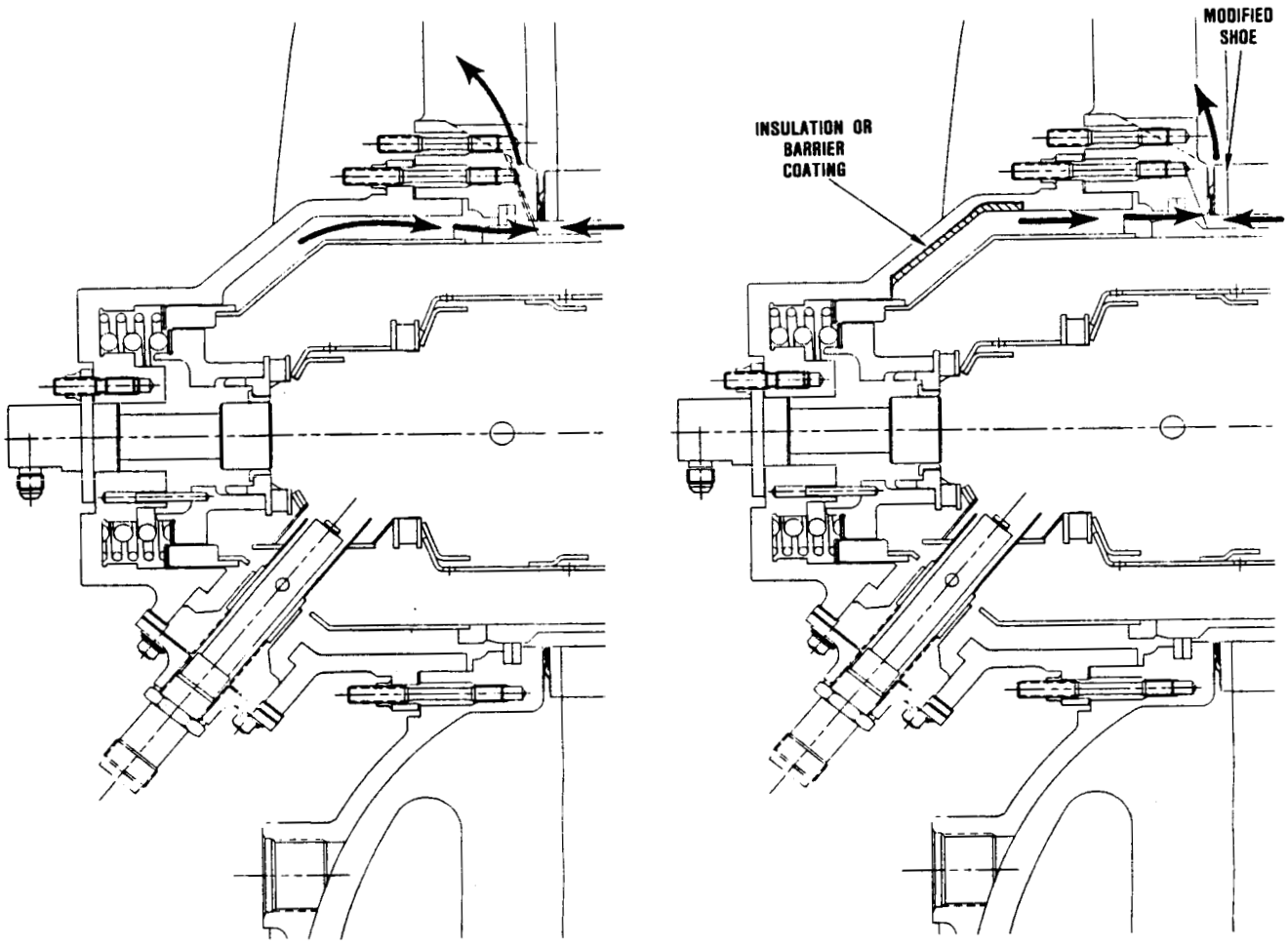

Figure 40. Comparison of Builds No. 1 and 2.

will incorporate these modifications into an engine for evaluation. The reduced leakage of the third build can be attributed to the new low leakage NGK core and/or the additional springs behind the nozzle piston rings. The higher leakage of the second build is attributed to the crack propagation of the old NGK core, which was subsequently retired.

4.4.1.4 Non-Diaphragm Seals

As an alternate approach to cooling the inboard (hot) seal crossarm diaphragm, a study was initiated during the previous report period to eliminate diaphragms from this seal (Figure 43). The core would run against a wear face coating applied directly to the FSH. The key

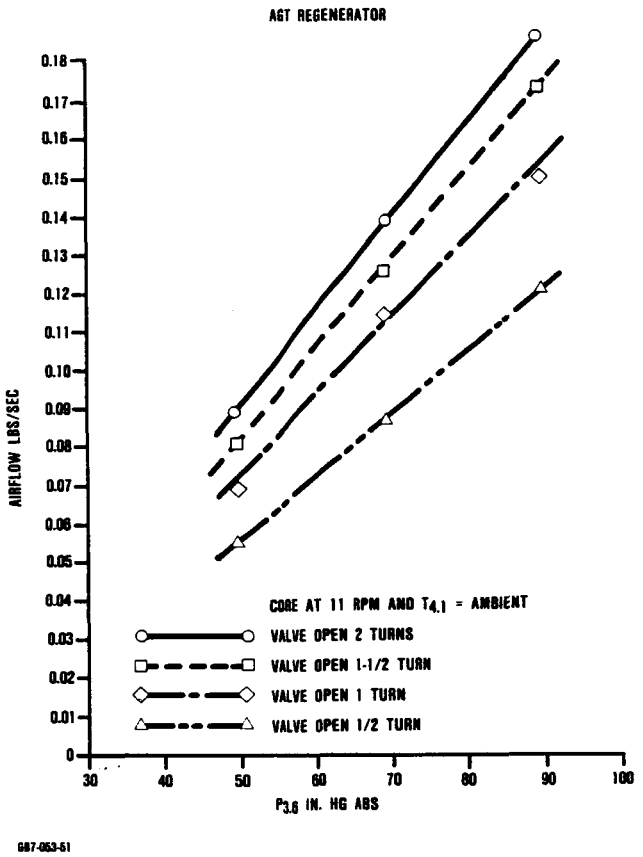

Figure 41. Effect of Valve Position on Leakage.

requirements for a successful non-diaphragm seal are low friction and wear coatings combined with minimum leakage gaps resulting from compatible platform deformations of the core and FSH. The work plan for this study consists of the following:

a) Thermal analysis

   1) Three dimensional finite element analysis of FSH distortion performed at Garrett

   2) Two dimensional finite element analysis of the regenerator matrix distortion performed at Ford

   3) Labyrinth seal leakage analysis for regenerator core - FSH gap performed at Ford

b) Attachment of ceramic coatings to the FSH

c) Evaluate coating wear and friction characteristics in the seal wear rig.

During this report period an analytical model based on labyrinth seal theory was developed to evaluate non-diaphragm seal leakage as a function of regenerator core and FSH distortions. The inboard (hot) seal consists of six leak path components as illustrated in Figure 44. Analytical expressions were developed for both the circular and linear components.

The hot face thermal distortion for the current Corning (AS) and NGK (MAS) materials were previously evaluated for cruise and full power conditions, which correspond to engine speeds of 60 and 100 percent, respectively. The results (Figure 45) indicate the Corning material has acceptable distortion variance (0.0006 inch), whereas the present NGK material variance (0.0030 inch) is unacceptable for a non-diaphragm seal system.

The AGT objective for regenerator system leakage is 3.6 percent maximum at full power (N = 100 percent) engine conditions. Based on static leakage data and analysis the total leakage consists of the following:

- Inboard (hot) seal assembly = 1.9 percent
- Outboard (cold) seal assembly = 1.2 percent
- Regenerator core carry-over loss = 0.25 percent
- Inboard seal diaphragm cooling allowance = 0.25 percent

Therefore a non-diaphragm inboard seal will have a design objective of 2.15 percent (1.9 percent seal +0.25 percent cooling) as a replacement for the present diaphragm seal system.

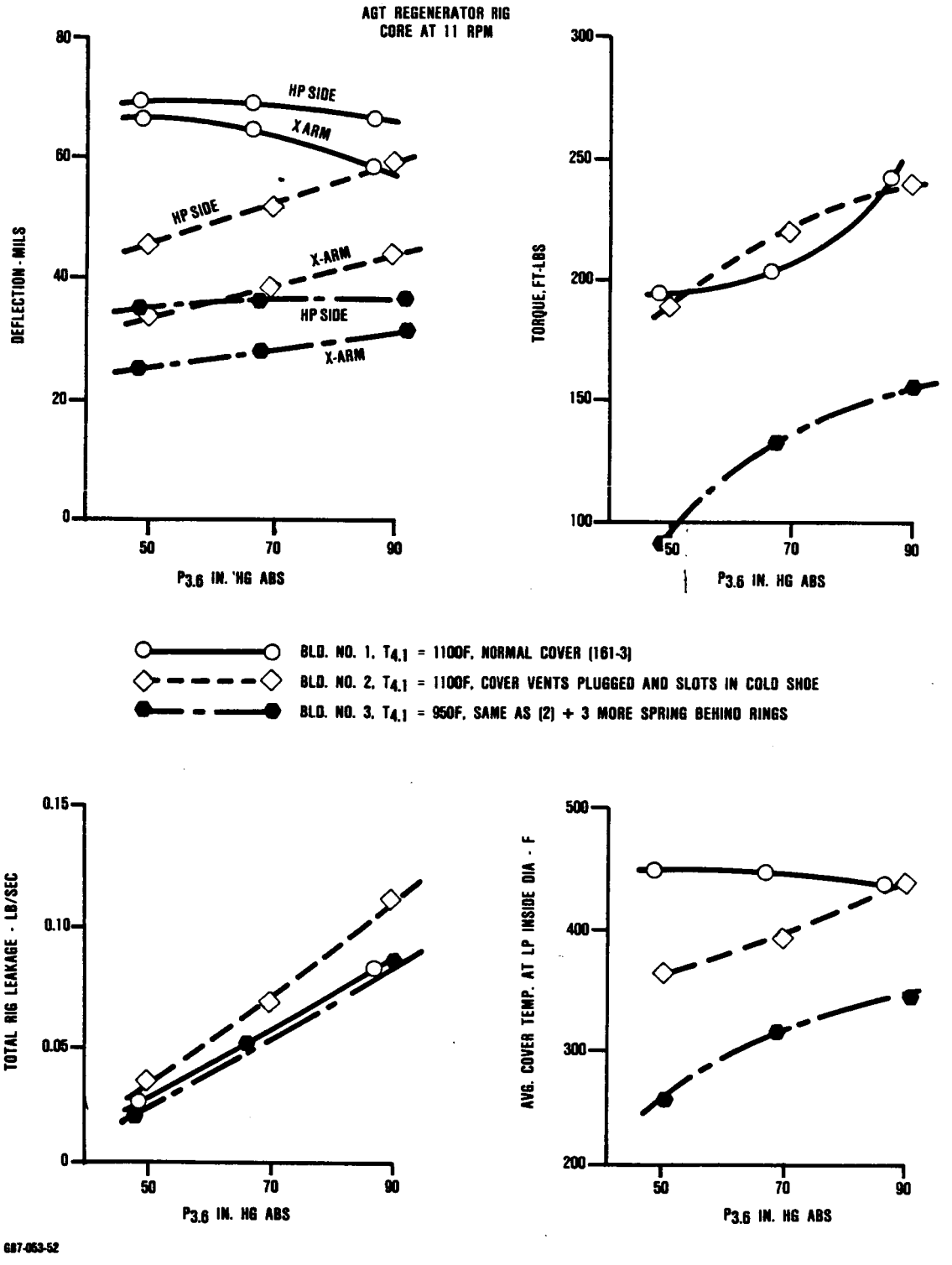

Figure 42. Rig Build Test Data Comparison.

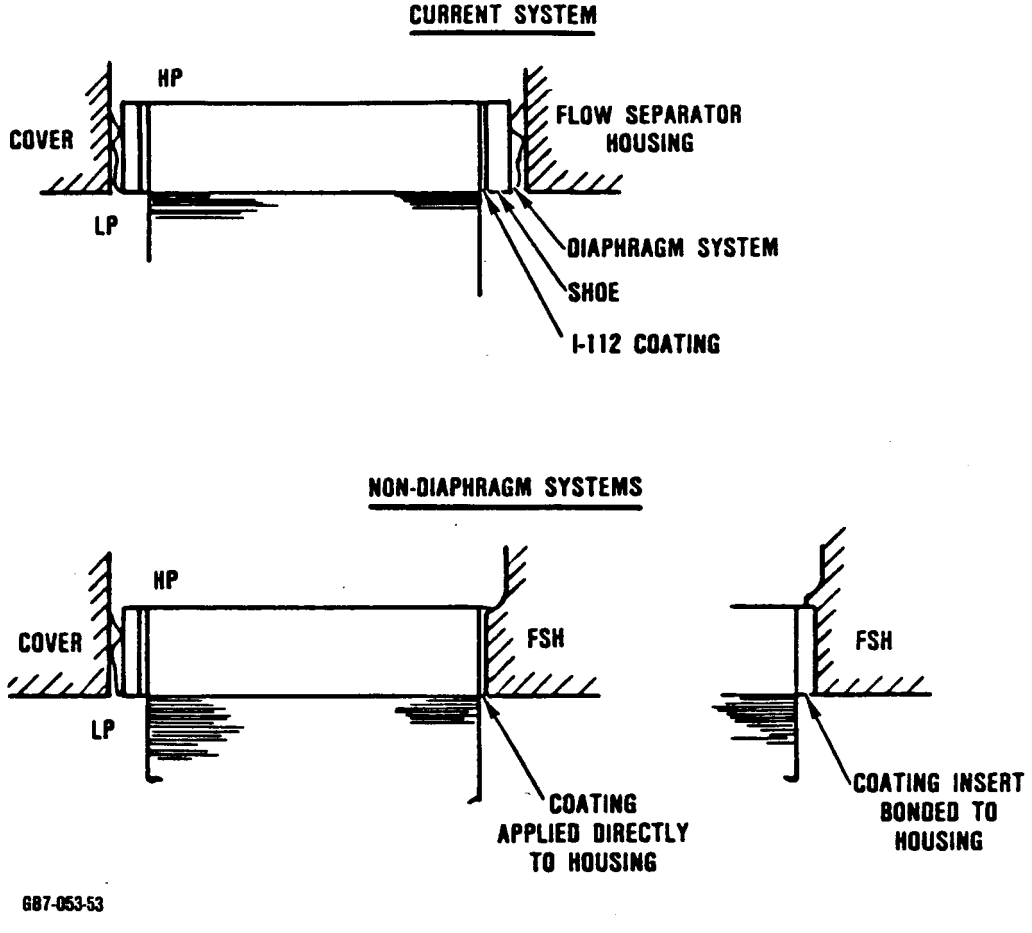

Figure 43. Seal System Comparison.

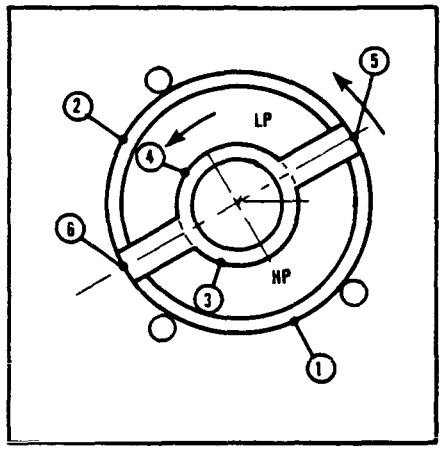

COMPONENT	SEAL LENGTH, IN.
1	26.6
2	26.6
3	10.8
4	10.8
5	4.3
6	4.3

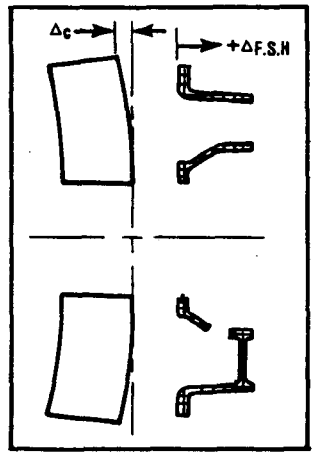

687-053-54

Figure 44. Non-Diaphragm Seal Schematic.

In order to evaluate seal system sensitivity the initial study consisted of evaluating seal component leakage as a function of a uniform gap at cruise (N = 60 percent) and full power (N = 100 percent) engine speed conditions, which are listed on Table 3. The results at cruise (Figure 46) and full power (Figure 47) demonstrate the powerful influence of leakage air temperature. As expected, the leakage for Components 1 and 4 (Figure 44) are minimal since pressure drop at these locations is very small (<1.5 psi). Conversely, the leakage for Component 2 is substantially higher than Components 3, 5, and 6 even though pressure drop is approximately the same. This is directly attributable to the much lower temperature of the compressor discharge air compared to the discharge air through the high pressure side of the regenerator. Component 2 leakage represents approximately 70 percent of the total leakage at both engine conditions (Figures 44 and 45). Leakage through Component 3 is more than the crossarm (Components 5 and 6) due to the following reasons:

- The seal width of the crossarm (1.50 inch) is twice the width (0.75 inch) of the peripheral seals
- For a wrapped process regenerator (Corning) the crossarm will have a geometrical advantage due to a substantially higher number of sealing points (labyrinths).

To further demonstrate the importance of air temperature, the leakage at cruise and full power were estimated based on ambient air as a function of uniform clearance (Figure 48). In this case the leakage with ambient air is approximately twice as high as leakage based on engine temperatures.

The next study consisted of evaluating seal leakage for the FSH distortions predicted by the Garrett 3-dimensional finite-element analysis, which is summarized on Figure 49. For the current Garrett model, one of the boundary conditions assumes axial constraints (Figure 49) at the ring support interface, which results in zero axial distortion of the outer ring of the FSH. Consequently, the distortions predicted are for the inner ring relative to the outer ring. In addition, to simplify the initial analysis, distortion due to temperature and pressure are evaluated separately. Distortion due to temperature was evaluated at engine cruise (N = 60 percent). Conversely, distortion due to pressure (isothermal) was evaluated at full power conditions (N = 100 percent).

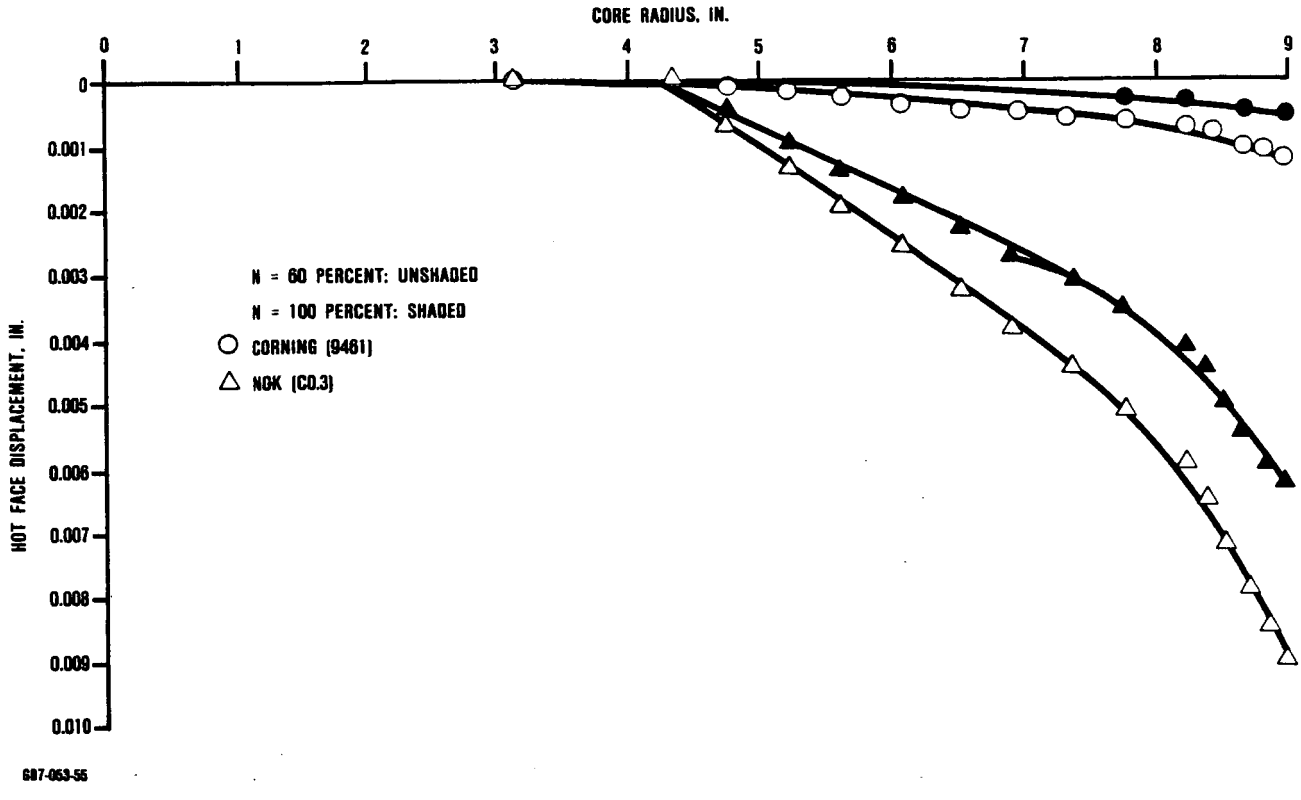

Figure 45. Regenerator Core Axial Distortion.

Table 3. Leakage Air Flow Conditions.

P_O: Leakage Inlet Pressure (psia)
P_N: Leakage Exit Pressure (psia)
T_O: Leakage Inlet Temperature (F)
$\dot{W}$: Engine Air Flow (lb/sec)

Component	P_o	P_n	T_o
N = 60%		$\dot{W}$ = 0.355	
1	29.8	29.6	210
2	29.8	15.2	210
3	29.6	14.7	1945
4	15.2	14.7	2000
5	29.6	15.2	1945
6	29.6	15.2	1945

Component	P_o	P_n	T_o
N = 100%		$\dot{W}$ = 0.832	
1	73.4	73.2	470
2	73.4	16.2	470
3	73.2	14.7	1677
4	16.2	14.7	1677
5	73.2	16.2	1677
6	73.2	16.2	1677

A total of thirteen combinations were evaluated and summarized on Figure 50. The maximum component gap is predicted by the contact point that results from meshing the axial distortion of the core with that of the FSH as illustrated in Figure 50. If the distortion of the core is greater than the FSH, then a gap will exist at the outer ring (Components

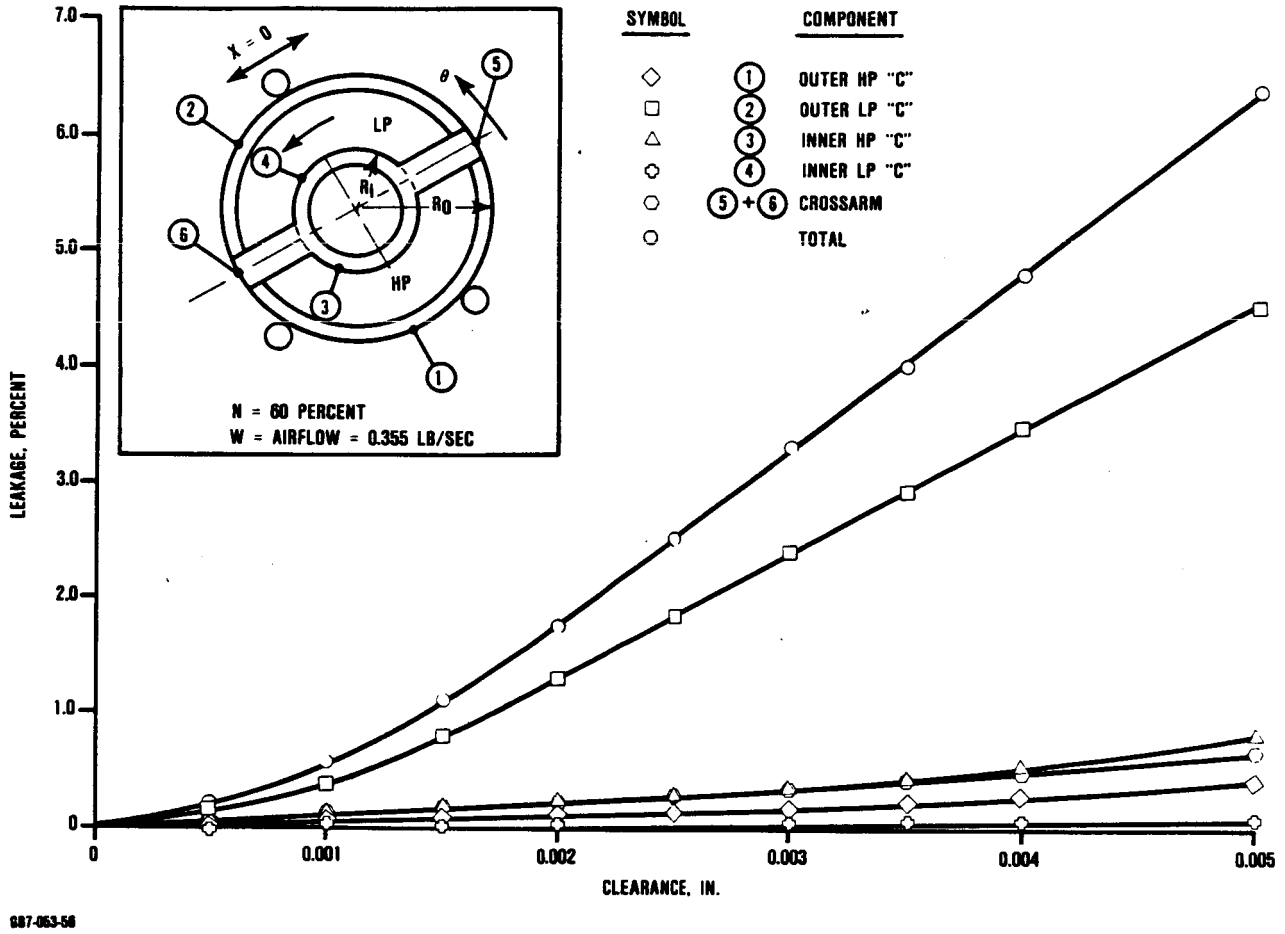

Figure 46. Non-Diaphragm Seal Leakage Versus Uniform Clearance.

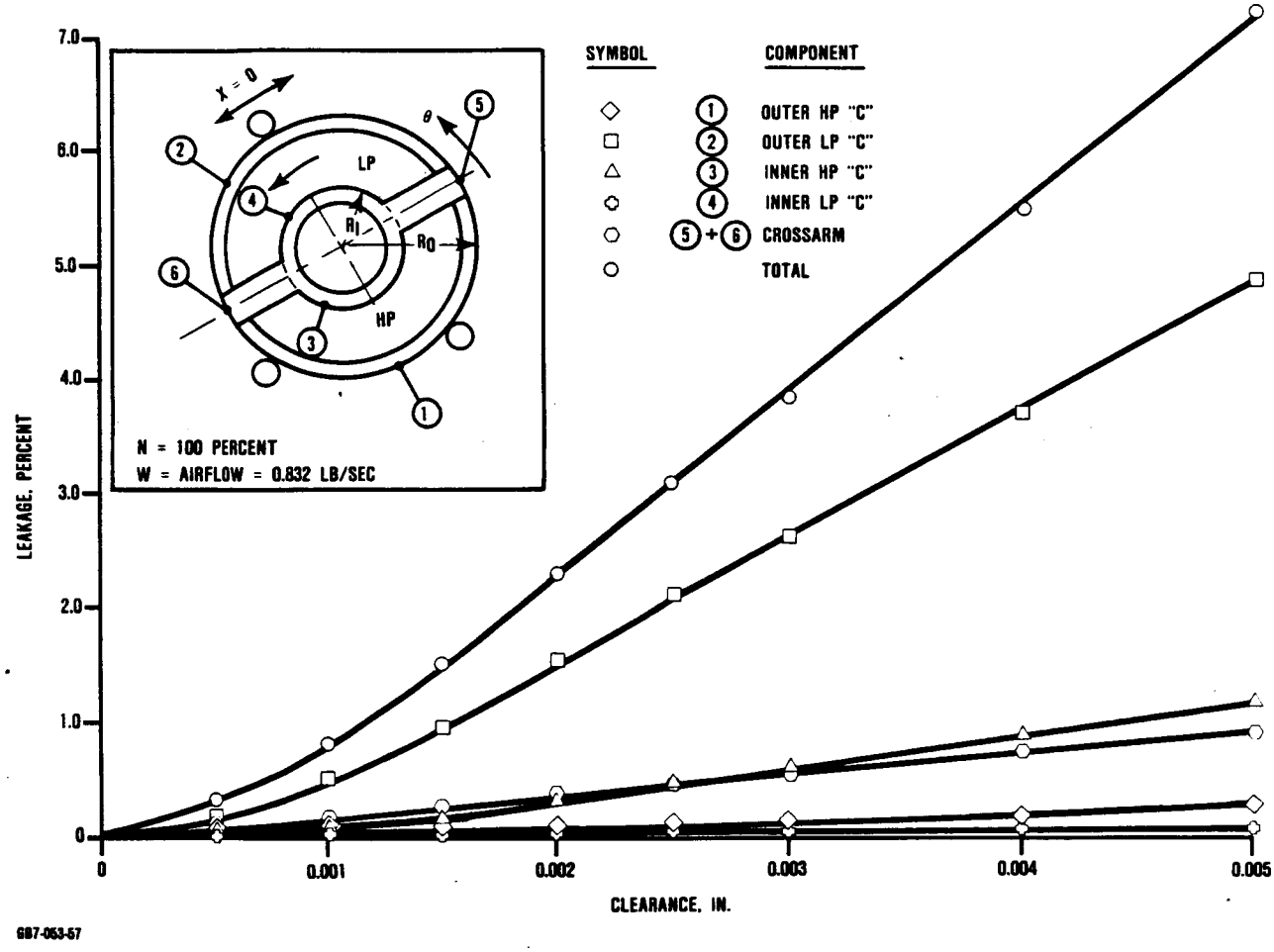

Figure 47. Non-Diaphragm Seal Leakage Versus Uniform Clearance.

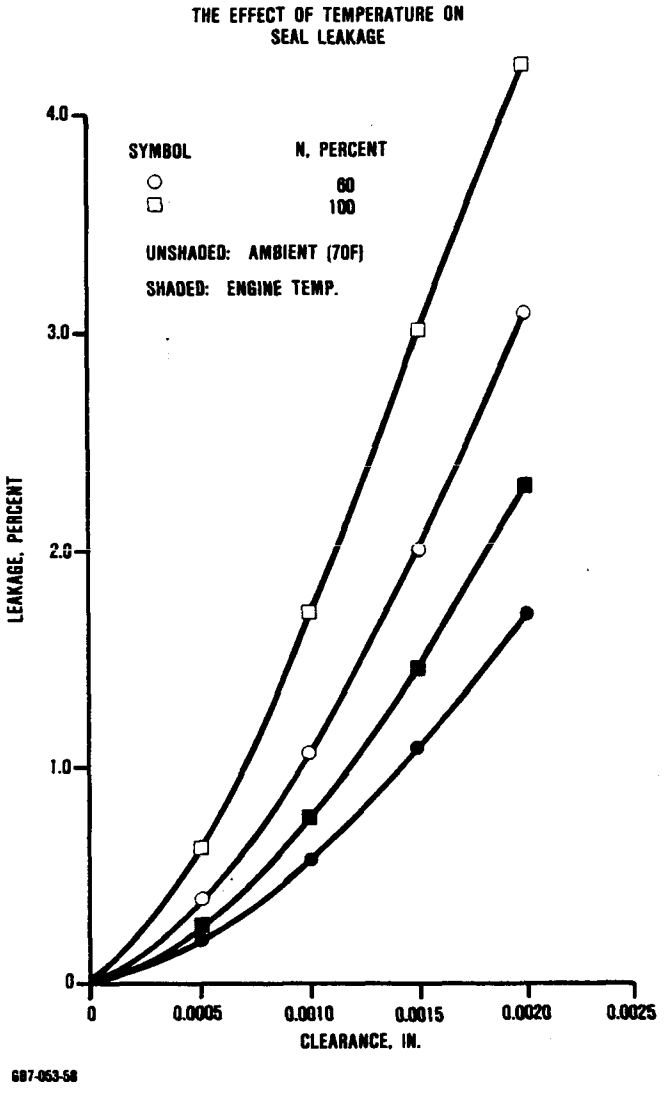

Figure 48. The Effect of Temperature on Seal Leakage.

1versely, when the axial distortion of the core is less than the FSH, then the gap at the outer ring is zero and leakage will be minimized.

For the thermal distortions without pressure at cruise conditions, leakage was calculated for both the current configuration (H = 5.0 Btu hr-ft^{2}F) and the simulation of a metal baffle (H = 1.0 Btu hr-ft^{2}F) around the outer perimeter of the FSH. Initial results indicated that by allowing the mounting flange of an RBSN housing to heat up by baffling the compressor discharge flow around it, the distortion is reduced significantly. In addition, distortion of an RSBN housing due to pressure is reduced significantly with the incorporation of struts.

Based on these preliminary results, the leakage of a non-diaphragm inboard seal system is projected to meet the objectives provided the clearance between the core and FSH at the outer ring is minimized.

To ensure this condition is met, the axial distortion of the core should be less than the axial distortion of the FSH inner ring (Component 3 and 4). In addition, to more accurately predict seal leakage, axial distortion of the FSH due to the combined effects of pressure and temperature must also be determined.

The evaluation of candidate coatings and method of attachment to LAS samples was initiated during the previous report period. Based on furnace exposure and seal wear rig testing, two wear face coatings developed at Ford continue to show promise. These coatings are zinc-oxide based and designated as I-112 and S-77.

A composite coating on a LAS ceramic wear rig substrate consisting of a pre-heat treated coating of Ford ATLAS glass frit, which provides an intermediate bond coating, and I-112 plasma sprayed wear face coating, was subjected to 2000F furnace exposure without failure. The sample accumulated 63 hours at temperatures up to 1800F in the seal wear rig against an LAS core without apparent difficulties. The coefficient of friction varied between 0.16 at 1800F and 0.22 at 1500F with negligible wear. A friction coefficient below 0.3 is considered excellent.

Another LAS sample with S-77 material applied without the Ford ATLAS intermediate bond coating has accumulated 120 hours in the seal wear rig at temperatures up to 1800F. The coefficient of friction varied between 0.15 and 0.20 with negligible wear. Minor chipping and delamination occurred after the 1800F exposure.

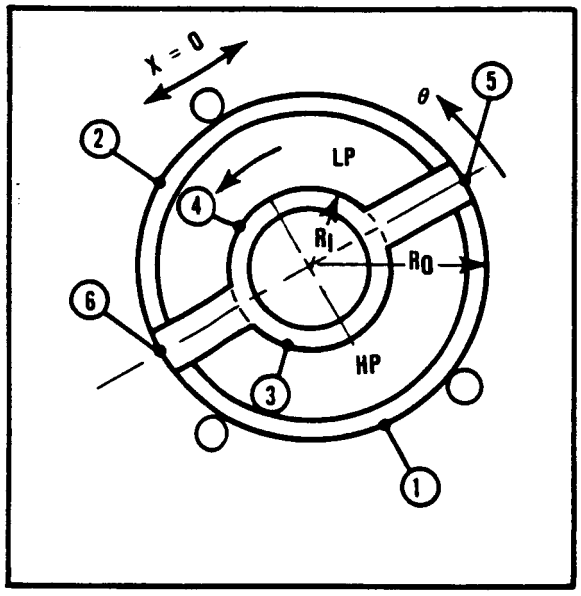

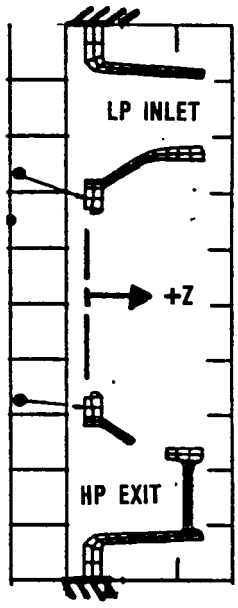

N, %		FSH		STRUTS		H_C (BTU/HR.-FT^{2}F)			COMPONENT DISTORTION MIN/MAX, MILS		
60	100	LAS	RBSN	YES	NO	0	1.1	5.5	3	4	5 & 6
*		*			*		*	*	4.9/5.8	5.8/5.8	0/5.5
									3.3/3.9	3.9/4.0	0/3.7
			*					*	9.5/10.7	9.7/10.5	0/10.0
							*		3.2/3.6	3.4/3.5	0/3.5
				*				*	1.5/3.9	2.6/3.9	0/3.9
	*				*	*			-0.2/-1.8	-1.8/-3.9	0/-1.8
				*					0.2/0.7	0/0.2	0/0.2
		*			*				-1.8/2.7	-1.8/-5.4	0/-1.8
				*					0.6/1.5	-0.2/0.6	0/0.6

GB7-053-59

Figure 49. Flow Separator Housing Axial Distortion.

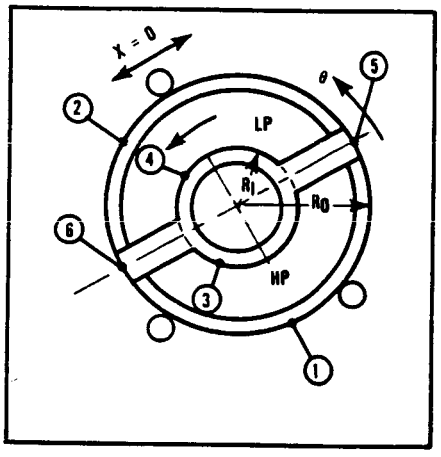

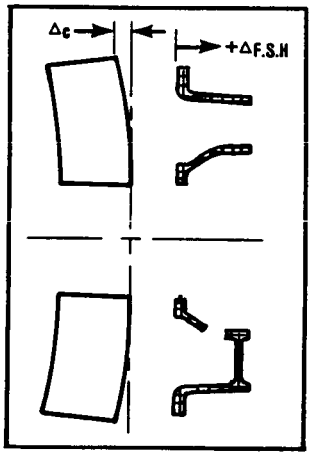

LEAKAGE
OBJECTIVE: 1.25 PERCENT MAX.

	N. %		F.S.H		CORE DISHING, IN		$H_{C.2}$ BTU-FT/HR-F	MAX. COMPONENT GAP, MILS					TOTAL LEAKAGE		COMMENTS
	60	100	LAS	RBSN	CRNG	NGK		1	2	3	4	5/6	LB/MIN	%	
1.	*		NO STRUT		0.0012		1.0	0	0	2.6	2.8	2.0	0.081	0.38	
2.							5.0	0	0	4.5	4.6	3.6	0.188	0.88	
3.						0.009	1.0	5.8	5.8	0.63	0.73	4.7	1.5	7.0	
4.							5.0	4.1	4.1	0.80	0.90	3.5	0.96	4.5	
5.				NO STRUT	0.0012		1.0	0	0	2.3	2.3	1.7	0.067	0.31	
6.							5.0	0	0	9.4	9.1	7.0	0.52	2.4	
7.						0.009	1.0	5.8	5.8	0.33	0.25	4.5	1.48	6.9	
8.							5.0	0	0	1.6	1.3	1.2	0.03	0.14	
9.				WITH STRUT	0.0012		5.0	0	0	2.5	2.4	1.4	0.06	0.28	
10.		*		W/O STRUT	0.0016		0	4.5	4.5	3.5	1.4	3.3	2.84	5.7	
11.				WITH STRUT				0.7	0.7	0.65	0.2	0.5	0.20	0.39	
12.			W/O STRUT					6.0	6.0	0.79	0.31	0.48	4.46	8.9	
13.			WITH STRUT					0.8	0.8	1.6	0.5	0.8	0.32	0.64	

687-053-88

Figure 50. Non-Diaphragm Seal Leakage Analysis.

Since flow separator housings made from silicon nitride are being considered in the AGT program, S-77 coating was sprayed on a silicon nitride substrate. It accumulated 75 hours in the wear rig at temperatures up to 1600F without distress. The coefficient of friction varied between 0.08 and 0.13. The test was terminated when the ceramic sample holder failed while attempting to run the 1800F condition.

A casting mold was fabricated to form reaction bonded silicon-nitride (RBSN) blocks as a replacement sample holder. One of these blocks has been sintered and is currently being machined into a sample holder.

In the interim period, testing was resumed with a metal sample holder, which restricts maximum temperature in the rig to 1500 to 1600F.

The seal wear rig accumulated 20 hours each at 1000, 1200, 1400 and 1600F with the modified metal holder containing a used I-112 coated LAS sample against an NGK MAS core impregnated with DES-1000 coating (chrome-oxide) from Kaman Sciences. It has demonstrated low friction and seal wear except on the trailing edge of the sample, which is attributed to cocking.

The core has been reversed to evaluate a new I-112 coated LAS sample. A 20-hour break-in run at 1000F has been completed.

Next, Ford will coat a thick-flange LAS flow separator housing with the special "non-diaphragm" seal coatings. Ford will thermal cycle the coated housing in a 2000F oven to test the coating integrity, and fabricate a cold seal with a heavy diaphragm to compensate for the diaphragms eliminated from the hot seal.

4.4.2 Regenerator System Development - Garrett

4.4.2.1 Hot Regenerator Leakage Rig

Hot regenerator leakage rig testing with ceramic flowpath components was initiated early in this reporting period. Previous testing of this rig had been done using metal flowpath components which were welded together so as to assure that leakage measured could be attributed to the regenerator system. This was not possible with the ceramic flowpath components, and so an attempt was made during this testing to isolate the leakages by injecting helium at various locations in addition to the HP inlet. By changing the location of the helium injection on the HP side, the difference in helium concentration at the LP discharge would then reflect the leakage between the two injection test points. Figure 51 shows the rig schematic with the helium injection stations.

An initial test attempt was made in July 1985 (Build 1). During rig installation and setup in test cell C-116, the observation was made that no regenerator drive torque was being read in the control room. A failed regenerator drive shaft was found, but disassembly revealed that the real problem was a massive ceramic parts failure; turbine shroud, stators, outer diffuser, and seal rings all were fractured. Some large pieces had badly broken up the core and gouged the hot seal at the crossarm.

Failure is thought to be a result of flow (and consequently pressure) being introduced to the LP side of the rig without any corresponding flow or pressure on the HP side. This condition is known to have existed during test cell setup for verification of flow calibrations. The high pressure on the LP side of the rig would have been sufficient to cause the transition duct to move axially toward the combustor overcoming the spring load. The subsequent equalization of pressures when the ceramic piston ring seals were unloaded then would cause the transition duct to be pushed back by the spring force. The resulting hammering effect is the most likely cause of the extensive damage. This hypothesis is constructed based on the facts that fracture occurred prior to any testing, and that at no time was there a flame in the burner.

The test plan now includes a note of precaution that the LP side of the rig must not be

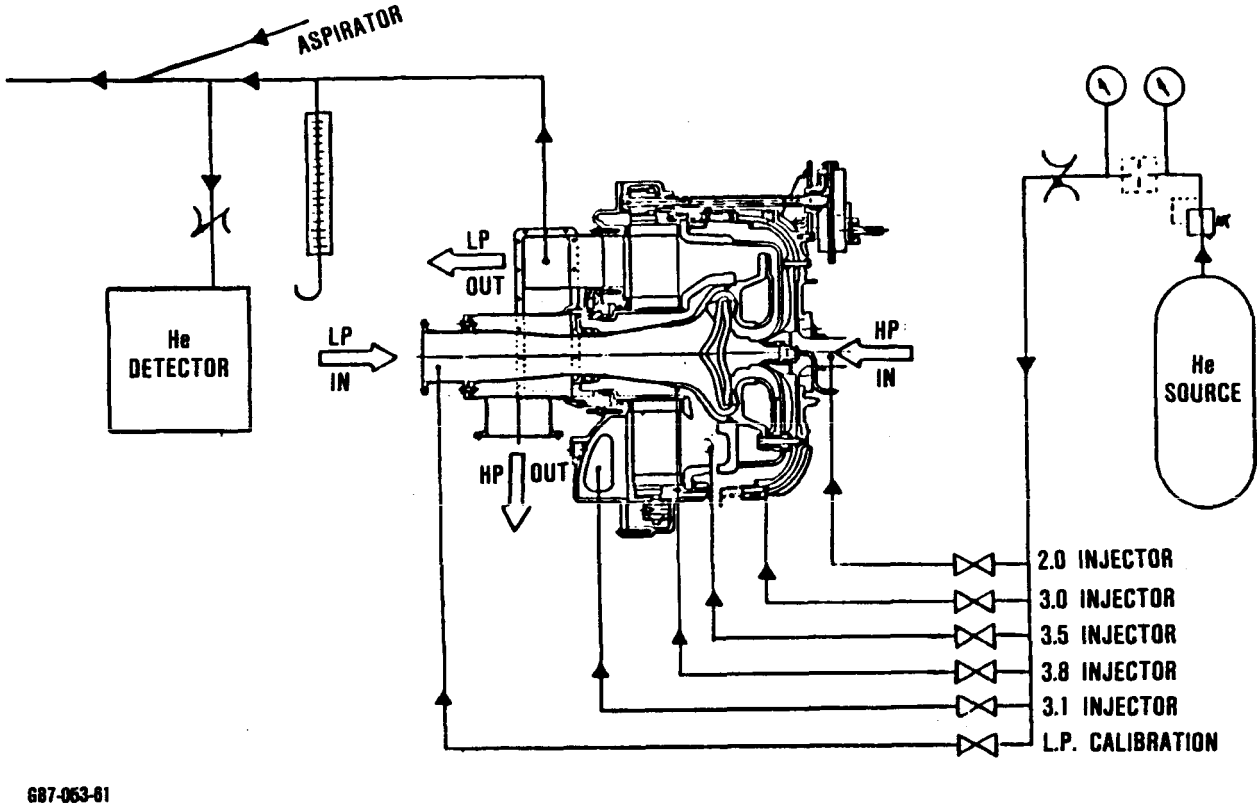

Figure 51. Hot Regenerator Rig Leakage Measurement.

pressurized unless a corresponding pressure is present in the HP side.

In August 1985, a second build was completed using components listed in Table 4 and the rig was again moved to test cell C-116. Although the entire test sequence was not completed as planned, some useful data was collected as given in Table 5.

As the test sequence progressed and pressures were increased, core torque exceeded the capacity of the drive motor, stopping the core and forcing a rig shutdown. Although the proper shutdown sequence was observed, an audible boom indicated a failure of ceramic components. Disassembly confirmed the fracture of several ceramic components, including: flow separator housing, transition duct, baffle, flow separator housing seal ring, and ceramic wave washer.

Fractography clearly indicates that an interference existed between the transition duct and the FSH. The reason for the interference was the use of an interim design transition duct. This duct incorporated bosses to accommodate turbine inlet temperature ($T_{4.1}$) thermocouples; separate grommets were previously used. The interim configuration had inadequate clearance as shown in Figure 52. A flow separator housing with excess stock in the walls also contributed to the interference, as shown in the schematic.

The best hypothesis for the fracture sequence of events is that a sharp change in differential pressure on fuel shutoff caused

Table 4. AGT Ceramic Component Quick Look.

TEST DATE 13 AUG 85

TEST TYPE/PURPOSE MEASURE ENGINE SEAL LEAKAGE AT VARIOUS LOCATIONS USING He LEAK DETECTOR.

CYCLE DESCRIPTION HEAT IN STEPS TO 1700°F, TAKE He LEAK MEASUREMENTS, COOL IN STEPS, S/D

RIG/ENGINE/BUILD HOT REGENERATOR RIG (HRR) BUILD 2 HREG2

CYCLES 1 (TOTAL) HOURS 1.0 (0.8) (TOTAL)

PARTS	PART NUMBER	SOURCE / MAT'L		SERIAL NUMBER	STATUS
INNER DIFFUSER	3609638	NGK	SN50	111	OK
OUTER DIFFUSER	3609637	NGK	SN50	115	OK
OUTER DIFFUSER SPACER	3609639-1	NGK	SN50	108-4	OK
ROCKER (3)	3609659-	KYOCERA	SN220M	119, 120, 121	OK
ECCENTRIC (3)	3609658-2	NORTON/GTEC	NC-132	137, 014, 015	OK
BOLT (3)	3609628	KYOCERA	SN220M	038, 039, 040	OK
CONTACT WASHER UPPER (3)	N.R.				
CONTACT WASHER LOWER (3)	3609625	KYOCERA	SN220M	126, 127, 128	OK
CROWNED WASHER	3609621	KYOCERA	SN220M	133, 134, 135	OK
TRANSITION DUCT	3610613	ACC	RBSN	640	FAIL
BAFFLE	3609614	CBO	SASC	120	FAIL (STRUT)
STATOR	3846162	CBO	SASC	SET 004	OK
SHROUD	3610670	NGK	SN54	124	OK
BACKSHROUD	3610238-	ACC	RBSN	678	OK
FLOW SEPARATOR SEAL RING	3610206	CORNING/GTEC	LAS	571	FAIL
WAVE WASHER PAP25302-1	3609653	ACC	RBSN	261	FAIL (SPLIT)
T SHROUD SEAL RING	3609651	ACC	RBSN	322	OK
FLOW SEPARATOR HOUSING	3609655-1	CORNING	LAS	57	FAIL
REGENERATOR SHIELD	3846154-1	CBO	SASC	104	OK
REGENERATOR SHIELD SEAL RING	3609650-1	PURE CARBON	RSS:C	105, 106	OK
INSULATION	PAP	ZIRCAR	ZAL-45	Z452	OK
TRANSITION DUCT BUSHING (3)	N.R.				
$T_{4.1}$ TC INNER SEAL (FEMALE) (3)	N.R.				
$T_{4.1}$ TC INNER SEAL (MALE) (3)	3609630	DURAMICS	ALUMINA	101 102 103	OK
$T_{4.1}$ TC INNER SEAL SPACER (3)	3609633	NORTON	NC-132	207 208 209	209 CHIPPED, OK TO H.F.
$T_{4.1}$ TC INNER LOAD SPACER (3)	3609629	NORTON	NC-132	207 208 209	OK
$T_{4.1}$ TC OUTER SEAL (FEMALE) (3) $+T_{5.1}$	3609620	NORTON	NC-132	213, 208, 209, 210	OK
$T_{4.1}$ TC OUTER SEAL (MALE) (3) $+T_{5.1}$	3609610	NORTON	NC-132	207, 208, 209, 260	OK

REGENERATOR CORE 44-08 CORNING

ROTOR

COMMENTS TEST ABORTED DUE TO CORE STOPPAGE. CERAMIC FRACTURE AT SHUTDOWN

ENTERED INTO COMPACT BY SCOTT WATSON DATE 15 AUG 85

TEST ENGINEER BOB MOREY DATE 15 AUG 85

687-053-00

Table 5. Hot Regenerator Leakage Rig Test Data.

P_{HP}, psig	P_{LP}, psig	$T_{5.1}$, F	Rig Station	Leakage, cm^3/sec	Leakage, percent	W_{leak}, lb/min
17	12	250-300	BG	2.6×10^{-8}	--	--
			LP	5×10^{-6}	--	--
			2.0	6.4×10^{-7}	12.3	2.47
			3.0	2.7×10^{-7}	4.9	0.98
			3.1	3.6×10^{-7}	6.7	1.34
			3.8	3.1×10^{-8}	0.1	0.02
17	12	1700	BG	1.2×10^{-7}	--	--
			LP	4.85×10^{-7}	--	--
			2.0	5.2×10^{-7}	8.5	1.70
			3.0	2.55×10^{-7}	2.9	0.57
			3.1	1.5×10^{-7}	0.64	0.13
			3.8	3.1×10^{-7}	--	--
27	12	1700	BG	1.15×10^{-7}	--	--
			LP	5×10^{-6}	--	--
			2.0	9.6×10^{-7}	17.3	3.46
			3.0	3.1×10^{-7}	4.0	0.80
			3.1	2.15×10^{-7}	2.05	0.41
			3.8	1.28×10^{-7}	0.27	0.053

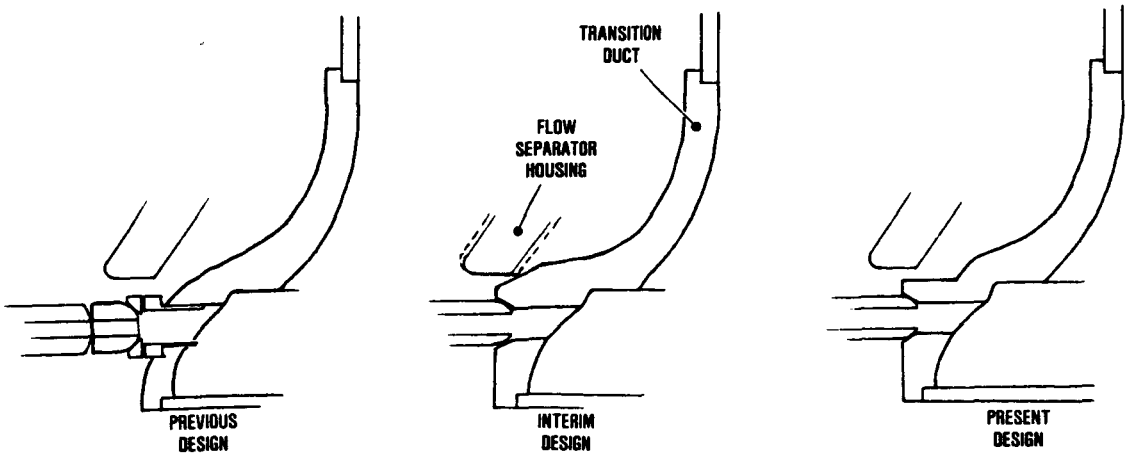

687-063-02

Figure 52. Source of Interference was Interim Design.

relative motion at the interference contact zone, resulting in the initiation of fracture. In the future, a "clay check" will be made to assure adequate clearance between the transition duct and the FSH at this potential contact point.

Other changes anticipated in the future include substitution of a single-hole transition duct, along with introduction of helium seeding at the 3.5 rig station through two specially-made $T_{3.5}$ probes.

In October 1985, the third build of the hot regenerator leakage rig was completed and the rig tested in test cell C-116. For this test, helium concentration was measured not only at the LP discharge, but at the HP discharge as well. Components tested are listed in Table 6.

Leakage data was taken at an airflow of 20 lb/min (on both the LP and the HP sides) and at a temperature of approximately 250F on both sides ("cold" condition). The pressure differential from HP to LP was 9 psid for this condition.

Following this, the LP air temperature was increased to 1600F. Difficulty was encountered in achieving a flow balance on both sides of the rig, which was thought to be due to very high leakages. Pressure differential from HP to LP was 7 psid during this phase of the testing.

The next test point required a higher differential pressure. However, the LP pressure tended to follow the HP pressure upward, thereby making it difficult to achieve proper test conditions. As the pressure in the HP side was increased above 30 psig, and the LP flow was being adjusted to achieve similar flows, the burner in the LP inlet blew out. A sharp reduction in the LP temperature was observed, followed by a reduction in the pressures on both sides of the rig. A significant acoustic event had occurred, and the rig was shut down.

Teardown revealed fractures of the baffle, backshroud, turbine shroud, stators, and seal rings and damage to the regenerator core and seals.

Fractography indicates a fracture origin on a baffle strut at the 10 o'clock position. The blowout of the the combustor was judged to have created a sharp pressure fluctuation in the LP side of the rig, and that this pressure fluctuation caused the transition duct to separate from the baffle strut, only to crash against it once again as the pressure dropped after the burner was out.

No firm conclusions were drawn from these tests due to the contradictory nature of the data obtained. A review of the data in Table 5, for example, shows that, at a HP side pressure of 17 psig and a $T_{5.1}$ of 1700F, more helium leaks across when injected at the 3.8 station than when injected at the 3.1 station. This typifies the inconsistencies in the data collected.

Some consideration was given to improving the mixing of the helium with the air as it is injected into the HP flow path, and to an improved probe arrangement for sniffing helium in the discharge ducts. Since Ford was set up to do similar work in their own hot regenerator rig, pursuing leakage testing in this rig by the helium injection method involved more effort and expense than the anticipated results could justify.

Hot regenerator leakage testing with ceramic structures would be more effectively conducted in the Ford rig. Their rig employs a single flowpath with an intermediate combustor orifice section. Ceramic flowpath components were sent to Ford and a Garrett representative spent a week at Ford's facility in Dearborn familiarizing Ford personnel with the build procedure and cautionary measures to be observed for the ceramic configuration. This testing will be continued at Ford's facilities in the next report period.

4.4.2.2 Regenerator Drive Bushing Materials Testing

A contributing factor to the failure of engine S/N 004C Build 4 was the rapid wear of the regenerator fixed roller bushing. This bushing, incorporating Pure Carbon 3310 graphite, was run in the subject engine using a

Table 6. AGT Ceramic Component Quick Look.

TEST DATE 25 OCT 85

TEST TYPE/PURPOSE MEASURE ENGINE SEAL LEAKAGE AT VARIOUS LOCATIONS USING HE. LEAK DETECTOR

CYCLE DESCRIPTION HEAT IN STEPS TO 1700°F, TAKE He LEAK DATA, COOL IN STEPS, S/D

RIG/ENGINE/BUILD HOT RECON. RIG BLD. 3 (H REC 3)

CYCLES 1 (TOTAL) HOURS 2.6 (2.1) (TOTAL)

PARTS	PART NUMBER	SOURCE		SERIAL NUMBER	STATUS
INNER DIFFUSER	PA3609638-1	NGK	SN50	111	OK
OUTER DIFFUSER	PA3609637-1	NGK	SN50	115	OK
OUTER DIFFUSER SPACER	PA3609679-1	NGK	SN50	108-4	OK
ROCKER (3)	PA3609659-5	NORTON	NC-132	112 113 114	OK OK OK
ECCENTRIC (3)	PA3609658-2	NORTON	NC-132	ON. 015. 137	CHIPPED, OK, OK
BOLT (3)	PA3609628-	KYOCERA	SN 220M	034. 035, 036	OK OK OK
CONTACT WASHER UPPER (3)	PA3609626-	NGK	SN 50	135. 136. 137	OK OK OK
CONTACT WASHER LOWER (3)	PA3609625-	KYOCERA	SN220M	123. 124. 125	OK OK OK
CROWNED WASHER	PA3609621-2	KYOCERA	SN220M	130. 131. 132	OK OK OK
TRANSITION DUCT	PA3609649	NGK	SN50	102	OK
BAFFLE	PA3609614	CBO	SASC	125	FAIL
STATOR	3B46162	CBO	SASC	SET 004	FAIL
SHROUD	PA3610670-1	ACC	RBSN	713	FAIL
BACKSHROUD	3B46148		SASC	107A	FAIL
FLOW SEPARATOR SEAL RING	PA3610206	CORNING	LAS	561	FAIL
WAVE WASHER PAP25202-1	PA3609653	ACC	RBSN	646	FAIL
T SHROUD SEAL RING	PA3609651	ACC	RBSN	360	OK
FLOW SEPARATOR HOUSING	PA3609655-1	CORNING	LAS	56	CHIPPED, OK
REGENERATOR SHIELD	3B46154-1	CBO	SASC	104	OK
REGENERATOR SHIELD SEAL RING	PA3609650-1	PURECARBON	RSSiC	105, 106	OK
INSULATION	PA3611436	ZIRCAR	ZAL-45	Z452	WORN, OK
TRANSITION DUCT BUSHING (3)	PA3609632-2	NGK	SN50	102	OK
$T_{4.1}$ TC INNER SEAL (FEMALE) (3)				?	OK
$T_{4.1}$ TC INNER SEAL (MALE) (3)	PA3609630-1	DURAMICS	ALUMINA	101	OK
$T_{4.1}$ TC INNER SEAL SPACER (3)	PA3609631-5	NORTON	NC-132	207	OK
$T_{4.1}$ TC INNER LOAD SPACER (3)	PA3609629-2	NORTON	NC-132	207	OK
$T_{4.1}$ TC OUTER SEAL (FEMALE) (3)	PA3609620-2	NORTON	NC-132	203, 210	OK
$T_{4.1}$ TC OUTER SEAL (MALE) (3)	PA3609610-2	NORTON	NC-132	207, 260	OK

REGENERATOR CORE FM44-005 HOT SEAL HX-027 COLD SEAL CX-039

ROTOR N/A

COMMENTS TEST ABORTED DUE TO AE EVENTS, LOSS OF T_4 & PRES.

☑ ENTERED INTO COMPACT BY SCOTT WATSON DATE 11/5/85

TEST ENGINEER BOB MOREY DATE 10/31/85

GB7-053-100

silicon carbide shaft. As a consequence of that test, a test matrix was devised to evaluate this and alternate shaft and bushing material combinations.

Test objectives were as follows:

- Evaluate shaft and bushing materials shown in Table 7 for wear characteristics

Table 7. Pin and Bushing Materials Wear Test Matrix.

↓ Pin / Bushing →	POCO ACF 10QE2	Pure Carbon 3310
SiC	X	X
Hard Chrome	X	X
Si_3N_4	X	X

- Make components from the best combination of materials tested available for engine use

Test matrix was as follows:

- Using the dynamic materials test rig shown in Figure 53, load and speed will be set to achieve a PV value of 15,000 to represent worst case load for the AGT fixed regenerator roller
- Rig temperature will be set to achieve 500F at the test specimen interface to represent the worst case temperature for the AGT fixed roller
- Operate rig for 50 hours at the preceding conditions, then disassemble and measure the wear of the shaft and bushing material samples.

Figure 54 shows published data for 347 stainless versus 3310 carbon. This will be used for comparison purposes. Table 8 shows the

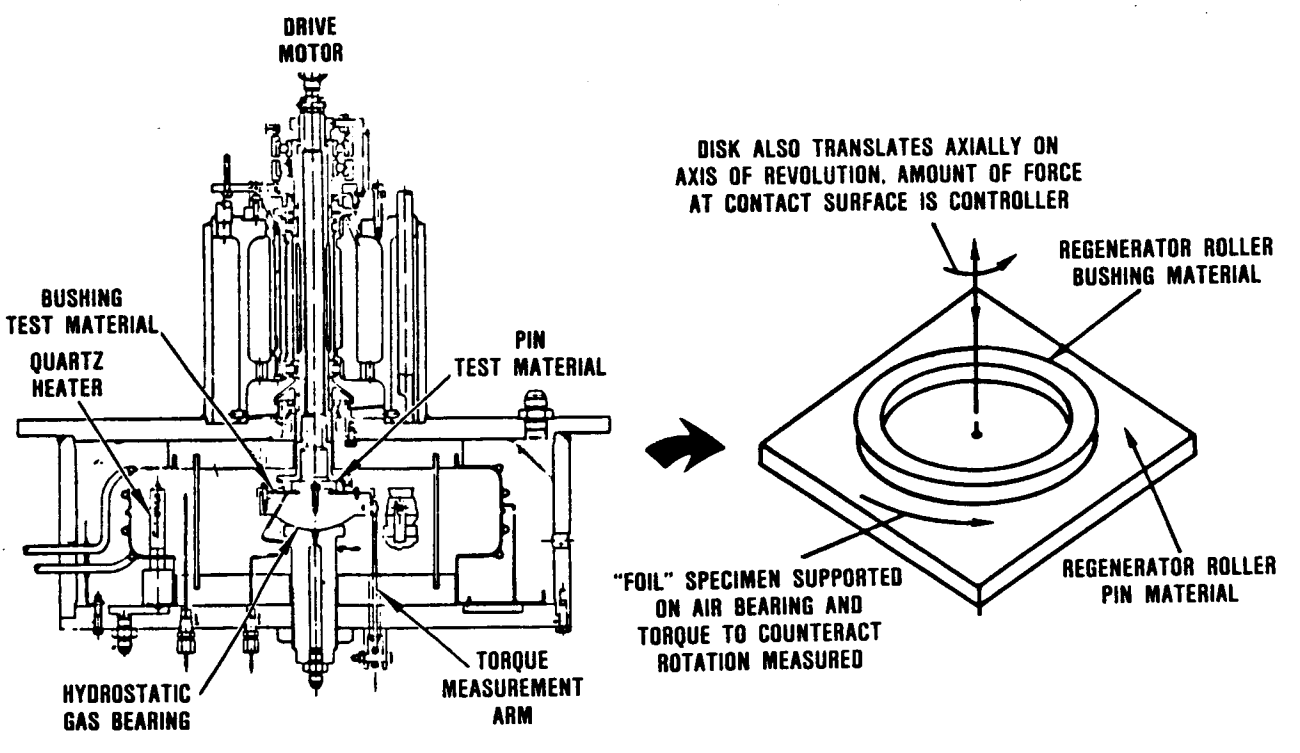

Figure 53. Dynamic Materials Test Rig Diagram at Right Shows Method of Operation. This Rig is Capable of Continuous Operation at 1200F.

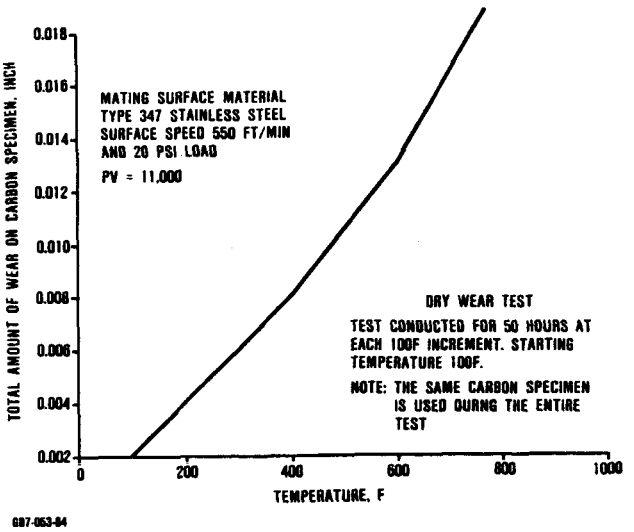

Figure 54. Wear Properties of Pure Carbon Grade 3310.

Table 8. Pin and Bushing Materials Wear.

Test Results		
Bushing → / ↓ Pin	POCO ACF 10QE2	Pure Carbon 3310
SiC	X	0.028 inch
Hard Chrome	In process	0.007 inch
Si_3N_4	0.024 inch	0.034 inch

results obtained to date. Note that results reflect wear of the bushing material and in all cases the shaft material wear has been negligible. Test completion is anticipated later in 1986.

4.5 Ceramics Development Activities

4.5.1 Ceramic Materials Evaluations

Fast and slow four-point flexural strength properties were measured on many AGT101 sintered silicon nitride (SSN) materials. The strength measurements were measured on longitudinally machined specimens with dimensions of 0.125 x 0.250 x 2.0 inch. The four-point flexure fixtures have an outer span dimension of 1.50 inch and an inner span of 0.75 inch. The fast fracture tests were conducted on an Instron test machine at a crosshead speed of 0.02 inch/minute.

4.5.1.1 Flexure Strength

The four-point flexure strength was measured on six sintered silicon nitride materials. These materials are considered to be candidate turbine rotor materials. The strength was measured at room temperature as well as at several elevated temperatures. The temperature where the strength begins to rapidly decrease has been identified for each material evaluated.

NGK SN-73

Four-point flexure testing was performed on the NGK SN-73 SSN material. Specimens of injection molded SN-73 and specimens of injection molded SN-73 bonded to dry pressed SN-73 also were tested for comparison. The location of the bond was in the center of the specimen, therefore the bond was subjected to the maximum tensile stress. The room temperature flexure strength measured on injection molded SN-73 was 116.7 ksi. The flexure strength remains above 100 ksi up to 1400F but drops to below 60 ksi above 1800F and continues to fall of as the temperature increased (Figure 55).

The flexure strength measured on the bonded SN-73 specimens was slightly lower than that measured on the injection molded specimens. Fractography was performed on the fractured bonded specimens to determine the origin location. None of the bonded specimens fractured at the bond.

NGK SN-81

Specimens fabricated from NGK SN-81 SSN by injection molding and by bonding injection molded material to dry pressed material were tested. The bonded specimens were tested so the bond joint would be in the area

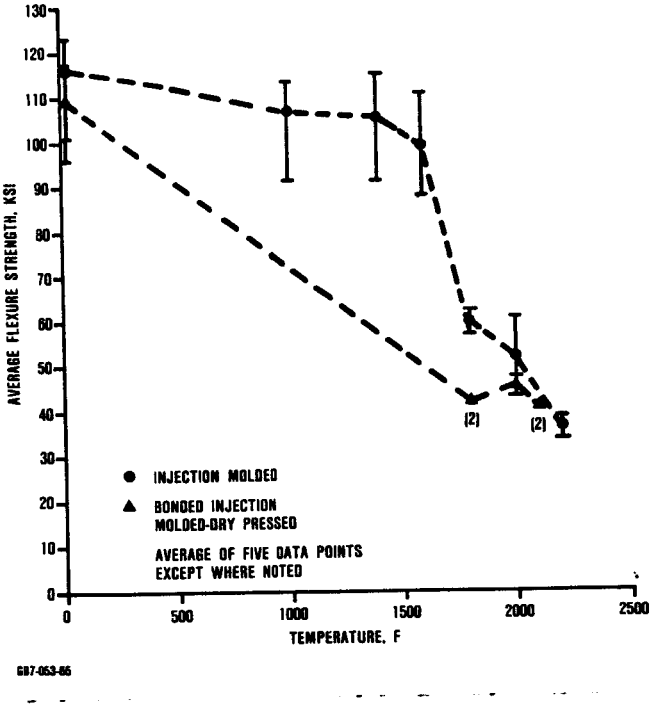

Figure 55. Four-Point Flexure Strength of NGK SN-73.

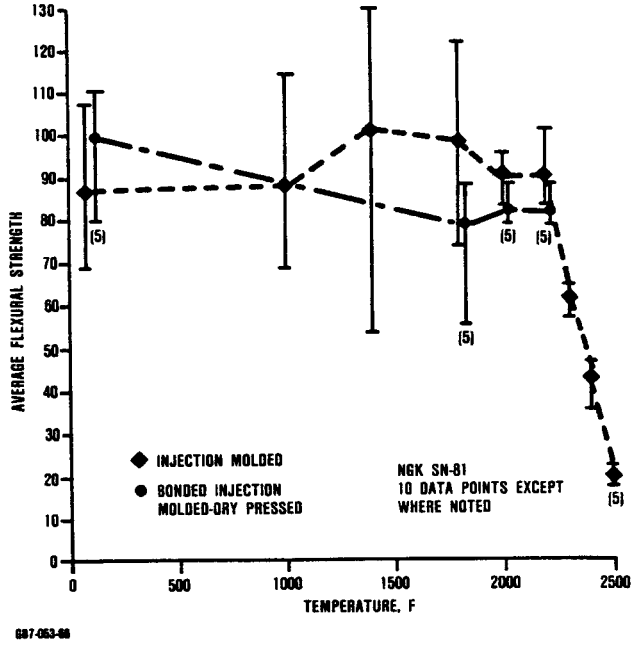

Figure 56. Four-Point Flexure Strength of Injection Molded NGK SN-81.

of highest stress. Both SN-81 materials showed very good elevated temperature flexure strength (greater than 80 ksi at 2200F). Flexure strength test results are shown in Figure 56. Fractography was performed on the bonded specimens. None of the specimens fractured at the bond.

NGK SN-82

Specimens of NGK SN-82 SSN were tested in four-point flexure. Ten specimens were tested at room temperature, 1000, 1400, 1800, 2000, 2200, 2300, 2400, and 2500F. The average four-point flexure strength of SN-82 as a function of test temperature is shown in Figure 57. The flexure strength remains high in the range of 70-100 ksi from room temperature to 2200F. Above 2300F the strength rapidly decreases with increasing temperature.

Kyocera SN 220M

The four-point flexure strength of Kyocera SN 220M SSN plotted as a function of temperature in Figure 58. The flexure strength of SN

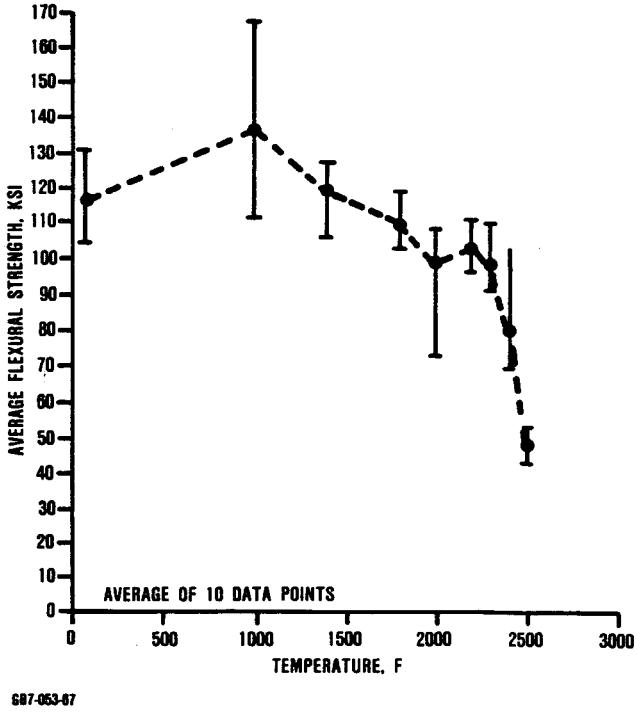

Figure 57. Average Four-Point Flexure Strength of NGK SN-82 Sintered Silicon Nitride.

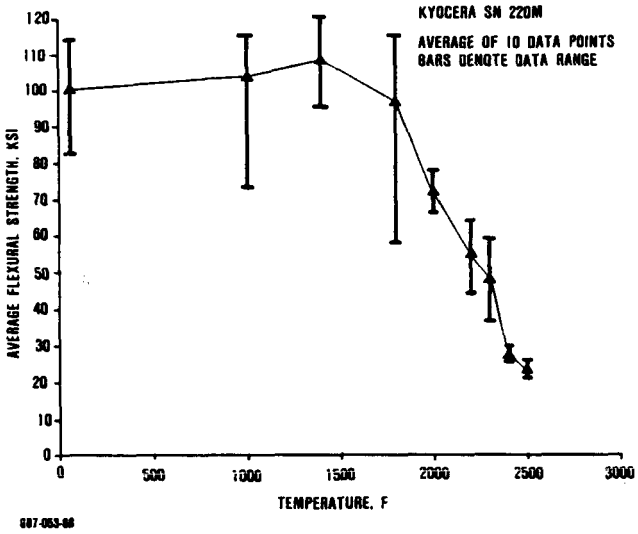

Figure 58. Four-Point Flexure Strength of Kyocera SN-220M Sintered Silicon Nitride.

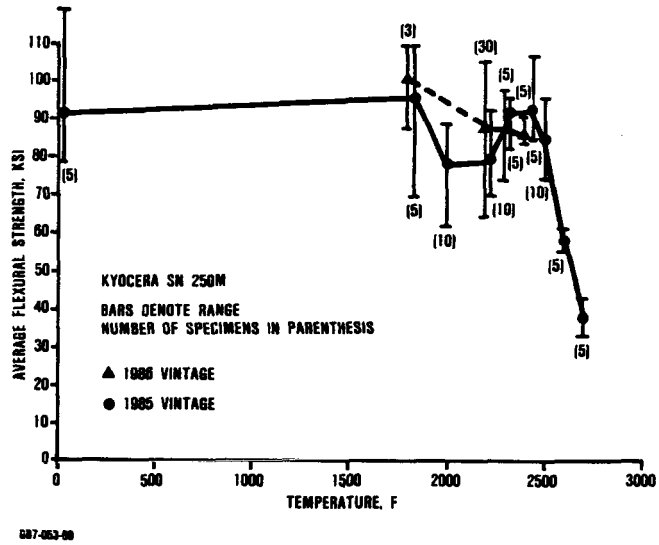

Figure 59. Four-Point Flexure Strength of Kyocera SN-250M Sintered Silicon Nitride.

220M remains above 95 ksi to 1800F; above 1800F the strength rapidly degrades with increasing temperature.

Kyocera SN 250M

The baseline four-point flexure strength of Kyocera SN 250M SSN is shown as a function of test temperature in Figure 59. Specimens fabricated in both 1985 and 1986 were evaluated. Kyocera SN 250M has excellent high temperature strength to 2500F. Above 2500F, the flexure strength rapidly decreases with increasing temperature.

Kyocera SN 270M

The flexural strength of Kyocera SN 270M is plotted as a function of temperature in Figure 60. SN 270M retains its high (>90 ksi) flexure strength to 2000F. The strength begins to slowly decrease with increasing temperature above 2000F. The flexure strength is still relatively high (>70 ksi) at 2500F.

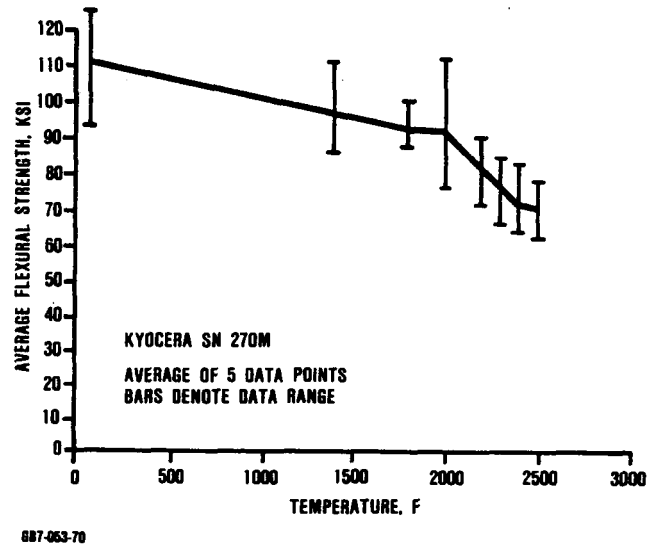

Figure 60. Four-Point Flexure Strength of Kyocera SN-270M Sintered Silicon Nitride.

4.5.1.2 Stress Rupture

Four-point flexural stress rupture testing was conducted on Kyocera's SN 220M, SN 250M, and SN 270M and NGK's SN-81 and SN-82 materials. Test temperatures and stress levels were chosen to measure stress rupture lives varying from several minutes to 150 hours. The test temperatures were chosen based on the fast fracture temperature capability of the materials. Typically, three tests

were conducted for each temperature and stress level.

The stress rupture data for the five materials is shown in Figures 61 through 65. Data points with arrows pointing to the right indicate the test was terminated before the specimen failed. The dotted line represents a very conservative projection of the stress rupture life at the temperatures indicated.

The five silicon nitride materials can be ranked for stress rupture life by choosing a temperature and stress and determining the time to failure. Tables 9 and 10 list the times to failure of a flexural test specimen under a 30 and 50 ksi load at temperatures of 2000, 2200, 2300, 2400, and 2500F. The stress rupture lives rank from low to high in the following order, Kyocera SN 220M, NGK SN-81, NGK SN-82, Kyocera SN 250M, and Kyocera SN 270M. This stress rupture data can be used to choose engine temperatures and operating cycles appropriate for each rotor material.

4.5.2 AGT101 Ceramic Component Screening and Proof Testing

4.5.2.1 Turbine Shroud and Stator Thermal Screen Tests

A total of ten screening tests were accomplished during this reporting period. The parts tested and the results obtained are given in Table 11. The thermal screening cycles employed are shown in Figure 66 and 67. Note that the thermal transient for screening stators is significantly different from that used for screening turbine shrouds.

Three screening tests were accomplished during the month of September 1985. In a previous attempt (May 1985) to screen stators in conjunction with an RBSN turbine shroud, the shroud fractured after the rig had been shut down, during what should be a cooldown mode. Insufficient data exists regarding the differences in heat transfer in the engine and the rig conditions to fully explain the RBSN shroud fracture. However, previous success in

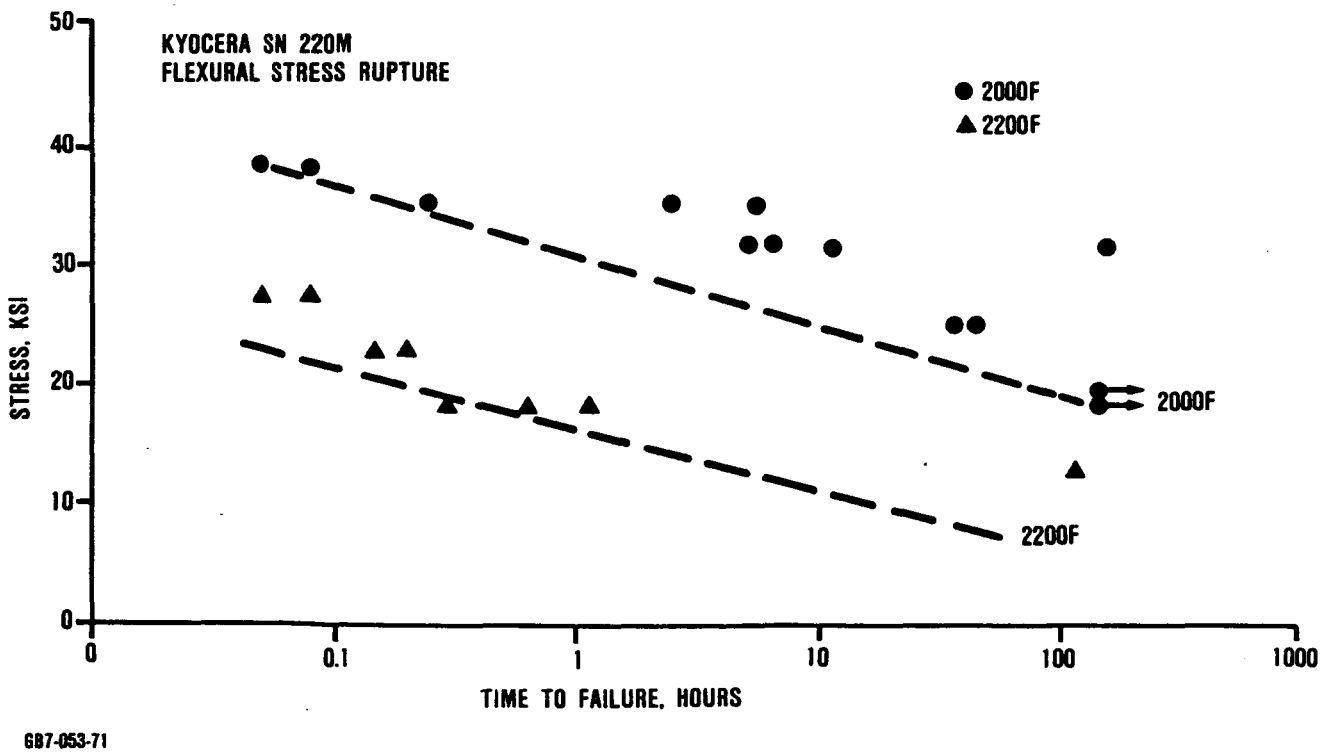

Figure 61. Kyocera SN-220M, Flexural Stress Rupture.

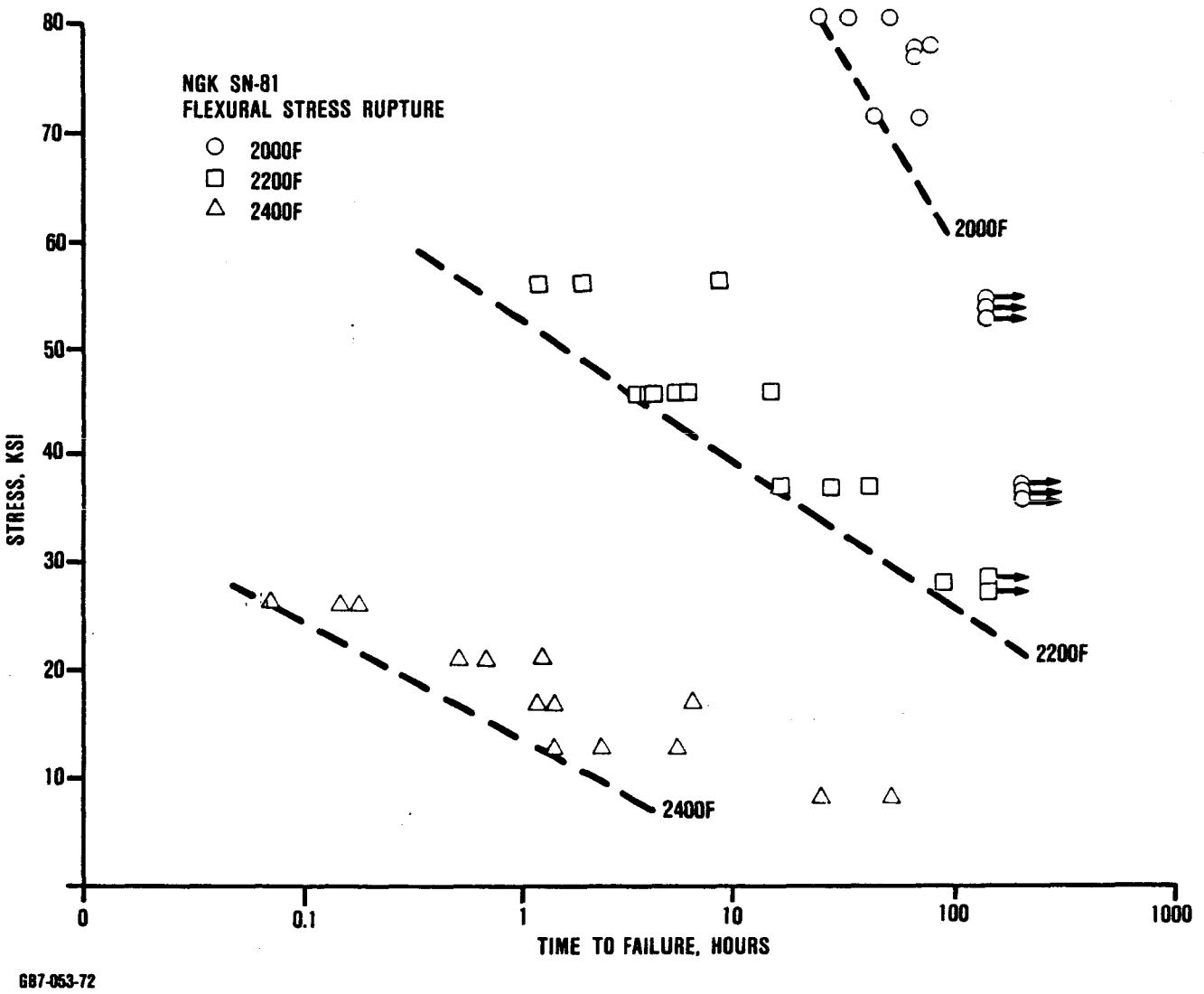

Figure 62. NGK SN-81, Flexural Stress Rupture.

screening stators in conjunction with an SSN shroud indicated that this was an acceptable approach. Therefore, no stator screening test was attempted for the build that included the RBSN turbine shroud; these tests were only done in builds that included an SSN shroud.

Thermal screen testing of turbine shrouds and stators resumed in January 1986. Two turbine shrouds and one set of stator segments were successfully screened to a thermal start transient condition representing engine normal start with 25 percent margin.

During the first test, the turbine shroud was subjected to the lightoff transient as shown in Figure 66. After two such cycles, the control system was reconfigured to execute the stator screening start transient cycle, shown in Figure 67 high level acoustic events were seen during this cycle, and the rig was shut down and disassembled. A fractured backshroud and several fractured stator segments were discovered. The stator fractures were determined to be secondary to the backshroud fracture. As a consequence of a shortage of ceramic hardware, the backshroud,

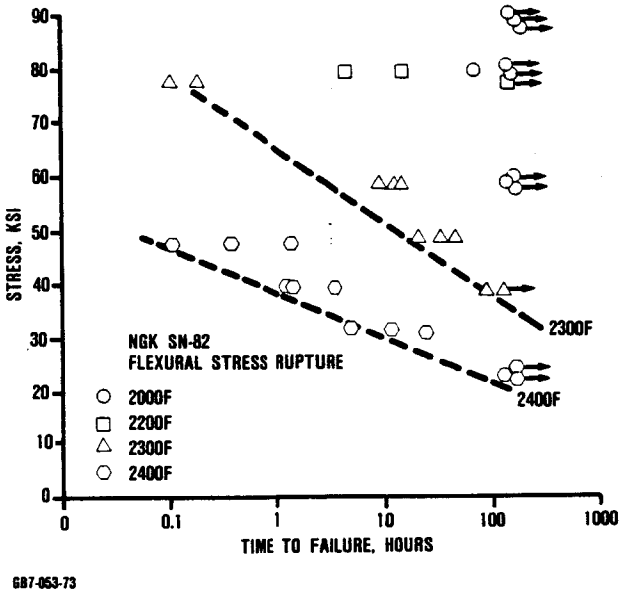

Figure 63. NGK SN-82, Flexural Stress Rupture.

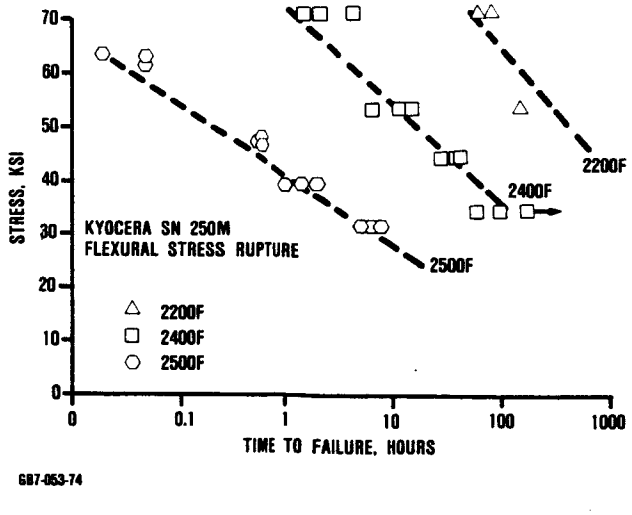

Figure 64. Kyocera SN 250M, Flexural Stress Rupture.

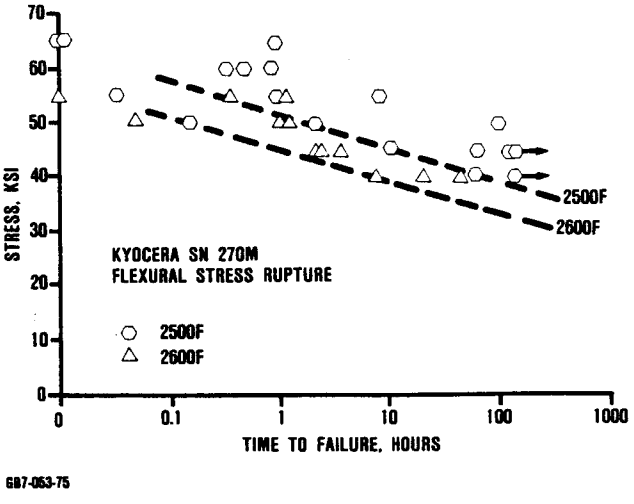

Figure 65. Kyocera SN 270M, Flexural Stress Rupture.

which exhibited a radial crack from the ID to the OD (note that this is the "stress-relieved" version with a center hole), was not cut apart for further examination. It was instead held as a piece of rig hardware until such time as additional spares were on hand.

The subsequent build of the rig was without incident. Both the turbine shroud and the stator set were successfully thermally screened to the prescribed thermal cycles.

During March 1986, one set of RBSN stators was thermally screened for two cycles to engine normal start conditions (with 25 percent margin).

Four screening tests were conducted during April 1986. During this period, one turbine shroud was re-screened and four sets of stators were tested.

Build 22 of this rig successfully re-screened turbine shroud S/N 126-1 (SN-54 NGK) following a turbine rub in Build 15 of engine S/N 002C. Stator set 015 (RBSN, ACC) was also tested in Build 22. Failure of back-shroud S/N 821 (RBSN, ACC) by a pre-nitriding internal flaw caused secondary damage to the stator set and rendered almost all segments unfit for further use.

Table 9. Comparison of Flexural Stress Rupture Lives of Japanese Sintered Silicon Nitride Materials Under 30 ksi Flexural Stress.

Material	Hours at Temperature				
	2000F	2200F	2300F	2400F	2500F
Kyocera SN 220M	1.5	0	0	0	0
NGK SN-81	1000	48	2	0	0
NGK SN-82	1000	400	100	12	0.1
Kyocera SN 250M	1000	1000	1000	230	75
Kyocera SN 270M	1000	1000	1000	1000	1000

Table 10. Comparison of Flexural Stress Rupture Lives of Japanese Sintered Silicon Nitride Materials Under 50 ksi Flexural Stress.

Material	Hours at Temperature				
	2000F	2200F	2300F	2400F	2500F
Kyocera SN 220M	0	0	0	0	0
NGK SN-81	200	1.6	0.1	0	0
NGK SN-82	1000	1000	15	0.1	0
Kyocera SN 250M	1000	1000	70	12	0.3
Kyocera SN 270M	1000	1000	1000	40	1.5

Table 11. Turbine Shroud/Stator Thermal Screening Rig.

Date	Build	Test Items	Transient Cycle	Result	Test Comments
Sept. '85	16	TShroud S/N 713 RBSN From ACC	Normal Start Per Figure	Qual'd	
Sept. '85	17	TShroud S/N 126-1 SSN From NGK Stator Set S/N 010 RBSN From ACC	Normal Start Per Figure Normal Start Per Figure	Qual'd Qual'd	Stator screening temperature of 2225F not achieved but sharp ramp up gives reasonable screen.
Sept. '85	18	Stator Set S/N 011 RBSN From ACC	Normal Start Per Figure	Qual'd	
Jan. '86	19	TShroud S/N 125 SSN From NGK Stator Set S/N 012 RBSN From SCC	Normal Start Per Figure Normal Start Per Figure	Qual'd Fractures	Backshroud failed during stator cycle, causing impact damage to several stators.
Jan. '86	20	TShroud S/N 126-2 SSN From NGK Stator Ser S/N 013 RBSN From ACC	Normal Start Per Figure Normal Start Per Figure	Qual'd Qual'd	
Mar. '86	21	Stator Set S/N 014 RBSN From ACC	Normal Start Per Figure	Qual'd	
Apr. '86	22	TShroud S/N 126-1 SSN from NGK Stator Set S/N 015 RBSN From ACC	Normal Start Per Figure Normal Start Per Figure	Re-Qual'd Fractured	Re-screen part due to turbine rub in engine testing. Backshroud failure due to internal flaw resulted in secondary damage to most stator segments.
Apr. '86	23	Stator Set S/N 016 RBSN From ACC	Normal Start Per Figure	Failed	Stator failure caused by pre-nitriding cracks, thermal shock and impact damage.
Apr. '86	24	Stator Set S/N 301 SSN From Kyocera	Normal Start Per Figure	Qual'd	
Apr. '86	25	Stator Set S/N 017 RBSN From ACC	Normal Start Per Figure	Failed	Stator failure caused by pre-nitriding cracks, impact damage.

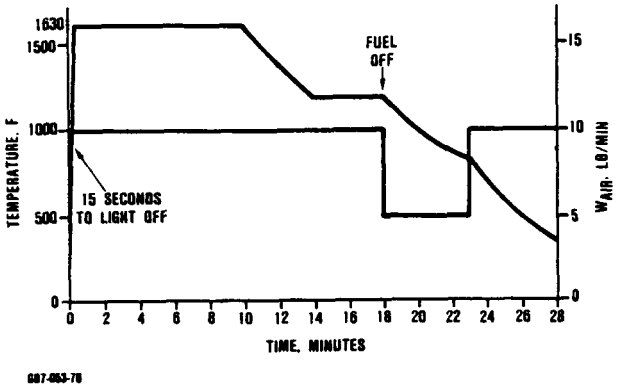

Figure 66. Turbine Shroud Screening Cycle.

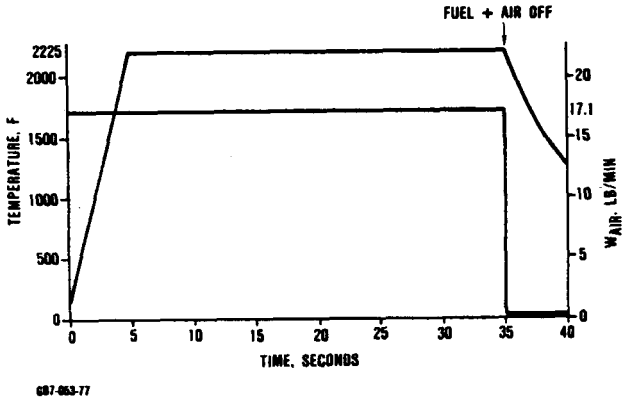

Figure 67. Turbine Stator Screening Cycle.

Build 23 tested stator set 016 (RBSN, ACC). Most segments of this set were fractured; some from internal flaws, and the remainder from impact (secondary) damage.

Build 24 successfully screened stator set 301 (SN 250M, Kyocera). This stator set did not have the trailing edges cut back for reduced stress, but used a straight trailing edge. For a comparison of the two configurations see Figure 68. During this test, transition duct S/N 124-6 (SASC, CBO) fractured with origin at the platform radius. Improved finish machining at this radius will enhance the survivability of future components.

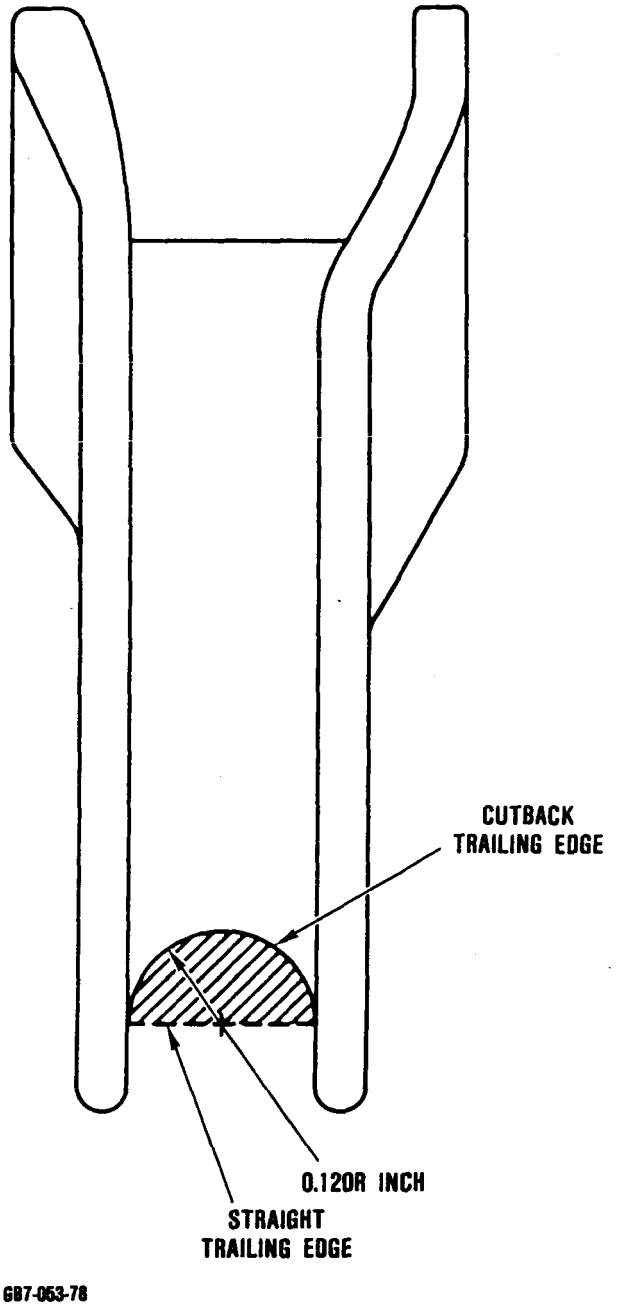

Figure 68. Comparison of Stator Vane With and Without Cutback on Trailing Edge.

Build 25 of the thermal screening rig tested stator set 017 (RBSN, ACC). Like set 016, the result was that most segments were fractured, some from internal flaws.

4.5.2.2 Transition Duct and Combustor Baffle Screening Rig

During this reporting period, six sets of transition duct and combustor baffle subassemblies were thermally screened as detailed in Table 12. All tests were performed to stress components to 125 percent of normal engine start conditions. The thermal cycle is given in Figure 69.

During the reporting period, two transition ducts failed due to inadequate sealing at the thermocouple locations. The problem was solved by modifying the rig so that an adequate, consistent spring load was applied to the parts.

Thermal screening also identified the combustor platform radius on the transition duct as a critically stressed area. Machining marks in the radius caused failure in an RBSN duct from ACC, and subsequent parts were polished in this area to alleviate this problem.

Table 12. Thermal Screening Results, Transition Duct and Baffle.

Part Name	S/N	Matl.	Source	Status
Transition Duct	824	RBSN	ACC	Fail
Transition Duct	123-5	SASC	CBO	Fail
Transition Duct	848	RBSN	ACC	Qual
Transition Duct	849	RBSN	ACC	Fail
Transition Duct	124-6	SASC	CBO	Qual
Transition Duct	122-5	SASC	CBO	Qual
Transition Duct	125-6	SASC	CBO	Qual
Baffle	128-5	SASC	CBO	Qaul
Baffle	362	RBSN	ACC	Qual
Baffle	132-5	SASC	CBO	Qual
Baffle	363	RBSN	ACC	Qual
Baffle	833	RBSN	ACC	Qual
Baffle	373	RBSN	ACC	Qual

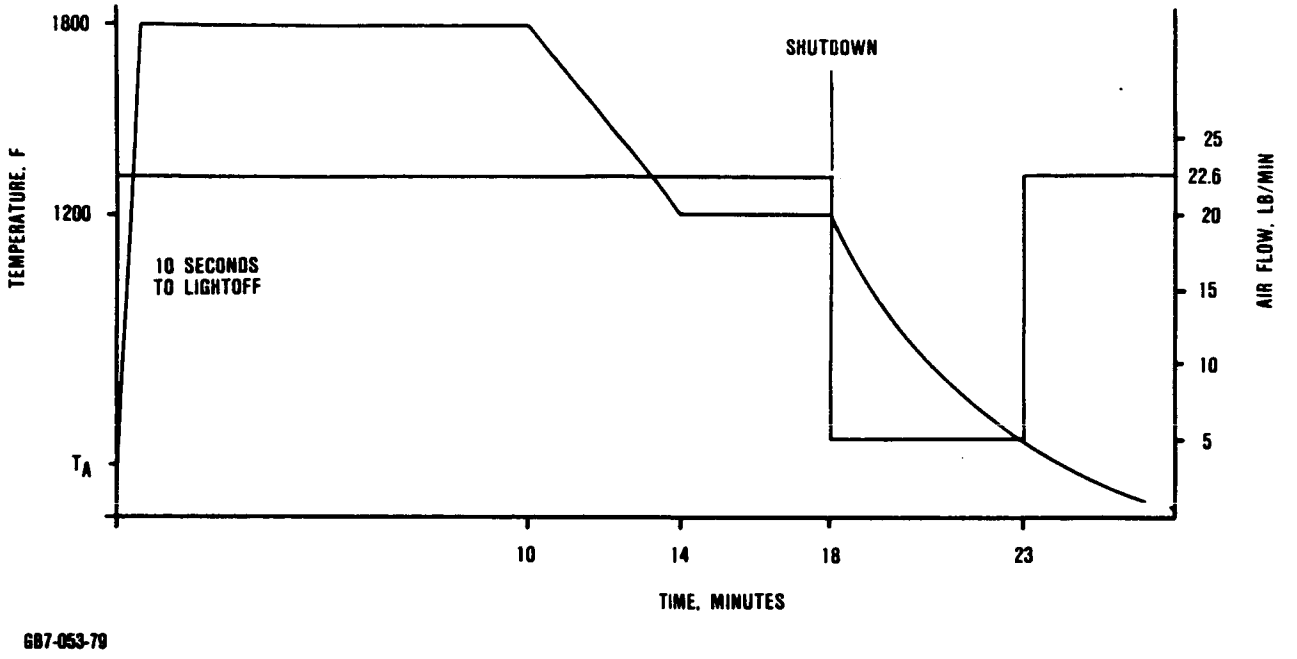

Figure 69. AGT101 Transition Duct/Baffle Screening Cycle.

Modifications to the rig included the use of an Accufiber temperature measurement system for several builds. Used in conjunction with a standard type K thermocouple, the Accufiber system was evaluated for its operating capabilities of up to 3600F, fast response, long life, and adaptability to the AGT101 program. The system uses an iridium or platinum coated sapphire probe which acts as a black body when placed in the gas flowpath. Radiation travels through the probe to a detector which converts the light into electrical signals that are sent to a signal processor. An IBM microcomputer displays the measured temperatures and acts as a system controller.

The rig insulation supporting the combustor baffle was damaged during a screening test. This was repaired by including a turbine backshroud in order to pilot the baffle. The backshroud is not at risk thermally since the backshroud stresses are low during the cycle.

4.5.2.3 Inner and Outer Diffuser Housings

Inner diffuser housing (IDH) and outer diffuser housing (ODH) thermal screening activity continued during the reporting period. Five sets of inner and outer diffuser housings (IDH/ODH) were thermally screened with no failures. Rig maintenance performed during the period included repair of the Babcock and Wilcox insulation inside the rig. A listing of qualified parts is provided in Table 13.

4.5.3 Ceramic Turbine Rotor

Table 14 summarizes the status of rotors received between July 1985 and June 1986. Twenty rotors representing three suppliers--NGK, Kyocera, and Ford were received.

NGK delivered four rotors, two each of SN-73 and SN-81 (SSN material). One of the SN-73 rotors was spun to 112,000 rpm at which

Table 13. Thermal Screening Results IDH/ODH.

Part	S/N	Matl.	Supplier	Status
IDH	555	RBSN	ACC	Qual
IDH	575	RBSN	ACC	Qual
IDH	547	RBSN	ACC	Qual
IDH	366	RBSN	ACC	Qual
IDH	337	RBSN	ACC	Qual
ODH	657	RBSN	ACC	Qual
ODH	340	RBSN	ACC	Qual
ODH	350	RBSN	ACC	Qual
ODH	576	RBSN	ACC	Qual
ODH	349	RBSN	ACC	Qual

speed it burst. The other SN-73 wheel was spin tested to 100,000 rpm. The remaining two were returned to NGK for further processing and spin tested before being returned to Garrett. This processing included additional heat treatment to recrystallize the grain boundaries in an attempt to improve the high temperature strength. Both rotors were respin tested before shipment to Garrett. One burst during this spin test; the second was spin tested to 95,000 rpm. There are no plans to test this remaining rotor in an engine at this time.

Ford submitted three turbine rotors, fabricated from RM-20, a sintered silicon nitride (SSN) for Garrett evaluation. This evaluation included visual and NDE inspection. All three rotors showed some possible defects in the hub section according to the NDE ultrasonic inspection, with no one rotor being any better or worse than the others. Visual inspection indicated that one had a better surface finish, indicating a greater chance of survival during spin testing. The spin test objective was to obtain 115,000 rpm; however, at 62,500 rpm the test was terminated due to blade tip failure (Figure 70). The remaining hub portion was sectioned in order to characterize the defects found in the NDE inspection. No defects were found suggesting that the defect locations were not determined accurately enough prior to sectioning. The hub portions were returned to Ford to aid in their material evaluation.

The remaining wheels were supplied by Kyocera. Six wheels were fabricated from SN 220M with the balance fabricated from SN 250M. (Both SN 220M and SN 250M are sintered silicon nitride). The engine test histories of these wheels are summarized in Table 14 with a fuller discussion in Section 4.5.1 Ceramic Materials Evaluation. The SN 220M wheels were spin tested to 110,000 rpm while the SN 250M wheels were spin tested 115,000 rpm, all at Kyocera. The lower spin speed of the SN 220M wheels was due to concerns of the material strength of SN 220M. In response, engine testing was limited in speed and temperature when testing the SN 220M wheels. The SN 250M material has a stronger room temperature strength and could thus be spin tested to the higher speed.

4.5.4 2500F Stator Rig

Twenty-six hours at 2500F were accumulated during this reporting period. The high temperature effects on ceramics, such as static fatigue, contact loading and endurance, were investigated. A total of five tests were run with the results summarized in Table 15. The material combination used in each test is summarized in Table 16.

Rig modifications to allow extended 2500F operation were completed in early July 1985. Figure 71 shows the rig cross section. A modified SC201 turbine shroud and RBSN inner diffuser housing were used to provide a means of loading the ceramic hardware. The loading force is provided by external springs as shown. The assembled rig is shown in Figure 72.

This rig configuration was tested for the first time in late July 1985 (Build 3) and was successfully operated at 2500F for 2 hours.

Table 14. Ceramic Turbine Rotor Test History.

Supplier Material	Serial Number	Date Received	Spin Test	Engine Test History
NGK SN-73	001	9/85	Burst at 112 krpm	
Kyocera SN 220M	0001-1	10/85	Proof Spin to 105 krpm	Eng 001 - 60 krpm. Rotor fractured during assembly into ceramic engine
Kyocera SN 220M	0002-1	11/85	Proof Spin to 105 krpm	
Kyocera SN 220M	0002-2	11/85	Proof Spin to 105 krpm	Eng 004C - 3 hr 40 min operation secondary failure
Kyocera SN 220M	0003-4	12/85	Proof Spin to 105 krpm	Inducer blade tip flaw caused failure
NGK SN-73	1001	12/85	Proof Spin to 100 krpm	
NGK SN-81	1002	12/85	Proof Spin to 105 krpm	Returned to NGK for further processing. Spin test there to 95 krpm
Kyocera SN 220M	0004-5	1/86	Proof Spin to 105 krpm	
NGK SN-81	1003	2/86		Returned to NGK for further processing. Burst during spin test by NGK
Ford RM-20	2673	2/86	Spin Test to 63 krpm Inducer Blade Tip Loss	
Kyocera SM 220M	0005-6	3/86	Proof Spin to 105 krpm	
Kyocera SN 250M	250	5/86	Burst at 89.5 krpm	
Kyocera SN 250M	251	5/86	Proof Spin to 115 krpm by Kyocera	

Table 14. Ceramic Turbine Rotor Test History. (Contd)

Supplier Material	Serial Number	Date Received	Spin Test	Engine Test History
Kyocera SN 250M	252	5/86	Proof Spin to 115 krpm by Kyocera	
Kyocera SN 250M	253	6/86	Proof spin to 115 krpm by Kyocera	
Kyocera SN 250M	254	6/86	Proof Spin to 115 krpm by Kyocera	
Kyocera SN 250M	255	6/86	Proof spin to 115 krpm by Kyocera	
Kyocera SN 250M	256	6/86	Proof spin to 115 krpm by Kyocera	
Kyocera SN 250M	257	6/86	Proof Spin to 115 krpm by Kyocera	
Kyocera SN 250M	258	6/86	Proof spin to 115 krpm by Kyocera	

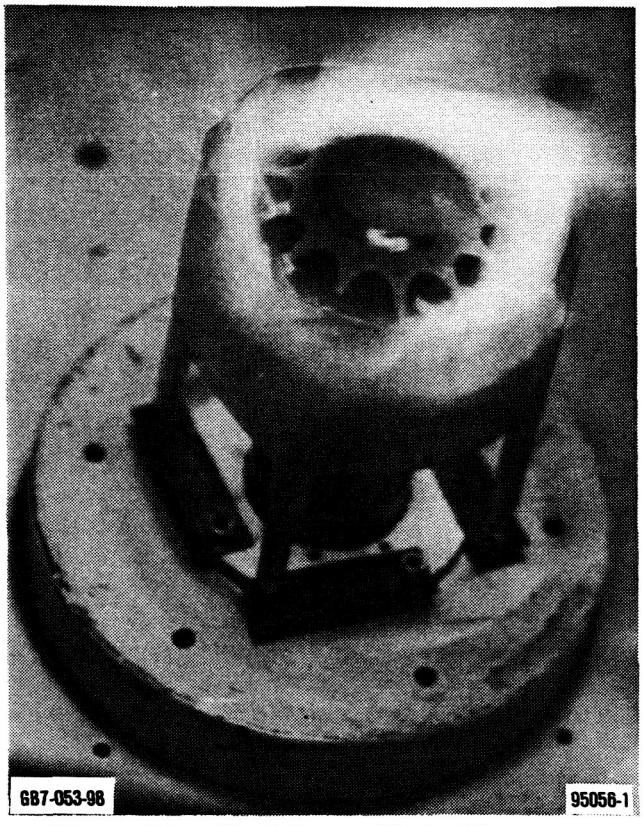

Figure 70. Ford Rotor Blade Tip Separation at 62,500 rpm.

Stators made of silicon carbide (SiC) and reaction-bonded silicon nitride (RBSN) were alternately used to evaluate interfacial sticking. Teardown inspection of the rig revealed glass formation, primarily on the stator and baffle feet surfaces; however, there was no evidence of sticking.

The next build (Build 4) incorporated an all RBSN stator set and RBSN turbine shroud to evaluate interfacial sticking at the shroud/stator interface. No results were obtained. A light-off was attempted using an off-the-shelf automatic control system. Thermocouple response in this rig (the thermocouples are shielded in a ceramic sheath) was too slow for adequate control, and as a result ceramic fracture ensued.

Builds 5 and 6 each accomplished 12 hours at 2500F. Build 5 showed sticking at the stator/turbine shroud and stator/stator interfaces. No damage was seen at either interface. Previous builds had showed the transition duct/baffle interface to be a problem when using the same material for both parts.

Table 15. 2500F Hot Stator Rig Testing.

Build	Date	Time at 2500F	Test Comments
3	July 1985	2 hrs	Glass formation on stator and baffle feet surfaces - no sticking
4	August 1985	—	Ceramic fracture at lightoff
5	September 1985	12 hrs	Sticking seen at RBSN/RBSN stator/shroud interface
6	September 1985	12 hrs	No sticking seen
7	November 1985	—	Ceramic fracture due to inadequate clearance

Table 16. 2500F Stator Rig Material Combinations.

	Build 3	Build 4	Build 5	Build 6	Build 7
Transition Duct	SACS	SASC	SASC	RBSN	RBSN
Combustor Baffle	SASC	SASC	RBSN	SASC	SASC
Turbine Back-shroud	SASC	SASC	SASC	RBSN	RBSN
Turbine Stators	SASC/RBSN	RBSN	RBSN	SASC	SASC/RBSN
Turbine Shroud	RBSN	RBSN	RBSN	RBSN	SASC

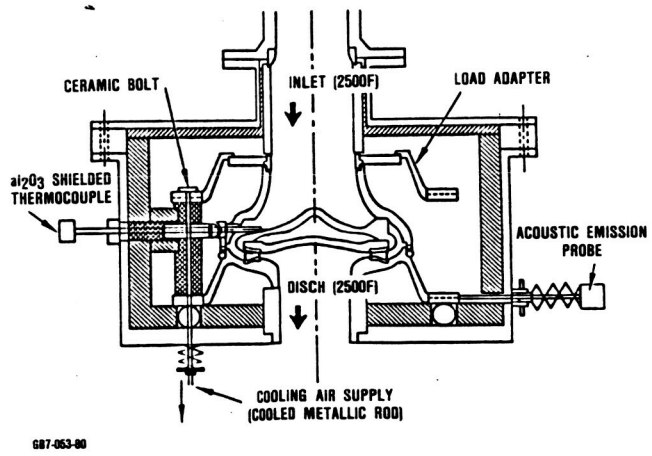

Figure 71. 2500F Stator Rig.

Figure 72. 2500F Stator Rig Shown with Ceramic Parts Assembled.

This problem can be eliminated by using an SASC transition duct/RBSN baffle combination.

Build 6 showed no sticking. Unlike the RBSN stators in Build 5, the SASC stators did not stick to either the turbine shroud or to each other. As in Build 5, alternating materials at the transition duct/baffle interface eliminated problems encountered in earlier builds.

The test objective of stator rig Build 7 was to determine the effectiveness of Al_2O_3 Sol-Gel coating on SASC parts to prevent sticking. Preliminary results using test bars have shown this to be an effective coating.

In this test, the coating was not satisfactorily evaluated due to rig failure caused by inadequate allowance for thermal growth differences between the SASC turbine shroud and the RBSN transition duct. Drawings have been revised as necessary to avoid a recurrence. No further coating evaluations were attempted in the rig during this reporting period.

To date, limited sticking at 2500F has been seen. No failure has occurred due to sticking. Interfacial distress seen between the transition duct and combustor baffle can be eliminated by using an alternating material stack in this area. More time at temperature is needed before drawing any conclusions about possible detrimental effects of the stator/stator and stator/shroud sticking that was seen.

4.5.5 Ceramic Seals Investigations

During this reporting period, attention focused on establishing cold baseline performance for three ceramic sealing areas in the engine. These seal areas are:

- o Turbine shroud/flow separator seal
- o Regenerator shield/flow separator housing seal
- o Regenerator shield/exhaust housing seal

Static seal leakage rigs were designed to evaluate existing and new seal configurations for each of these areas. Each of these rigs makes extensive use of engine hardware to speed rig fabrication.

Characteristic of the rigs is the capability to measure seal leakage as a function of force

on the seal and pressure contained. In addition, each rig has the capability of establishing the degree of concentricity between parts being sealed so that seal performance can be measured and compared to predetermined amounts of eccentricity. The rigs are also able to compare cold performance data for new seal designs with data from current seals indicating the potential of the new designs.

Since the turbine shroud/flow separator piston ring seals are believed to be most critical with regard to engine performance, this rig design was chosen for initial fabrication and is provided in Figure 73.

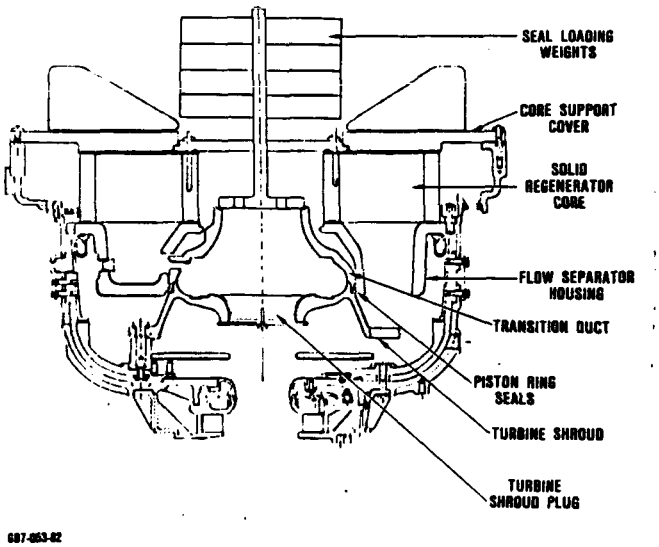

Figure 73. Components Required for Piston Ring Seals Rig.

The turbine shroud/flow separator housing ceramic seals rig was designed to evaluate seal performance as a function of the following variable conditions:

- o Mechanical spring load applied to the seal
- o Number of wave spring lobes
- o Effect of lobe contact on seal axial distortion
- o Radial and axial movement of the turbine shroud relative to the flow separator housing
- o Alternate loading configurations
- o New seal designs

Rig leakage checks were performed to measure total rig leakage without ceramic seals. This measurement included leakage through the graphite bushing and around the O-ring seals intrinsic to the rig, with O-rings also being used in place of the ceramic piston ring seals. This data was subtracted from piston ring seal leakage data to accurately determine piston ring seal leakage. Test results gathered from two separate builds are given in Figure 74.

This rig leakage test was repeated on a periodic basis to verify the integrity and performance of the rig seals.

Initial ceramic seal configurations tested in the rig included:

- o Baseline rig configuration
- o Single LAS flow separator seal
- o Dual LAS flow separator seal

The configuration that showed the largest decrease in seal leakage was the dual LAS flow separator seal shown in Figure 75. This configuration uses a wave spring between the combustor baffle and the turbine backshroud to redirect the hot section load path. This altered load path allows a solid stack seal arrangement with increased seal loading compared to the single seal configuration. The dual LAS flow separator seal configuration has the advantages of uniform loading around the circumference, and two leak path restrictions instead of one. Leakage measurements, shown in Figure 76 indicated a 50 percent reduction over the single seal configuration.

Effects of axial spring load on seal performance were studied using a single LAS flow separator seal. Seal loading was varied from 5 to 55 lbs over the range of engine pressures. Data shown in Figure 77 indicate that there was no significant benefit derived from increased spring loading for this seal configuration. More testing is necessary to determine the effects using other seal configurations.

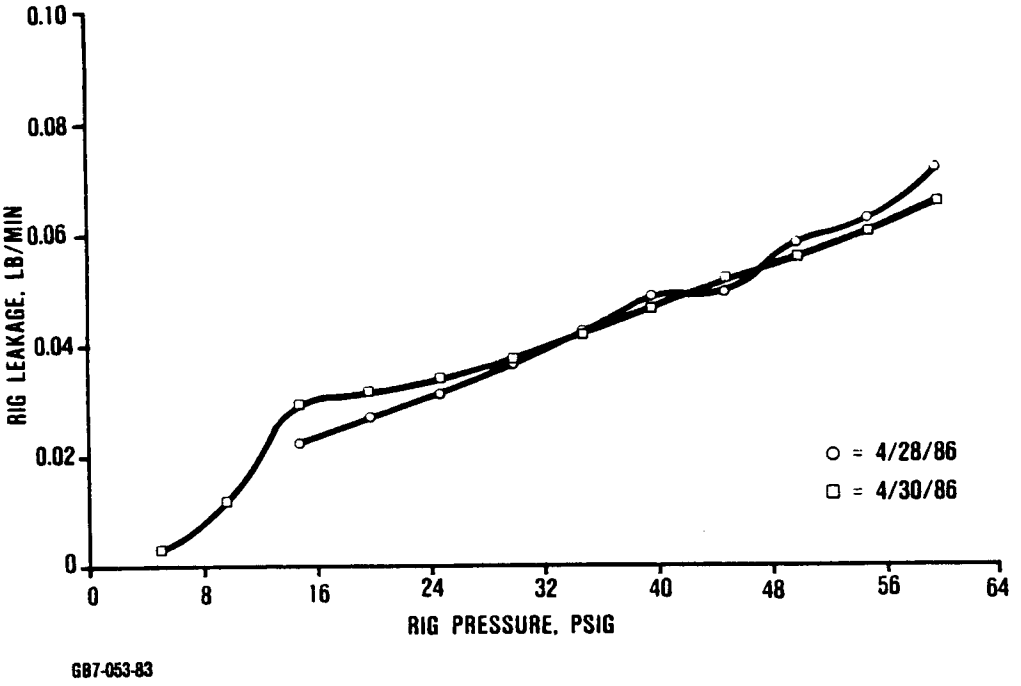

Figure 74. Piston Seals Rig: Rig Leakage Tests, April 28 and 30, 1986.

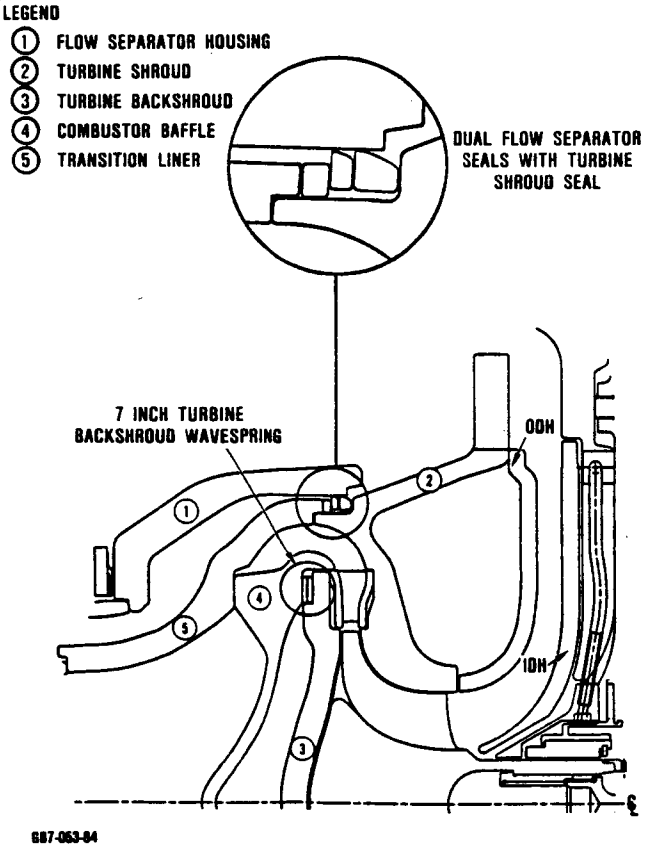

Figure 75. Revised Seal Design Gives Substantial Leakage Improvement.

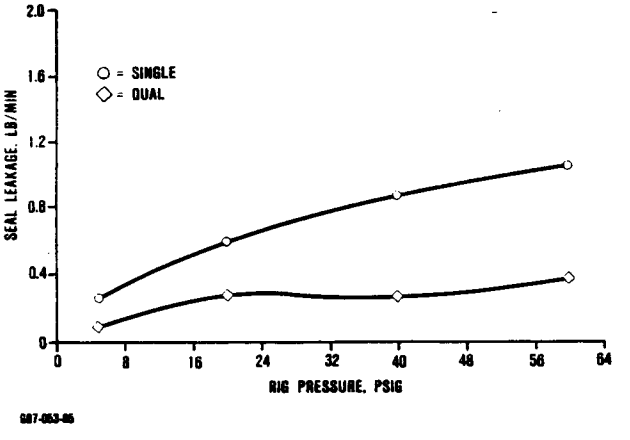

Figure 76. Single Versus Dual Piston Ring Seals.

Single LAS flow separator seal testing also indicated that eccentricity between the turbine shroud and the flow separator housing has a significant effect on seal performance. Seal leakage was measured for 0, 0.04, and 0.06 inch of eccentricity with results as shown in Figure 78 These measurements showed increases in leakages of 12 to 25 percent as eccentricity increased over leakages measured without eccentricity.

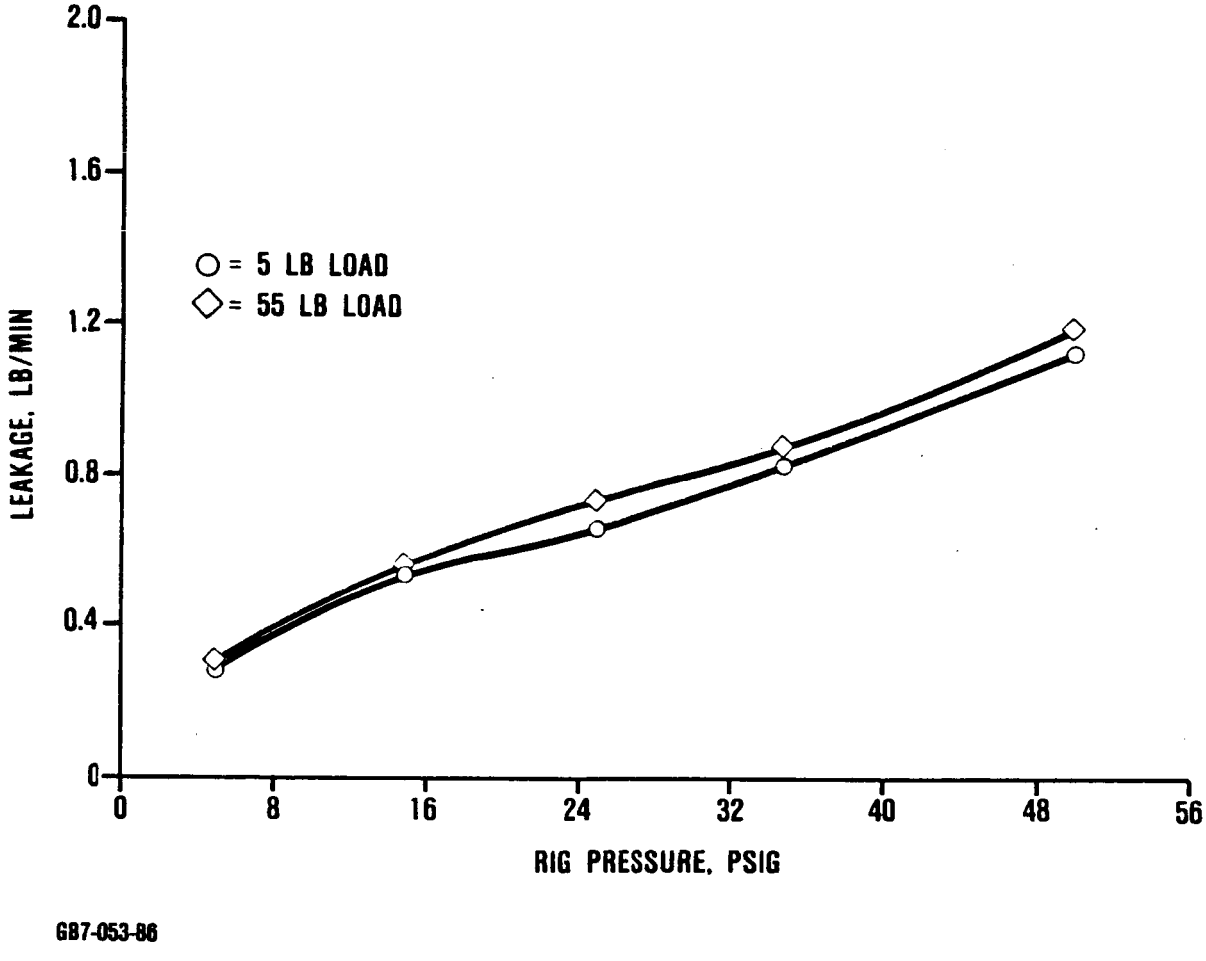

Figure 77. Increased Loading Effect on Single LAS Seal - 5-28-86.

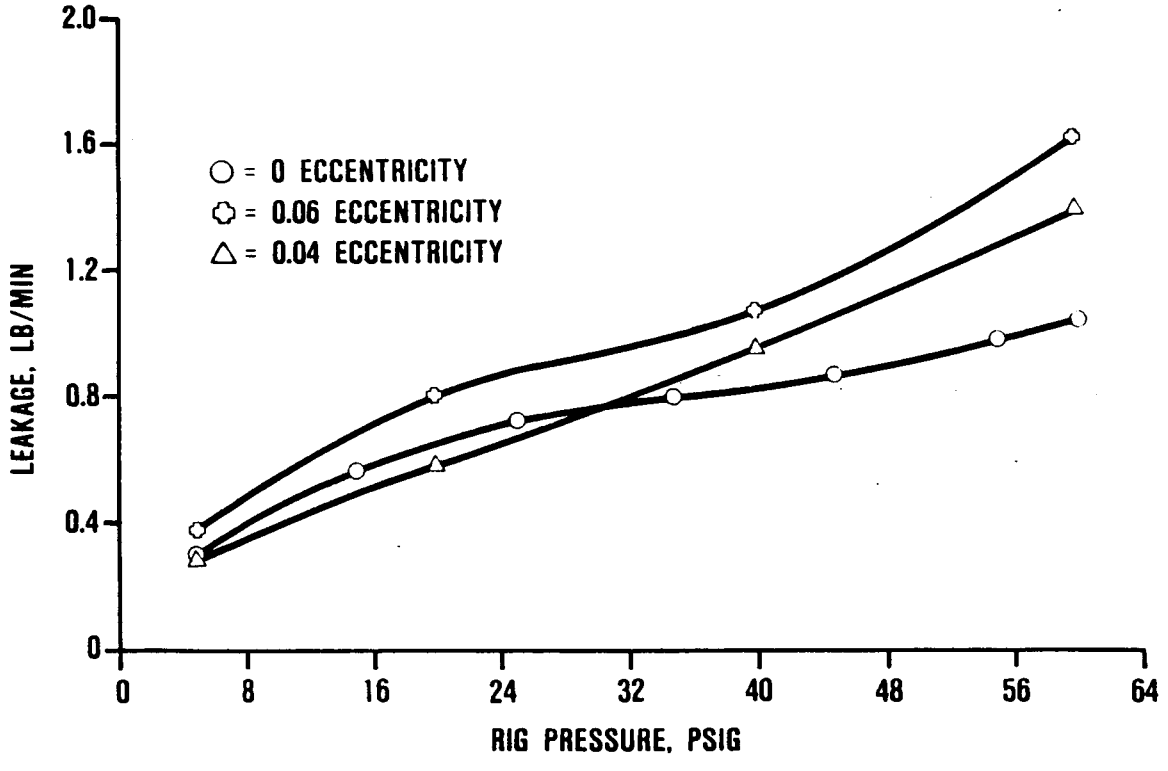

Figure 78. Increased Eccentricity Increases Leakage.

Testing of the regenerator shield/flow separator housing interface indicated a very low leakage rate as diagrammed in Figure 79.

In summary, the seals rigs were used to evaluate two ceramic sealing areas in the engine. After identifying deficiencies in the turbine shroud piston ring seal area, significant improvements were made by modifying the seal configuration. Testing of the regenerator shield/flow separator interface revealed performance that met design criteria.

4.5.6 Ceramic Components Received

The following components were received during this reporting period:

ACC delivered two turbine shrouds, three transition ducts, five turbine backshrouds, five wave washers, five combustor baffles, nine turbine shroud seal rings and thirteen flow separator housing seal rings. All were fabricated from RBSN.

Corning delivered seven flow separator housings, all fabricated from LAS.

Ford submitted three turbine rotors for evaluation at Garrett. All were fabricated from RM-20 (sintered silicon nitride).

Standard Oil (CBO) delivered six transition ducts, six combustor baffles, fourteen regenerator shields and twenty-one combustor liners. All were fabricated from SASC.

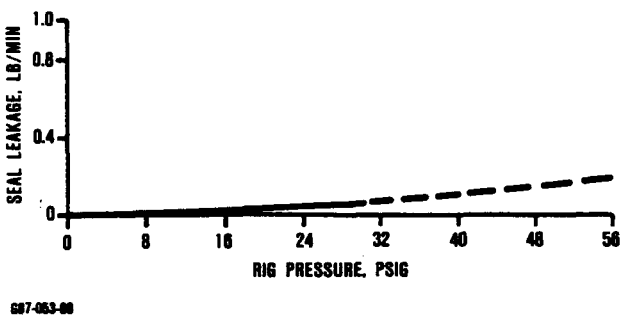

Figure 79. Regenerator Shield/Flow Separator Housing Interface Exhibits Minimal Leakage in Initial Testing.

Kyocera delivered one turbine stator set (19 vanes), fabricated from SC201. Kyocera also delivered six turbine rotors, five sleeve spacers and two pilot combustors. All fabricated from SN 220M (SSN). Additional parts fabricated from SN 250M (SSN) are as follows: one transition duct, two turbine shrouds, three stator sets (19 vanes/set), three turbine backshrouds, four combustor baffles, five turbine shroud seal rings, seven turbine rotors, seven flow separator housing seal rings and eight wave washers.

NGK delivered four turbine rotors. Two were fabricated of SN-73 and two of SN-81. Both are a sintered silicon nitride material.

4.6 Rotor Dynamics Rig Testing

4.6.1 Honeycomb Seal Evaluation

A honeycomb seal was tested to assess whether it could contribute to dynamic stability and also limit leakage through the foil bearing area. Honeycomb seal data analysis was completed during this reporting period. Testing was accomplished using the rotor dynamics rig shown in Figure 80. The following four configurations were tested:

- Configuration 1 - As shown in Figure 80, except swirl vane assembly was not installed and the honeycomb seal had a uniform diametral clearance of 0.010 inch. This configuration is not representative of engine conditions.
- Configuration 2 - Buffered labyrinth seal assembly removed, swirl vane assembly was not installed, and the honeycomb seal had a uniform diametral clearance of 0.010 inch.
- Configuration 3 - Buffered labyrinth seal assembly was removed, swirl vane assembly was installed, and the honeycomb seal had a uniform diametral clearance of 0.010 inch.

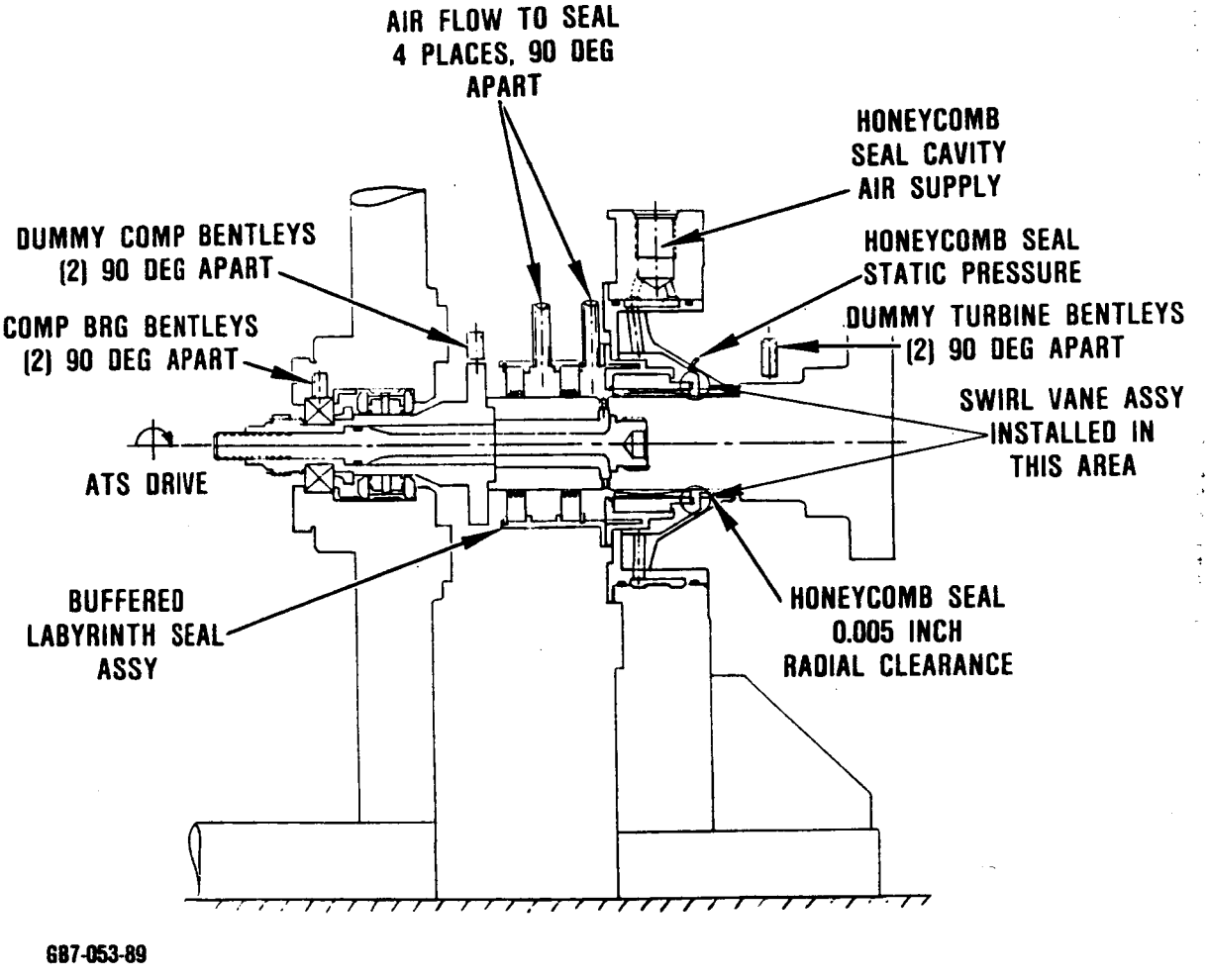

Figure 80. Rotor Dynamics Rig Configuration Used for Honeycomb Seal Testing.

- Configuration 4 - Buffered labyrinth seal assembly was removed, swirl vane assembly was installed, and the honeycomb seal had a convergent taper.

4.6.2 Honeycomb Seal Test Results

Configuration 1 test results initially indicated an improvement in rotor stability when both the honeycomb and labyrinth seals were pressurized. Figure 81 shows the typical results of pressurizing the honeycomb seal in this configuration. Figure 82 shows the result of pressurizing only the labyrinth seal assembly, incurring a dramatic increase in subsynchronous response. Figures 83 and 84 show the foil bearing, bearing journal and honeycomb seal damage resulting from the high amplitude subsynchronous motion. The honeycomb seal was abraded by the rotor resulting in a tapered bore with an increase in clearance at the turbine end of approximately 0.008 to 0.009 inch. The foil bearing was completely unserviceable.

For Configuration 2, the labyrinth seal assembly was removed to duplicate the engine configuration and allow evaluation of the

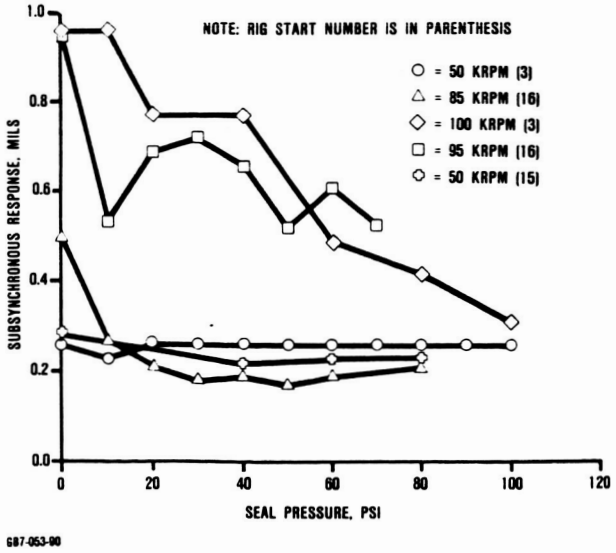

Figure 81. Honeycomb Seal Pressurized.

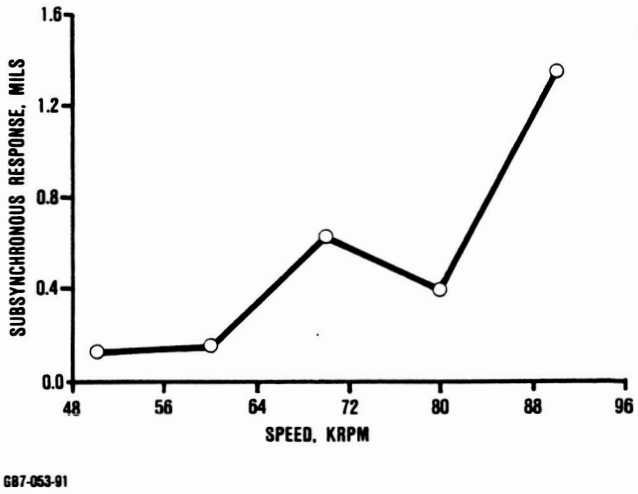

Figure 82. Labyrinth Seal Pressurized to 100 psi, Rig Start No. 2.

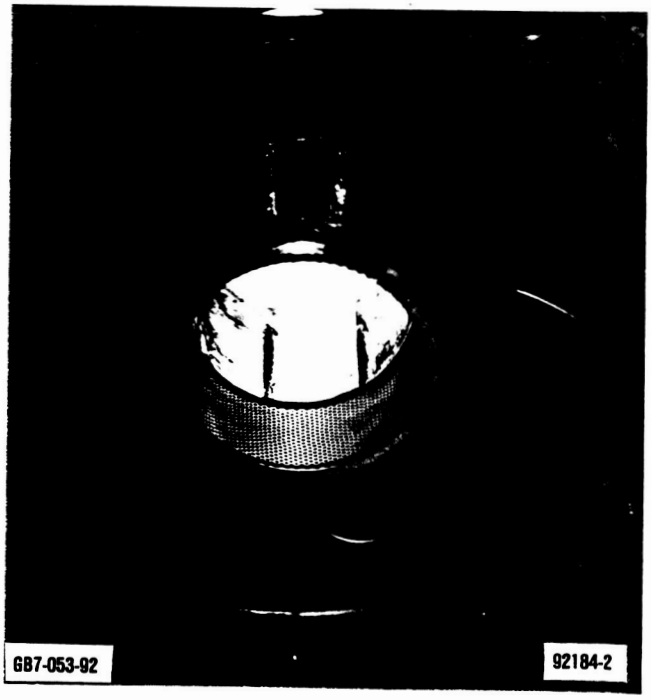

Figure 83. Damage to Honeycomb Seal and Foil Bearing from High Subsynchronous Motion.

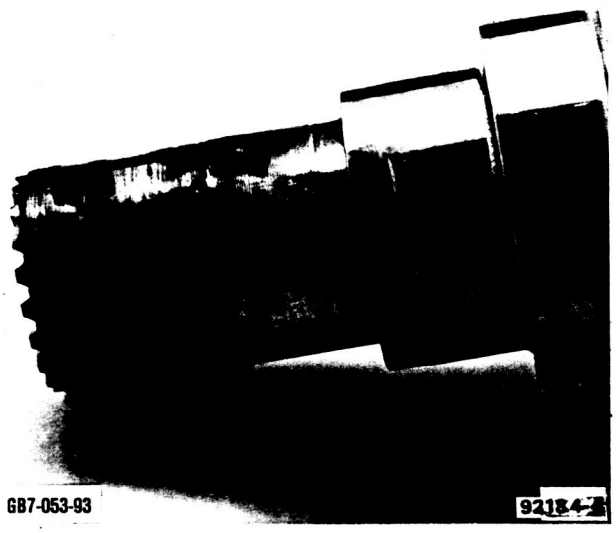

Figure 84. Bearing Journal Damage Incurred During Configuration 1 Testing.

honeycomb seal without the effects of the labyrinth seal. Figure 85 is typical of the rotor response experienced during Configurations 2, 3, and 4 when the honeycomb seal was pressurized.

Configuration 3 used the swirl vane assembly shown in Figure 86. This was installed as shown in Figure 87. The intent of this seal was to direct air flow into the honeycomb seal tangential to the bearing journal and opposite the direction of rotation. High subsynchronous response again was observed when the honeycomb seal was pressurized.

Configuration 4 was the same as 3 except the honeycomb seal ID was machined with a taper converging toward the turbine end with an enter-to-exit clearance ratio of 1.5. Exit diametral clearance was 0.010–0.011 inch. Again, high subsynchronous response on pressurizing the honeycomb seal resulted in rotor instability.

The honeycomb seal also was tested for leakage by conducting a static leak test, which closely approximates dynamic leakage. Figure 88 shows the results achieved. Further testing of the honeycomb seal in the rotor dynamics rig is not anticipated because of detrimental effects on rotor dynamics. Consideration is being given to the use of the honeycomb seal in the engine to limit leakage through the foil bearing.

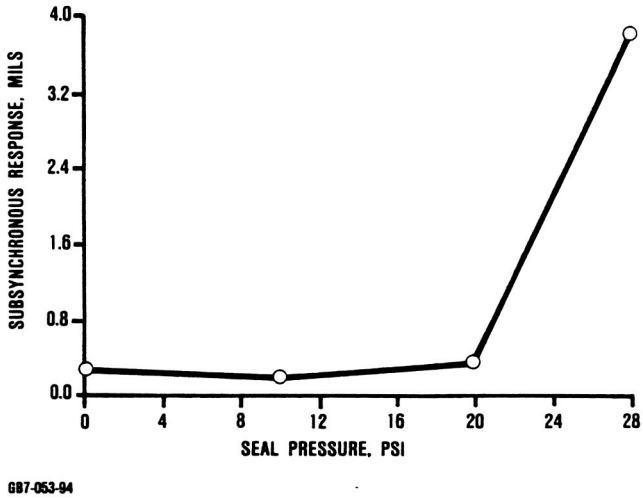

Figure 85. Rig Build 2, (Configuration 2) Honeycomb Seal Pressurized at 70,000 rpm.

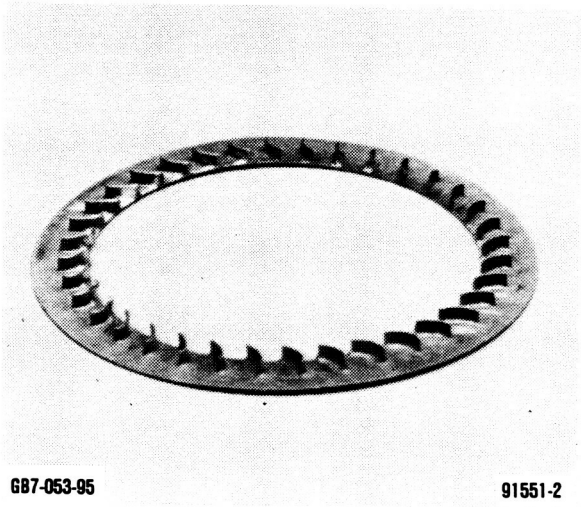

Figure 86. Swirl Vane Assembly Testing in Conjunction with Honeycomb Seal.

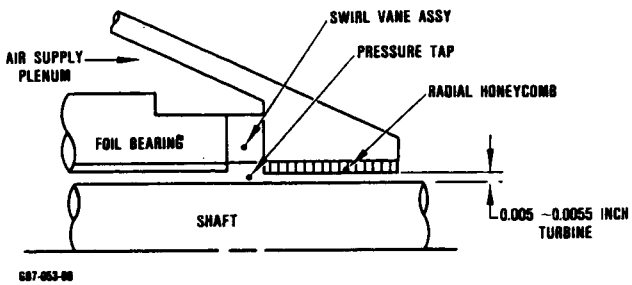

Figure 87. Honeycomb Seal Test Configuration 3.

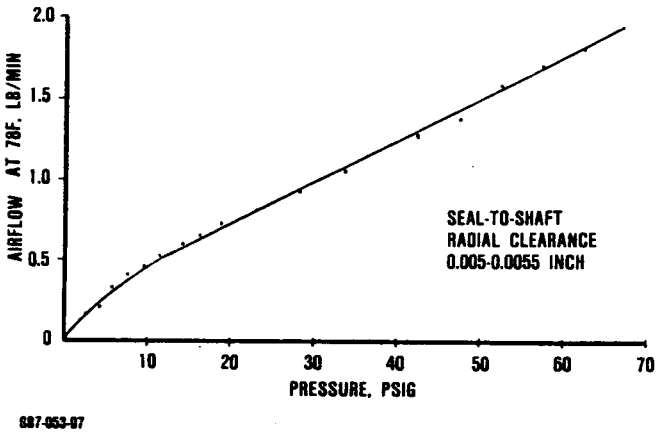

Figure 88. Honeycomb Seal Leakage Flow Versus Pressure.

This Page Intentionally Left Blank

APPENDIX A

FORD MOTOR COMPANY
ADVANCED GAS TURBINE (AGT)
TECHNOLOGY DEVELOPMENT PROJECT
1986 ANNUAL
TECHNICAL PROGRESS REPORT

1.0 TASK 2.3 - CERAMIC ROTOR

1.1 RM-20 Introduction

Prior to 1985, sintered reaction bonded silicon nitride (SRBSN) was the prime candidate for AGT101 turbine rotor fabrication at Ford. This material was preferred because its inherent low sintering shrinkage would permit the fabrication of rotors to near net shape. Efforts to fabricate rotors using the silicon-water slip cast system, however, were unsuccessful. Problems were encountered with stability of the silicon-water base slip, and as a result of these problems and the inherent weakness of the silicon castings, SRBSN components could not be made that were free of blade cracks.

Material iteration RM-20, a sinterable silicon nitride (SSN), provided a solution to some of the problems encountered with SRBSN.

The following sections characterize the RM-20 SSN material, and describe the Ford effort associated with fabricating a crack-free AGT101 turbine rotor. During this phase of the program the rotor material composition was held constant and the primary objectives of the program were:

- Development of process techniques for casting crack-free turbine rotors using the fugitive-wax process
- Fabrication of rotors of the RM-20 materials with identical physical properties to those of test bars

1.1.1 RM-20 Silicon Nitride Process

RM-20 is a silicon nitride-based material originally developed by Ford for cutting tools and other wear type applications. This material is made by pressureless sintering a silicon nitride chemical composition. The process concept involves a form of SRBSN and the use of yttria as a major sintering aid. Property data based on test bar specimens (Table 17) and the inherent process flexibility of RM-20 indicate that this material is suitable for slip casting of the AGT101 ceramic turbine rotor.

Figure 89 shows the process for fabricating RM-20 SSN gas turbine rotors. This process consists of dry ball milling selected silicon powders and additives to yield an intimate mix and cold pressing round plates under uniaxial pressure. These plates are nitrided to yield silicon nitride contents greater than 89 percent by weight and second phase oxynitride crystallites of $Y_{10}Si_6O_{24}N_2$ composition. Thereafter, the plates are broken into coarse particles (14 mesh) suitable for primary reduction by roll crushing.

Table 17. Physical Properties RM-20 Material*

Flexural Strength, (Room Temperature)	126 ksi
Weibull Modulus	13
Density	3.29 g/cm^3
Strength (2200F)	82 ksi

*Strength data are reported here for a cold pressed material, nitrided and sintered. Complete processing details are given elsewhere. (Reference 12).

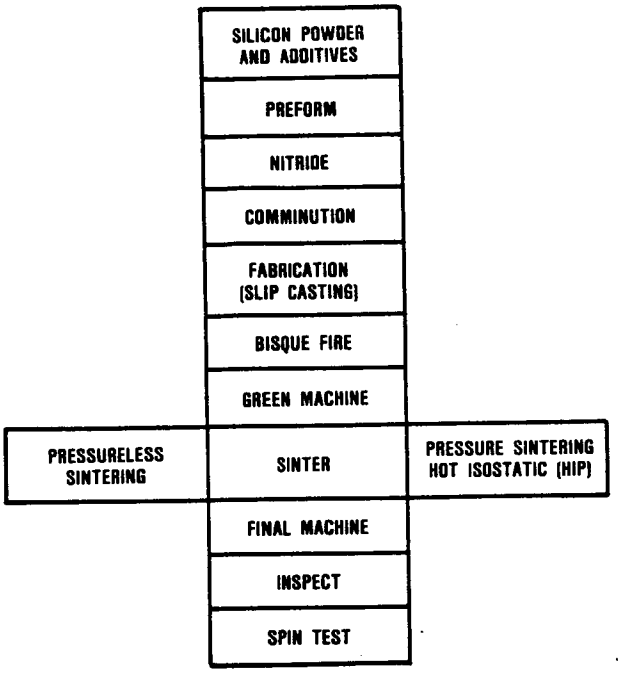

Figure 89. Sintered Silicon Nitride Process For Advanced Gas Turbine Rotors.

Ball milling is used to reduce further the particle size after roll crushing. By most standards the resultant powder is relatively coarse for slip casting, but a stable slip can be prepared using deflocculant systems that provide both physical and chemical suspension mechanisms. These deflocculant systems are covered in the following section on RM-20 slip preparation.

As in the case of SRBSN, slip casting - combined with the fugitive wax process - was used to fabricate RM-20 rotors. After slip casting, rotors are dried to remove the residual water, bisque fired for green strength, pre-machined and sintered. Both pressureless sintering and hot isostatic pressing were employed during this reporting period.

1.1.2 RM-20 Rotor Fabrication

Slip Cast Material Preparation

Early studies (Reference 2) examined the production of stable slips for the casting of RM-20 rotors. The objective of that work was the development of a slip, free of outgassing, with good flow characteristics, stability within the casting time period, and demonstrating little thixotropic behavior. Slip deflocculants evaluated were: a) Keltex, b) Dispex A-40, c) Dispex N-40, and California 226/35.

Of this group, Dispex A-40, in concentrations of 0.26 percent, produced the best results. Figure 90 shows the viscosity relationship with spindle rpm for various levels of Dispex A-40. Recently, a problem was encountered in casting the shaft (the last portion of the rotor cast), wherein the slip became thixotropic, causing slumping and distortion. This problem was eliminated by substituting N-40 deflocculant for approximately 50 percent of the A-40 deflocculant.

One problem associated with slip consistency is the presence of agglomerates in the slip. These agglomerates are formed during dry milling of the RM-20 powder. The agglomerated powder, when placed into slip suspension, would break down over a long period of time, resulting in poor viscosity control. Wet milling and screening experiments were designed to eliminate agglomerates in the RM-20 casting slip. Screening was only partially effective, and wet milling drastically changed the powder particle size distribution.

The best result was achieved with a combination of dry ball milling and a limited amount of wet milling.

Table 18 illustrates this procedure with calls for 48 hours of dry milling, followed by removal of the balls, and the addition of water. This suspension was then tumbled 72 hours. The mill was then recharged with grinding media and the suspension was wet milled for 1.25 hours. The grinding media were then removed, viscosity of the slip

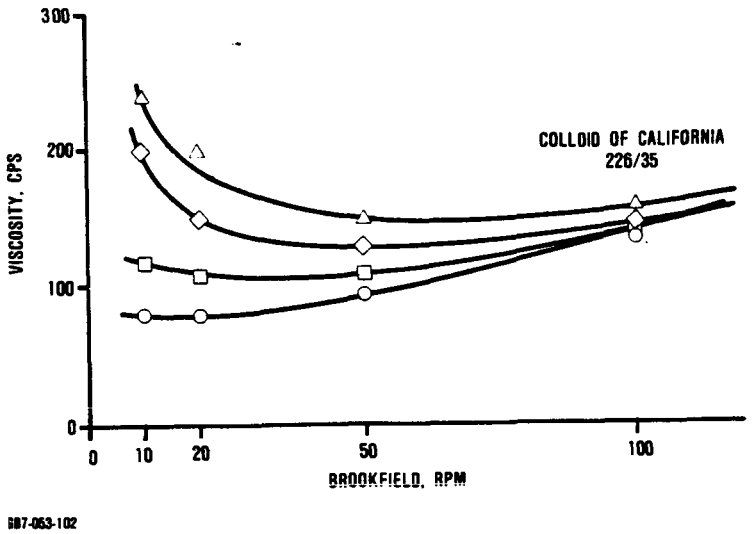

Figure 90. Relationship of Viscosity Versus Spindle Speed for Various Concentrations of Dispex A-40 Deflocculant.

Table 18. Improved RM-20 Slip.

Operation	Media	Duration, Hours
Dry Milling	None	48
Tumbling	Water	72
Wet Milling	Grinding	1.25
Tumbling	None	16

adjusted to 125-150 cps via water addition, and the slip tumbled 16 hours. This procedure produced a casting slip of good stability and excellent consistency. Several rotors have been cast with this improved technique of slip preparation.

Rotor Slip Casting

Several changes have been made in the slip casting process to improve rotor quality. Historically, blade cracks and poor grade material in blade tip regions resulted in low rotor yield. Also, a high proportion of spin pit failures originated in blades that appeared sound, which suggested that subsurface defects were controlling quality, even in rotors that passed visual and zyglo inspections. To overcome these problems, a systematic review of all the steps in the casting process was undertaken, starting with the composition of the waxes used to make the molds.

Thermal Expansion of Negative Fugitive Wax

The wax used for casting molds at Ford was a product of the Freeman Company, called "Dip Seal". Late in 1985, Freeman ceased marketing this product and an in-house analysis of the wax was undertaken to determine whether it could be made at Ford. The analysis showed the wax to be mostly paraffin (65 percent) and the remainder methyl stearate. Methyl stearate is undesirable because it is insoluble in toluene, the solvent used to remove the wax from the casting. Investigation of the properties of paraffin disclosed a large change in the thermal expansion rate at rather modest temperatures (28 to 34F). This is caused by a change in crystal structure of the wax in the solid phase and is accompanied by a five-fold increase in an already-high thermal expansion rate. This knowledge led to change in the casting process. All casting and wax removal is now done at constant temperature to avoid any expansion damage to the casting.

To replace the Freeman Dip Seal wax, a casting wax (LN-209-218) was purchased from the J.F. McCaughin Company. This material, a beeswax - paraffin-carnauba mixture with a melting temperature of 150F, was preferred.

Mechanical Strength of Negative Fugitive Wax

Because of the low elastic modulus and low strength of waxes, slight forces or loads cause

large deflections in thin sections of the casting molds. The molds had the form of a rotor sitting on a flat disc and clamped to the plaster base which loaded the wax mold on the webs formed between blade tips. Mismatches between the plaster and mold caused distortion in the wax. This type of mold, and the technique used to clamp it, were changed to eliminate distortions in the wax.

A new method of dipping the wax mold, using an aluminum contoured plate, was developed (Figure 91). The plate matched the base contour of the water soluble positive wax and had the web sections between blades machined away, leaving a ledge of aluminum 0.060 inch in width. The positive was held down with a bolt and a cap. Tightening of this bolt was minimized as any stress on the positive wax could cause a crack which would translate into a web inside the wax mold and a corresponding crack in the cast part. The contour of the aluminum dipping plate that matched the back of the positive wax was produced in a computer-controlled mill. The same program was used to mill this exact contour into the matching surface of the plaster on which sits the wax mold, thus assuring a perfectly matched interface. The first mold produced by three dips into a 155F McCaughin dip wax were heavy enough to allow filling of the mold without mechanical clamping. This arrangement was slightly modified when the thickness and weight of the molds were changed; however, the unstressed mold feature (except for stress caused by the slip itself) was retained.

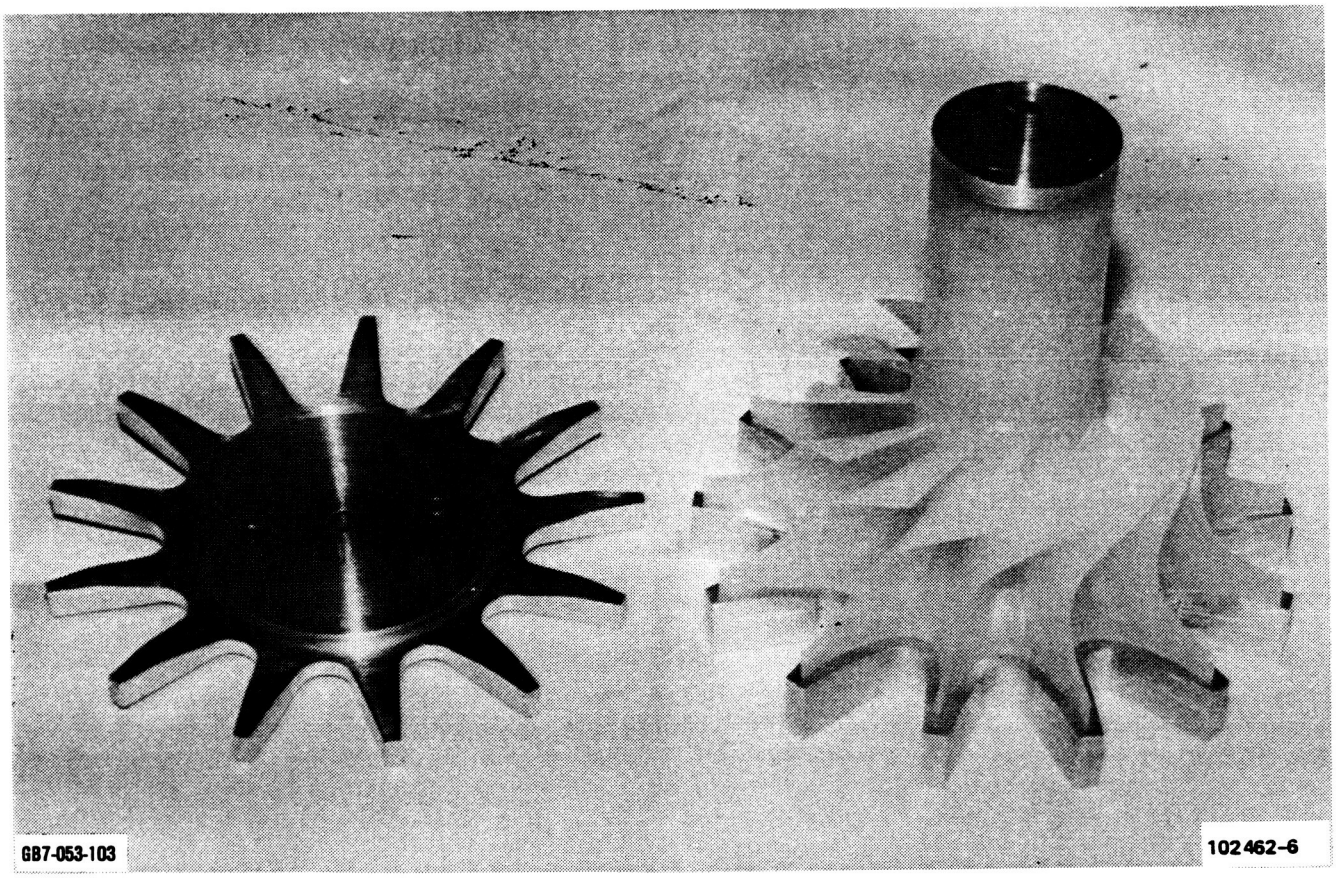

Figure 91. Fugitive Wax Dipping Fixture.

Wax Removal

While the 3-dip molds produced a high percentage of crack-free rotors, a long time (24 hours) was required for wax removal. Removal was accomplished by allowing the wax-covered casting to sit in toluene without agitation and at constant temperature. Thinner molds could be expected to dissolve quicker and less time in toluene would be a desirable result. It was also suspected that soaking the wax would cause a slight swelling, stressing the blades of the casting. Hence, thicker molds could be expected to stress the castings more than thin ones. Initial attempts at a single dip, thin mold produced problems in the wax positives.

Positive Wax Preparation

Cracks and roughness in the wax positive were found to cause problems in the cast parts. Polishing the positive wax with 4-0 steel wool eliminated these problems. This step removed surface defects and improved wax removal from the casting. Two new problems were associated with thin wax molds: splitting of the mold down the blade edges and surface blemishes caused by contamination of the white wax surface with mold release agent. The blemishes were caused by traces of oil used in the injection molding of the wax positive. This problem was eliminated by two consecutive cleanings in an organic solvent. The problem of mold splitting was caused by the uneven coating of wax around the edge of the blades. At the corner of the surfaces the wax deposit is very thin. Chamfering this edge on all blades caused a more even layer of wax and reduced this tendency to split. With these modifications, experiments were initiated with single dip wax molds.

Single Dip Molds

Initial attempts to use single dip molds proved difficult (Figure 92). The wax molds were 70-80 grams lighter than previous molds. Unless slip was added to the mold slowly and carefully a leak would start at the mold/plaster interface, quickly draining the slip and

Figure 92. Single Dip Negative Wax.

ruining the casting. To overcome this, a steel ring about six inches in diameter, one inch high and 0.060 inch thick was fabricated. This ring weighed 70 grams, and, when placed on the wax mold at the tip of the blades, the ring held the mold down (Figure 93). Because of the perfect fit of the wax to plaster, there was no deflection of the wax.

Subsequent wax removal was accomplished in six to eight hours, versus 24 hours for the 3-dip wax mold. Removal was aided by the use of an eye dropper and a small artist's brush.

Material Quality in Rotor Blades

Spin pit tests of visually sound rotors produced a large percentage of blade failures which suggested that the blades had subsurface cracks that caused failure at speeds well below that at which hub failures occurred. To assess the quality of the subsurface blade material, a light glass beading of the sound blade surfaces was undertaken after the rotors

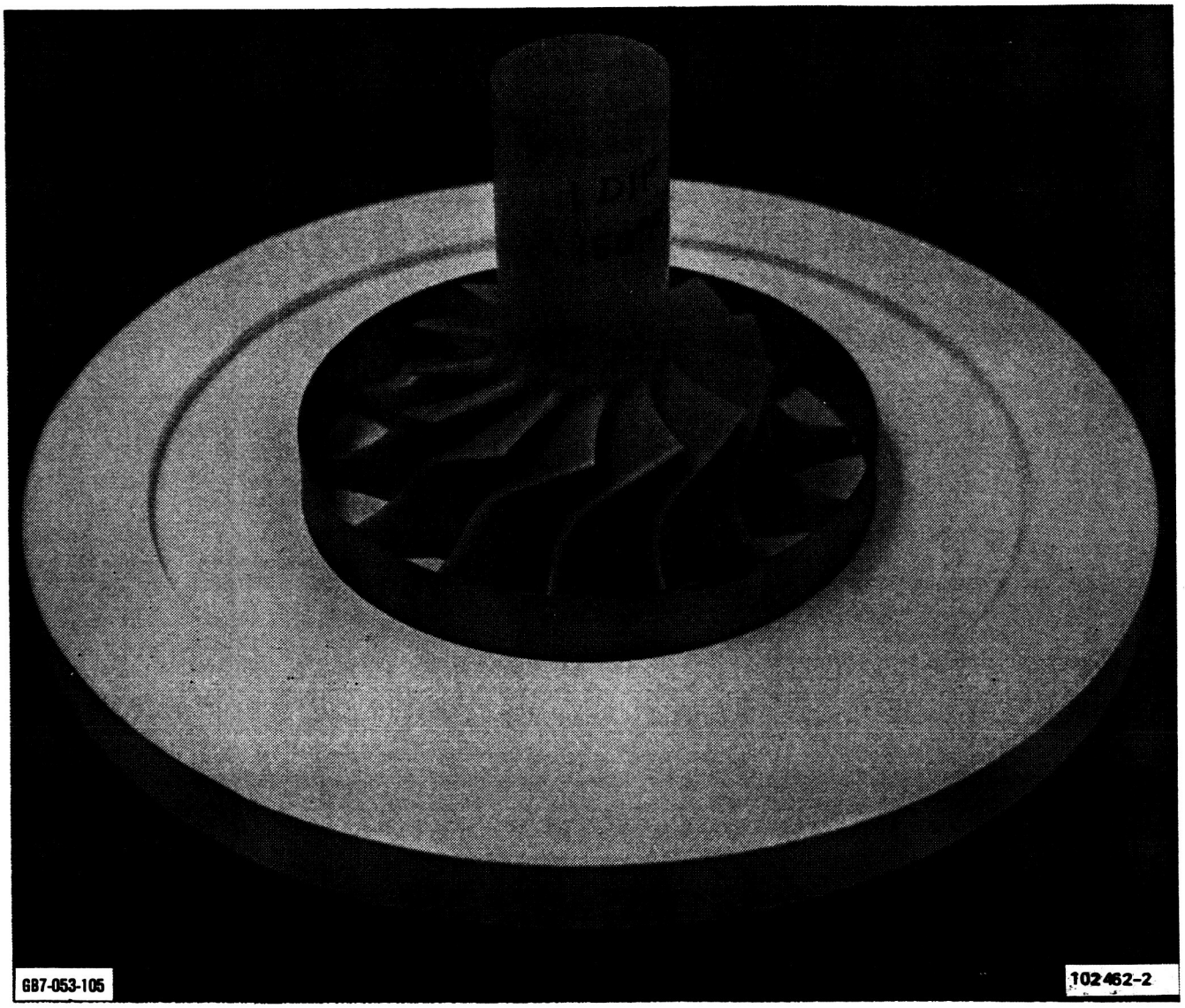

Figure 93. Single Dip Wax, Plaster Base and Steel Retaining Ring.

had been bisque fired. This surface removal disclosed porous material at the blade tips. To overcome this, the castings were spun, while casting, at 100 rpm. This increased centrifugal force caused a migration of material to the tip and significantly reduced the problem.

Remaining Problems With Wax Molds and Wax Positives

Two problems remain with the wax system. First, the positive had a tendency to distort with shelf time. This tendency to stress-

relieve and hence distort is well understood in the dental profession where critical dimensions in wax patterns must be maintained. As yet, we have not addressed this problem, but it will be a deterrent to accurate blade forming. This deformation also caused the shaft diameter of the wax positive to ovalize by 0.010 to 0.020 inch over a few weeks. Blade deformation has not yet been defined. Possible solutions for this problem include refrigerating the wax positives until they are used or using them immediately after they are molded.

Secondly, the inside surface of the wax mold develops a rough surface even though the wax positive is polished smooth before dipping. Apparently, the 150-160F melting temperature of the water soluble wax is too close to the 150F melting temperature of the dip wax. Lowering the temperature of the dip wax to its lowest usable point improved the surface texture, whereas raising the temperature or holding the positive in the dip wax longer than required heightens the effect.

The rough surface appears as bumps on the casting not only destroying the smoothness of the component surface, but giving the mold wax a rough surface, making removal more difficult. The surfaces can be smoothed after bisque firing by sanding, but this is tedious job and best avoided.

In summary, the above mentioned process modifications have produced a marked improvement in rotor fabrication quality. Approximately 70 percent of slip cast rotors have been crack free. There is, however, a need for better quality material in the blade tip region of the rotor.

1.1.3 Rotor Heat Treatment and Equipment

Pre-Sintering of Rotor

Once dried, the RM-20 rotor castings become extremely fragile and are difficult to handle through inspection and subsequent sintering. This problem is most severe during the placement or "packing" of the rotor in a powder blanket for sintering. Therefore, a presintering or "bisque" firing treatment was developed to partially consolidate the casting and provide the required handling strength.

The bisque firing cycle consists of slowly ramping in a nitrogen atmosphere to 1500C and holding at this temperature for two hours. During this cycle the casting will undergo partial consolidation, as indicated by 2.5 percent linear shrinkage, which is sufficient to impart suitable handling strength. An additional advantage of bisque firing is that it permits machining of the casting with standard high speed tool steel, and thus reduces costly diamond grinding of the final component. This pre-sintering cycle does not impede the final sintering kinetics. This process is now being used on all castings.

Sintering of Rotor

The sintering time/temperature profile initially developed was a single-step densification cycle. This cycle was adequate for the densification of the original platformed rotors but yielded unpredictable blade distortion in redesigned rotor castings. In addition, considerable fusion of the packing powder occurred increasing the difficulty of removal, particularly between the blades. Packing powder compositional changes reduced but did not eliminate the problem.

A two-step sintering cycle was developed to reduce blade distortion and facilitate removal of the packing powder. The first step of the dual cycle utilized a packing powder (boron nitride, silicon nitride, yttria and silica) and a 12-hour temperature ramping schedule that had three discrete temperature holds: 0.5 hours at 1520C, 0.5 hours at 1620C, and four hours at 1720C. Negligible fusion occurred within the packing powder.

The second step of the sintering cycle utilized a compositional change in the packing powder and a single temperature hold of 12 hours at 1800C. This compositional change and increase of temperature and hold time provided greater availability of SiO (gas) thereby maintaining the required oxynitride

composition within the rotor, so that full densification could be achieved. This packing powder could be readily removed.

Upon conclusion of the two-step cycle, a nominal 18 percent sintering shrinkage was realized and a final density of 3.24 to 3.28 g/cm^3 was obtained. Observed blade distortion was minimal.

The two-step cycle approach, although much improved over the earlier one-step cycle, did increase considerably the complexity and total time needed to complete the sintering cycle. The main factor in the longer total time needed was the two steps, with each step involving a complete temperature cycle with repacking of the rotor (powder pack) between cycles. In addition, one more handling of the fragile rotor was undesirable.

Consequently, a new cycle was developed which is currently being used. Its main features are:

- o A <u>one</u> step sintering cycle
- o 36 hours compared to the 12 hours hold at the maximum temperature
- o Two discrete temperature holds. One hour at 1500C and 36 hours at 1800C
- o Two discrete temperature ramp rates. Three hundred Celsius per hour up to 1500C, followed by 50C per hour to 1800C.
- o The packing powder, which includes 24 percent boron nitride, is packed loosely.

Upon conclusion of this one step sintering cycle, a nominal 18 percent sintering shrinkage is realized and a final density of 3.28 to 3.29 g/cm^3 is obtained. The packing powder is readily removed and blade distortion is minimal.

Post Sintering Heat Treatment of RM-20 Rotor

All pressureless sintered rotors have shown a duplex zoning structure (Figure 94). The exterior casting is generally dark in color and shows a well crystallized secondary phase. The interior region of the rotor is lighter in color and shows by X-ray diffraction a predominantly glassy second phase. Scanning electron microscopy indicates that the densities and chemical compositions of both regions are identical. Cold spin testing of several rotors produced blade separation failures at the intersection of the two regions. Fracture origins could not be identified but separation in all blades occurred near the interface of the duplex zones. This zoning interface may be acting as a stress riser and thereby producing premature failures.

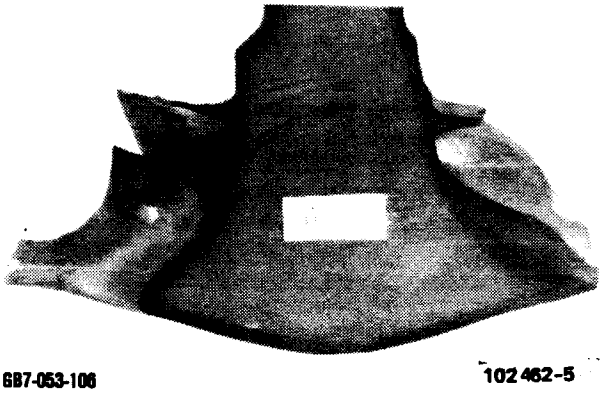

Figure 94. Typical RM-20 Rotor Duplex Zoning.

An investigation was initiated to develop heat treatment techniques for crystallization of the interior region of the rotor and the elimination of the duplex interface. A half-fraction of a 2^4 (i.e., 8 data points) statistically-designed experiment was used to study four variables (nucleation temperature and time, growth temperature and time) at two levels each, requiring eight heat treat cycles.

Test bars cut from a sintered rotor (40) were heat treated. A 0.025 inch layer was ground from each test bar. X-ray diffraction examination showed that all eight heat treatment cycles resulted in a crystallized second phase. However, when the 0.063 inch level

(maximum depth of test bar) was examined, four of the eight bars were found to retain some glassy phase.

Table 19 describes the eight heat treat cycles and X-ray diffraction test results. These initial test results indicated that the devitrification of the glassy second phase throughout the rotor (over one inch depth) would require further cycle modifications.

Full size rotors were heat treated, sectioned, and examined by X-ray diffraction to determine phase composition. One rotor (64) was heat treated using a cycle similar to cycle HT4; however, the hold time at the "growth" temperature of 1450C was increased from four hours to 96 hours. A rotor (63) was heat treated using a cycle similar to cycle HT7 with an identical increase in hold time. The relevant differences in their cycles, as shown in the table, were in their "nucleation" temperatures and duration times.

The results of these tests show that the two heat treatment cycles did affect the second phase throughout the interior of the two rotors although not to the same degree. The original HT4 cycle, which was used on the test bars, resulted in some retained glass (see Table 19). Similarly, the modified HT4 cycle (rotor 64) results in more glass than the modified HT7 cycle (rotor 63).

The secondary phase composition of rotor 63 was identified as:

$Y_{10}Si_6O_{24}N_2$ ("H") + $Y_2Si_2O_7$.

The secondary phase composition of rotor 64 was identified as:

$Y_{10}Si_6O_{24}N_2$ ("H") + $Y_2Si_2O_7$ + Y_2SiO_5 + a small amount of glass.

After the heat treatment, MOR test bars were made from rotors 63 and 64 and from rotor 65 which did not undergo post-sintering heat treatment.

Room temperature, four-point MOR bending tests were then carried out on five test bars from each rotor. The results are summarized in Table 20.

These results show some deterioration of room-temperature strength with decreasing levels of glass in the secondary phases. However, high temperature strength is expected to be greatest in the rotor with the least amount of the glassy secondary phase.

Table 19. Comparative EDX Inspection Results of Different Heat Cycles.

Cycle No.	Bar No.	Nucleation		Growth		Glassy 2nd Phase
		Temp, C	Hours	Temp, C	Hours	
HT1	8A	1050	1	1300	1	Some
HT2	9B	1200	1	1300	4	Some
HT3	6B	1050	1	1450	4	No
HT4	6A	1200	1	1450	4	Some
HT5	5A	1050	4	1300	4	No
HT6	8B	1200	4	1300	4	Some
HT7	7B	1050	4	1450	4	No
HT8	7A	1200	4	1450	4	No

C-2

Table 20. Mean MOR Results For Heat-Treated Rotors.

Rotor	Mean MOR, ksi	Std. Dev., ksi	Heat Cycle (See Table A-3)
65	87.6	3.4	None
64	79.5	4.8	HT-4 (96 hrs)
63	74.6	7.2	HT-7 (96 hrs)

The overall strength level of these rotors is approximately 30-35 percent lower than the test bar strengths of 125 ksi previously reported. A chronic problem in any material-component development program is that of obtaining material properties in a large component, such as the AGT101 rotor, similar to those of the test bar material. In this case, the difference in strength has long sintering times required to achieve density. An effort to eliminate porosity in RM-20 rotors with a hot isostatic pressing (HIP) process has been initiated.

Sintering Equipment

The pressureless sintering process utilized a cold walled vacuum furnace and a refractory metal hot zone. The major draw-back of this system was the reactivity of the SiO (gas) with the hot refractory metal. The hot zone was limited to approximately 15 to 18 cycles before a complete rebuild was required. Significant in-house modifications increased the furnace life to approximately 25 cycles, but further life improvement was necessary. Therefore, a furnace manufacturer was contracted to redesign the hot zone and other deficient areas to improve the sintering environment.

The new design provided for a smaller, more efficient hot zone faced with 0.005 inch thick tungsten sheet. After several cycles, deterioration was noted which rapidly accelerated with subsequent cycles. The hot zone became unusable after 23 cycles.

An in-house redesign and rebuild effort resulted in an improved hot zone. Reconstruction included the replacement of the 0.005 inch tungsten face with 0.020 inch molybdenum sheet, and molybdenum rods added to the ceiling structure for support. A sacrificial molybdenum sheet was placed over the floor in order to reduce the faster deterioration of the floor relative to the rest of the hot zone, caused by spilled packing powder reacting with the floor. To minimize downtime needed for hot zone rebuild, two additional hot zones were built in-house. Table 21 below shows the marked improvements achieved with in-house furnace modification.

Table 21. Life Improvements Resulting From Furnace Redesign.

Category	Previous Design	Latest Design
Total number of cycles	23	32 (still usable)
Number of cycles with max. temperature >1750C	8	12
Number of cycles with max. temperature between 1510C and 1750C	0	20
Number of cycles with max. temperature between 1300C and 1510C	15	0
Number of hours at temperature above 1750C	96	316

1.1.4 Spin Testing RM-20 Rotors

General Review

Extensive changes have been made in the methods used to mount spin pit arbors to AGT101 rotors and the manner in which the rotors are balanced. Previously, the final spin pit arbor was mounted using "loctite" and a 0.001 to 0.002 inch loose diametral fit between the arbor and the rotor. This technique did not produce perfect concentricity between rotor shaft and the outer diameter of the steel arbor on which the assembly is mounted and spun during balancing. Tests revealed that this method introduced unbalanced forces which then had to be removed by grinding away rotor surfaces, usually the blades. Obviously, this was unacceptable for rotors which might be engine candidates. To overcome this problem, a press fit arbor was designed and the balancing process was split into two parts; an initial balance check and a final balance operation.

Initial Balance Check

To reduce the extensive grinding previously required to balance rotors, a method of relocating the geometric center of the rotor shaft through the mass center of the part was adopted. The mass center was located and the shaft portion of the rotor was ground as close to the center of the blades as possible. A steel sleeve (Figure 95), 3.50 inches long with 0.070 inch wall thickness was press-fitted to the shaft. The press was 0.0015 inch on the diameter and the sleeve was fitted by heating before installation. The sleeve was installed while the rotor was still mounted to the grinding machine. When cooled, the O.D. of the sleeve was ground to fit the half bearings of the balance machine. The initial check of unbalance was then made. Results revealed from 40 to 60 percent less unbalance than rotors mounted with loctite. With the direction and size of the unbalance known, the offset of the rotor shaft could be calculated. The geometrical center of the shaft could be relocated in greater proximity to the mass center, further reducing the unbalance and allowing final balancing with minimal grinding.

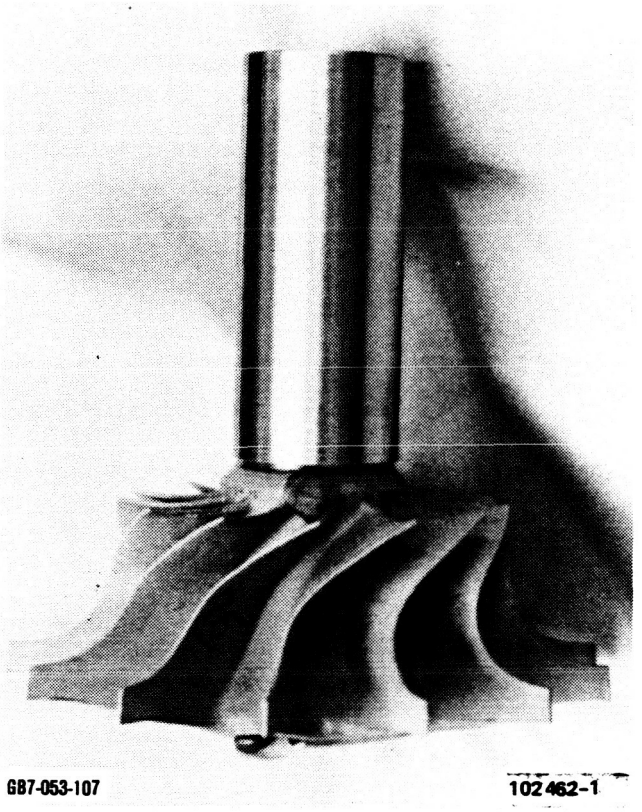

Figure 95. AGT101 Rotor Press Fitted with Steel Sleeve for Initial Balance.

Final Balancing

After the initial check, the sleeve was removed by heating it to a temperature of 300 to 400F. The rotor was returned to the machine shop, mounted and adjusted so the shaft portion had zero runout. The machine check was then adjusted to reposition the mass center at the rotational center and the shaft was reground to run true to the mass center. The steel spin-pit arbor (Figure 96) was installed with a 0.003 to 0.004 inch diametral press fit and its O.D. ground to fit the balance machine half bearing. The quill shaft hole was also ground true to the mass center during this stage. These steps were all accomplished without dismounting the rotor from the original machine position used to regrind the

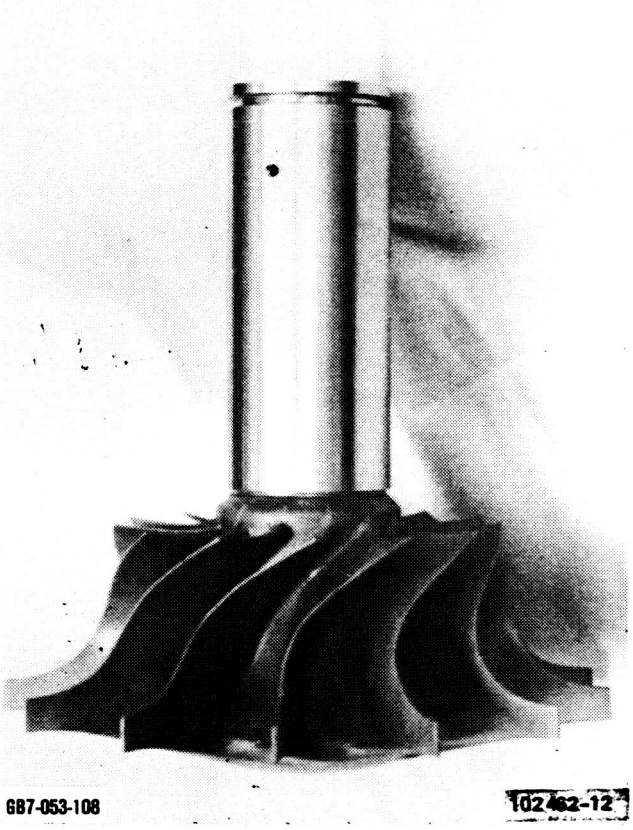

Figure 96. AGT101 Rotor With Press Fitted Spin Pit Arbor for Final Balancing.

shaft to the new location over the mass center. The rotor was then final balanced by grinding on the back and on the shaft just forward of the blade root on the exducer end. These steps reduced the unbalance from the 0.160 to 0.200 oz-in. previously encountered to 0.010 to 0.040 oz-in. an amount which can be corrected by grinding without destroying the rotor blades.

Spin Tests

Actual spin tests were conducted in a vacuum pit using a Barber Stockwell 150,000 rpm air turbine. A summary of recent testing, along with a failure analysis, is shown in Table 22.

Table 22. AGT Rotor Spin Test Results.

Rotor No.	Failure Speed, rpm	Analysis
55	98,000	Quill failure*
65	95,600	Hub burst
66	95,000	Hub burst
69	88,480	Blade failure, rotor destroyed

***Quills previously used were soft steel. After tests on rotor 55 they were replaced with quills hardened to R_c 45.**

This series of tests reflects an increasing uniformity in speed and type of failure. All rotors in this group were crack free, based on visual and zyglo inspection, and fully bladed. All were cast with the same techniques, by the same people, from RM-20 SSN material. Although previously tested rotors have failed at higher speeds, they were not fully bladed and blade failures predominated. Most the of the former tests were done on rotors of SRBSN material.

A higher percentage of these latest test rotors failed through hub burst, reflecting the higher quality of the blades. This suggests that the larger flaw size of the cast rotor material (as compared to test bars) is now controlling the ultimate failure speed of these rotors. All of the RM-20 rotors at this point in the program were pressureless sintered with the 36-hour hold. As shown earlier in Table 20, this long hold at peak temperature resulted in increased porosity and strength lower than obtained for test bars. HIPping RM-20 rotors is expected to reduce this porosity and improve spin test results.

APPENDIX B -

STANDARD OIL (CARBORUNDUM) UNIQUE WORK ADVANCED GAS TURBINE (AGT) TECHNOLOGY DEVELOPMENT PROJECT 1986 ANNUAL TECHNICAL PROGRESS REPORT

1.0 INTRODUCTION

This report, submitted by the Structural Ceramics Division of the Standard Oil Company, presents the annual Progress Report for the AGT101 program. Work reported herein covers the period of July 1, 1985 through June 30, 1986. Standard Oil continued development activities throughout this period as a subcontractor for the Garrett Turbine Engine Company (Garrett).

Work focussed primarily on four static structures made of sintered alpha silicon carbide: combustor liners, regenerator shields, combustor baffles and transition ducts (Figure 97). Early during the report period, the workscope included the development of dimensionally acceptable stator segments. This effort was terminated during the first half of this period due to unresolved dimensional problems and resources were reallocated on the fabrication of transition ducts as a higher priority component. A dual path fabrication approach was chosen for the transition duct. Isopressing and advanced green machining was continued to satisfy ongoing delivery requirements. In parallel, injection molding was initiated as a near net shape process and the preferred solution for fabricating a configuration with nonsymmetrical features. Injection molding was also the forming technique chosen for the combustor baffle. The remaining two components, combustor liner and regenerator shield were isopressed and green machined. All of the components were sintered on individual high temperature mandrels and then submitted for NDE in the as-fired state and after final grinding.

Routine NDE for initial inspection after sintering consists of visual examination, density determination, microfocus X-ray, fluorescent dye penetrant inspection and dimensional evaluation. Final NDE is accomplished by visual examiniation, a second fluorescent dye penetrant inspection, and a verification of ground dimensions.

A summary of all component deliveries for the report period is given in Table 23. Table 24 shows the actual shipment dates for each of these components.

2.0 COMPONENT/PROCESS DISCUSSION

2.1 Combustor Liner

Deliveries for the report period consisted of 18 combustor liners and 3 shorter combustor rig liners. All combustor liners were made by isostatically pressing tube stock and machining in the green state. Initial green dimensions were based on a shrink factor previously determined when the powder lot was qualified. The first green machined component was then test sintered and dimensioned. These results were then used to adjust the shrink factor, if necessary, for the remaining tube stock.

After sintering and initial NDE each unit was cut to length, inspected, and annealed. The last six shipments required grinding on the O.D. to meet new print specifications which were received after components had already been processed through green machining.

All delivery requirements for FY1986 have been completed. No failures have been reported by Garrett on rig or engine tested components.

Figure 97. AGT101 Components for FY1986.

Table 23. Component Deliveries.

Component	Delivery	Serial Numbers	Drawing	Condition
Combustor Liner	18+3*	5-117 - 6-137	PA3609611 PAP255863* PAP254020 PA3611755-2 Mod.	Ground
Regenerator Shield	10	5-111 - 6-120	3846154-Rev. A 3846154-Rev. B	Ground
Combustor Baffle	6	5-128 - 6-133	PA3609614-A PA360916-A	3 as-fired/ 3 ground
Transition Duct	6	5-120 - 6-125	PA3609649 Mod. PA3610213-B-2	4 w/brazed ports 1 w/TC holes, diverter 1 integral ports, diverter

Table 24. Delivery Time Table.

	1985						1986					
	July	Aug	Sept	Oct	Nov	Dec	Jan	Feb	Mar	Apr	May	Jun
Combustor Liner		2		4+1*	2+2*		2		2	4	2	
Regenerator Shield			2		2				4		2	
Combustor Baffle				3	1	1				1		
Transition				4				1+1**			1	1***

*rig components, **rework, ***display

2.2 Regenerator Shield

Six components were delivered during this period completing FY1986 requirements. All regenerator shields were fabricated similar to the combustor liners using isopressed tube stock and machining in the green state. An attempt was made to decrease the grinding time by incorporating the I.D. radius feature during green machining. Slight deviations in shrinkage from piece to piece, however, resulted in a more complicated set-up for final grinding. After the first four deliverables, the decision was made to return to the initial green machining format using a tube blank with constant wall thickness. After sintering and as fired Q.C. each unit is ground to length, and the various O.D. features and the large I.D. radius are incorporated. Components have been screened in several rig and engine tests without any failures.

2.3 Combustor Baffle

Six combustor baffles were delivered during the report period. The components were made by injection molding a bimodal compound which sinters to about 90 percent of theoretical density. This specific compound was chosen because of the good test results achieved on slip cast components of similar density and composition.

Previously supplied combustor baffles were produced by drain casting using a water-based bimodal SiC slurry. The drain casting method was eventually abandoned in favor of an injection molding approach with its better net shape and high volume capability. An advanced design iteration incorporated variable wall thicknesses which were easily included in the injection molding tool, in contrast to the casting approach which would have required substantial green machining to achieve the desired features.

The injection molding tool was modified to produce components to the new PA3609614 Drawing. Two different injection molding machines of different sizes were used to mold components. The in-house available 250-ton horizontal screw machine had only marginal clamping pressure. To complement in-house capabilities, custom molding houses were investigated and three outside molding trials were conducted during the past year. The machines used were of 375-ton capacity. One of these molding trials was cut short because of inadequate controls and sensitivity of the machine. The few components molded during this trial exhibited severe flow lines and burn marks.

Two different bimodal compounds, P2 and P5, were used for the molding trials conducted during this period. During the previous year, a third compount P6 had been investigated as a possible candidate. MOR bars of all three compounds were fabricated and ground. Standard MOR testing was completed early during the report period. The data are summarized in Table 25.

The MOR data indicate no significant difference between the three compounds. However, compound P6 exhibits a higher density as a result of increased sintering shrinkage than either P2 or P5 rendering the compound unsuitable for the current mold.

Each molded combustor baffle was processed through a sprue removal step in the green state. This procedure was optimized during the last quarter of this period. Difficulties were experienced during this step which were attributed to the chuck arrangement and also to the process sequence e.g., before or after binder bake out. The optimized procedure provides sufficient green strength to avoid cracking during handling.

Combustor baffles processed through sintering during the first half of the report period showed some degree of flow profile distortion. Several iterations of firing mandrels were investigated before achieving good consistency of the current profile.

Of the six combustor baffles supplied during this period, the first four were shipped in the as-fired state. The remaining two were ground on the stacking dimensions and the gas

Table 25. Evaluation Of Bimodal Injection Molding Composition.

Compound	No. of Specimens	Density range, g/cm^3	Room Temperature MOR, ksi	Std. Dev, ksi
P2	23	2.86-2.95	42.77	6.98
P5	20	2.87-2.94	40.96	7.35
P6	5	2.92-3.00	43.13	3.72

flow profile. Two additional sintered units were submitted for grinding and eleven in-house molded parts are currently in green machining for sprue removal.

Two of the injection molded units have been thermally screened to date, both passed the test successfully. This performance suggests that the injection molded baffles are of comparable quality as the previously supplied slip cast components which have successfully passed several rig and engine tests.

2.4 Transition Duct

A dual fabrication approach was pursued for the transition duct. Isopressing/green machining and injection molding were the two paths which were investigated in parallel for the latest design iteration (drawing PA3610213 - Modification B, Configuration 2). This design has two major changes from previous designs: a 180-degree flow diverter and three integral thermocouple port holes. The addition of these features were initially thought to make it impractical to fabricate transition ducts by green machining. Injection molding was considered the prime approach for producing the latest configuration early in the period.

Nine transition ducts molded during the previous report period were sintered to approximately 98 percent theoretical density. However, the overall shrinkages were lower than expected. A dimensional analysis was conducted for this group of transition ducts with special emphasis on the shrinkage behavior of the O.D./I.D. contour profile. Minor machining stock is required on all stacking dimensions. The necessity became evident to incorporate shrinkage factors which varied slightly with direction.

The tool was revised before the end of 1985 and a molding run on a 1000-ton horizontal screw machine was conducted at an outside vendor yielding 79 components. All units were molded with solid thermocouple bosses. This change was made from the first molding trial when port holes were molded directly into the bosses and weld lines occurred.

An initial group of 20 transition ducts was designated for evaluation and optimization of the binder removal process and the presinter treatment procedure. In addition, adjustments were made to process some of these parts through sintering and conduct in depth dimensional analysis. This lot consisted of components which were produced early during the molding trial when the packing pressure and the ejection mechanism had not been optimized. Unexpected difficulties were experienced during binder removal. Over 50 percent of the components exhibited cracks after bake out. The majority of rejects were located in one specific bake oven. Additional investigations were conducted, which showed that the standard loading procedure was inadequate.

Special measures had to be implemented to allow for sufficient support of the components during binder bake out, also to accommodate the thermal expansion/contraction movement during the bake cycle.

Following the binder removal procedure the components were subjected to a presinter preparation. Units exhibited an unusual amount of fragility and susceptibility to blow-outs. Steps were implemented to modify the cycle and a revised procedure was implemented. An additional group of 20 transition ducts was processed using the revised procedure.

Five transition ducts have been processed through sintering during the report period. They showed some flow lines and cracks in the push-out pin locations. The units exhibited good densities and showed good consistency on the flow profile. Evaluation of the stacking dimensions showed that only marginal stock was present on these initial components.

Additional transition ducts, which are of better molding quality than the first two groups, are currently in binder removal. These units will be used to evaluate all the newly revised procedures. These changes are expected to yield initial test pieces which have sufficient grind stock by fine tuning the sintering cycle and by optimizing the fixturing. Detailed assessment of component integrity through fluorescent dye penetrant and microfocus X-ray evaluation will be conducted to assess the overall quality of the sintered components.

Based on a reevaluation of the two fabrication approaches and improved progress on the green machined transition ducts, priority was placed on green machining over injection molding to supply deliverables with an integral diverter and integral ports.

Two transition ducts with separate ports (inserted in the green state and then shrunkfit during sintering) were supplied during the previous report period. In both cases, the application of a high temperature braze after the initial shrinkfit was necessary to reduce joint leakage at 5 psi to an acceptable level. Both of these units were successfully screened at Garrett. This assembly approach led to problems in producing crack free components with no leakage.

A decision was made early in this report period to sinter the transition ducts and the inserts separately, machine each individually to a close fit, and attach the ports during a subsequent brazing step. Experiments were conducted to determine the optimium clearance and configuration of the joint. Four brazed assemblies were supplied for testing in October 1985. Three of these brazed assemblies were tested and each of these cracked near one of the ports. Subsequently, tests were conducted to assess the strength of SASC with and without a thin layer of braze applied. Standard size MOR bars (1/8 x 1/4 x 2 inch) were used for a room temperature 4-point bend test. The tests revealed that MOR bars, which had a thin layer of braze applied, exhibited 30-50 percent lower strength than comparison samples. As a conclusion of this brief study, it was decided to rework the fourth unit. The brazed ports were removed and replaced with separate close fitting inserts. This unit subsequently passed thermal screening.

In a parallel activity, the green machining program was revised to incorporate the 180 degree diverter for improving overall rig and engine performance. The first unit with this additional feature was completed February 1986. The component was delivered in the as-fired state with port holes.

Figure 98 illustrates the sequence of steps which are necessary to produce the transition duct by isopressing/green machining. An oversized tube blank is produced using a rubber bag to shape the outside and a steel mandrel to form the inside. This blank is then preturned and finally green machined using a CNC lathe and mill. A large amount of green machining stock has to be removed to produce the desired configuration and clearly shows the built-in inefficiencies of this process. As a

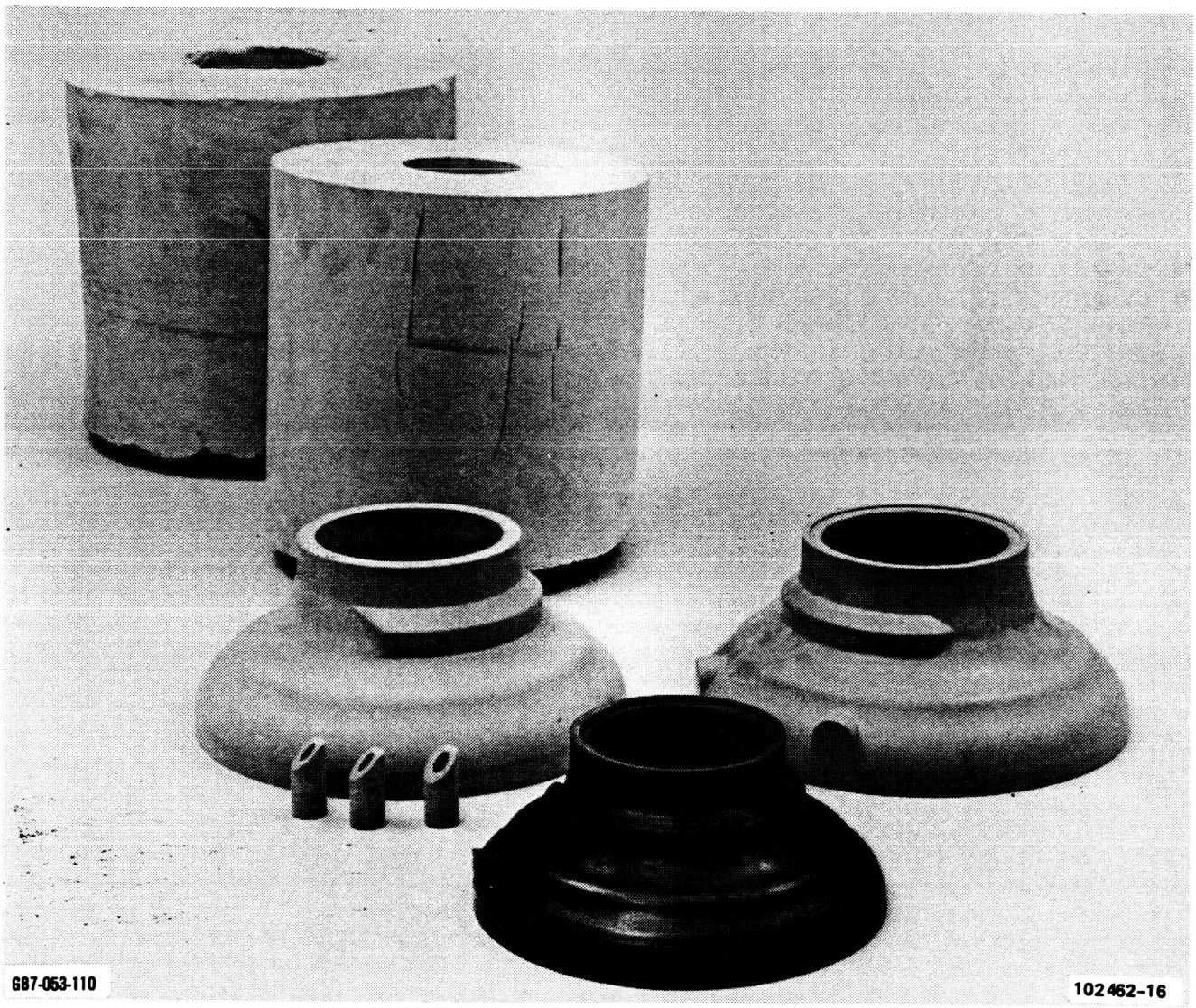

Figure 98. Transition Duct - Fabrication Sequence.

contrast, the transition duct on the right depicts a near net shape injection molded transition duct in the as-molded state after sprue removal.

In an effort to eliminate loose fitting ports, as well as brazed or shrunk-fit inserts, additional empahsis was placed on obtaining a green machining program which allowed for integral ports. The first unit with all the features of Drawing PA3610213-B-2 completed green machining and sintering at the end of the third quarter of the report period. The unit was ground inspected, annealed, and shipped in May 1986. A second machined integral unit which had a visual defect on the O.D. was shipped to Garrett for evaluation. A third unit is currently in green machining. Additional green tube stock has been pressed to meet delivery requirements of FY 1986.

Figure 99 represents a sintered transition duct made by isopressing and green machining. The unit contains all features of the most recent drawing and only minor touch up grinding is required.

2.5 Turbine Stator

Work continued on individual stator segments through the first half of the report period. Components molded during the previous period were processed through sintering and several fixturing techniques were investigated, however, some distortion on the platforms near the leading edge could not be eliminated.

Several sets of stator segments supplied during the previous period were thermally screened. Failure analysis conducted on screened components that developed trailing edge cracks indicated no discernible defects in the fractured regions. Detailed stress analysis identified a maximum principle stress of about 43 ksi in the respective region. Subsequent tests conducted on stator segments with a cut back trailing edge were positive - no fractures observed. However, the dynamic performance was severely reduced. Development work on this component was put on hold at the end of 1985 because of fabrication difficulties as well as design/performance issues.

3.0 SUMMARY

Standard Oil continued its subcontract development work on several hot flow path static structures for the AGT101 program with all components manufactured from sintered alpha silicon carbide. FY 1986 requirements were completed for two of these components, the combustor liner and the regenerator shield. Combustor baffle deliveries are expected to be completed in August 1986. Significant progress has been achieved in fabricating dimensionally reproducible transition ducts with integral features, and further effort continues on the fabrication of this component using two parallel forming approaches.

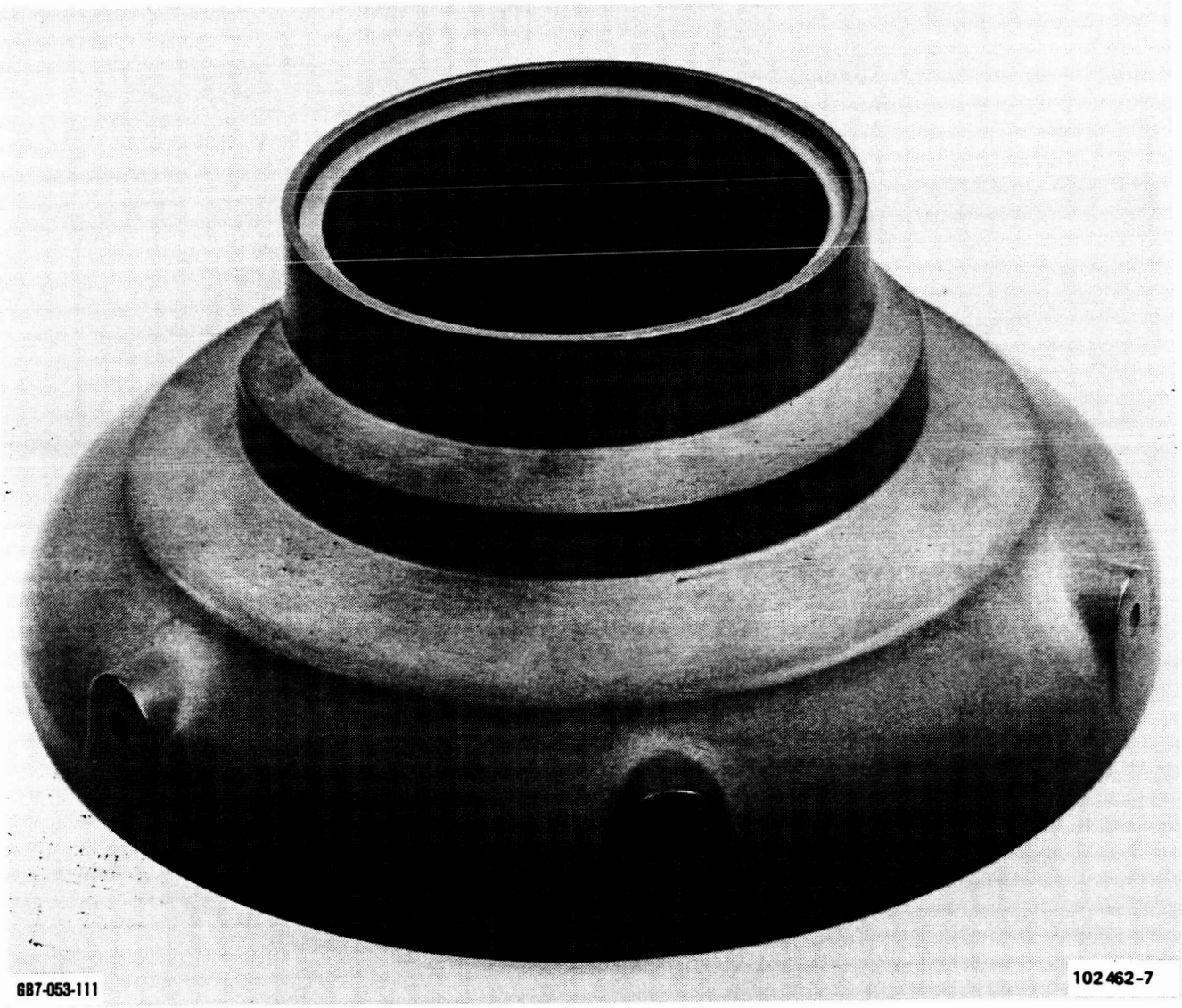

Figure 99. Integral Isopressed/Green Machined Transition Duct.

This Page Intentionally Left Blank

APPENDIX C

AIRESEARCH CASTING COMPANY
ADVANCED GAS TURBINE (AGT)
TECHNOLOGY DEVELOPMENT PROJECT
1986 ANNUAL TECHNICAL PROGRESS REPORT

1.0 INTRODUCTION

This report, submitted by AiResearch Casting Company (ACC), will cover the efforts of ACC in support of the Advanced Gas Turbine (AGT101). The program was conducted as a subcontract to the Garrett Turbine Engine Company (Garrett), and the report will cover ACC's materials and fabrication development efforts. These efforts are concerned with the materials development and fabrication of rotors and ceramic structures by slip casting and the fabrication of stator vane assemblies by injection molding.

2.0 SUMMARY

Early in the beginning of this reporting period, the program was restructured to obtain a better understanding of the potential impact of raw materials and tooling changes on casting quality. Side-by-side casting and further processing was used with the same slip in various tooling design configurations. This effort suggested that the A-2 generation rotor design was most suitable for the development of a documented fabrication process specification.

Considerable effort was directed toward isolating the persistent discoloration/segregation problem. Tests included casting both test blocks and rotors with variations such as pressure casting, adding plaster to blade edge, inverted casting plus additional plaster in the shaft area. Several other variations were evaluated which included low to high viscosity range, higher percent solids, binder additions and changes in amount and techniques in adding of sintering aids.

A second-stage evaluation was inaugurated which involved the preparation slip batches of sufficient quantity to cast five rotors for each selected material/process combination. A total of seven material/process combinations were selected to insure that all castings produced from the same material under identical processing conditions could be evaluated with more meaningful results. A total of 94 rotors were slip cast at ACC during this reporting period.

A wide variety of casting iterations were evaluated in an effort to produce static component structures. These iterative casting evaluations substantiated that even small surface and sub-surface porosity and flow lines were detrimental in the final part used in testing. A total of 32 turbine shrouds, 30 transition ducts and approximately 14 backshrouds were cast during this reporting period. Earlier in the year, five baffles were fully processed and shipped to Garrett. Thirteen flow separator housing seal rings and eight, 3-lobe, 0.050 inch deflection wave springs were also shipped.

RBN 124 baseline injection molded stator vanes were processed. Nine of these were rejected, some visually (30X), some after X-ray. Eighteen passed inspection and were shipped to Garrett.

In an effort to improve the high temperature strength of injection molded stator vanes, the blended material (SRBSN) approach was evaluated. The results were promising as indicated by sintered/HIPped densities ranged from 3.22 to 3.24 g/cm^3 which is higher than 99 percent of theoretical.

3.0 ROTOR MATERIALS AND FABRICATION DEVELOPMENT

3.1 Productivity

A total of 94 rotors were slip cast at ACC during this reporting period. These cast rotors are categorized as follows: GTE Si_3N_4, 49 rotors; UBE Si_3N_4, 18 rotors; Starck H-2, 3 rotors; Si_3N_4 with Si, 24 rotors.

3.2 New Restructuring Plan

In September 1985, the program was restructured to strengthen both casting as well as support activities. All processing steps were fully documented and controlled. The new program was aimed at understanding the impact of raw materials and tooling changes on casting quality.

The plan was to perform side-by-side casting and subsequent processing using the same slip in the various tooling and design configurations to determine the sensitivity of processing to each tooling approach. Yearly trends suggest that B1 (water soluble wax pattern, closed blades) approach generally leaves hollow blade tips and the B2 (water soluble wax pattern, open blades) approach produced excessive blade flash. A B2 (water soluble wax pattern, modified open blades) significantly reduced the excessive flash and associated blade damage during subsequent processing. Figure 100 shows differences between A and B generations.

No obvious differences were found between A1 or A2 rubber pattern configurations (14.5 percent and 17.0 percent shrinkages, respectively) on processing yield. Continued processing of A2 generation rotors suggest that the A2 tooling is the most suitable for the development of a documented rotor fabrication process specification.

3.3 Technical Progress

3.3.1 Contamination

A series of tests designed to isolate the persistent discoloration/segregation problem

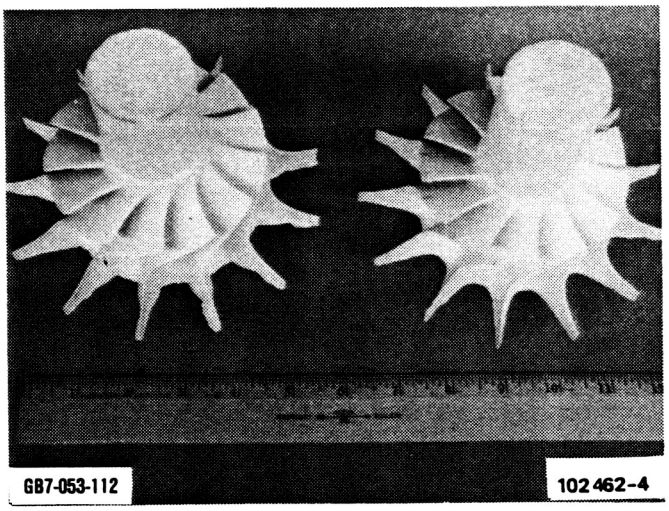

Figure 100. Differences Between A and B Generations.

was initiated. Tests included casting test blocks and rotors with variations such as pressure casting, additional plaster area on blade edge region, casting with dome side up (inverted) plus additional plaster in the shaft area. Figure 101 shows discoloration evident in a test block and Figure 102 shows the setup arrangement used for inverted rotor casting.

These variations do affect the location of the discoloration indicating a segregation or migration of additives, fines or water-soluble compounds.

Additional experiments included casting with low to high viscosity slips and higher percent solids. Castings still exhibited discoloration.

Tests on sample blocks led to the casting of additional rotors to evaluate alternate deflocculants, binder additions and the isolation of sintering aids. Binder additions were suggested by Allied Corporate Research Labs. A rotor cast with 100 percent Si_3N_4 with no sintering aids evidenced no discoloration. Rotors cast with Y_2O_3 additions only appear to be discoloration free. Rotors containing Al_2O_3 only showed some degree of discoloration.

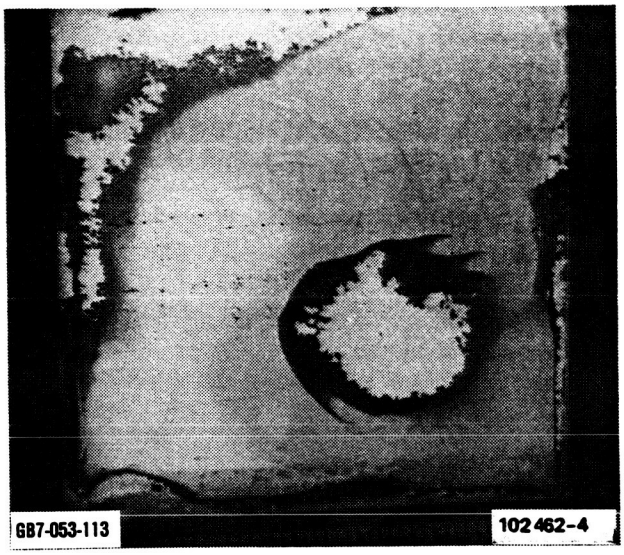

Figure 101. Test Block with Discolored Area.

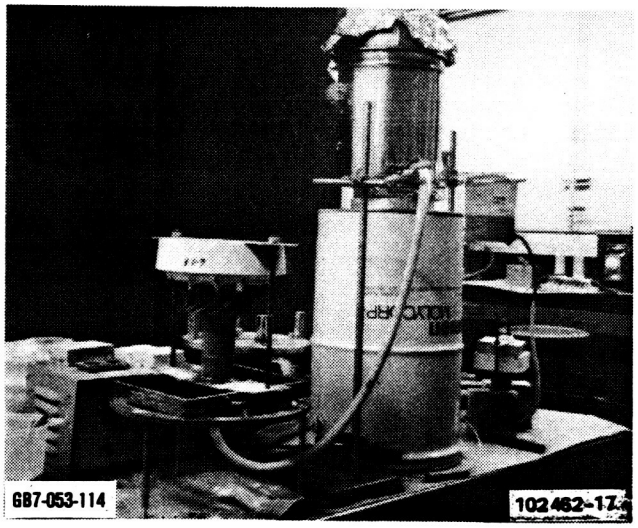

Figure 102. Setup for an Inverted Casting.

Alternate deflocculants were investigated. However, castings were not of good quality and results were not reproducible.

Alternate raw materials were also evaluated. A blend of Starck H-2 Si_3N_4 and Kemanord Si powders was cast into rotors and processed through nitriding. The blended materials consistently showed weight gains of 97-98 percent of theoretical. However, a group of five rotors cast with conventional casting, pressure casting, and inverted casting all showed discoloration on the blades.

UBE SN-E02 Si_3N_4, surface area (S.A.) = 2 m^2/g, UBE SN-E05 Si_3N_4, S.A. = 5 m^2/g, and blends of SN-E02 and SN-E05 were evaluated.

In March 1986, the first stage processing parameters trend/screening evaluation concerned with discoloration was completed. This evaluation included alternate raw materials, different levels of sintering aids (including no sintering aids), deflocculant types and concentrations, viscosity effect, casting techniques, methods of dispersing deflocculant, binders, and detailed chemical analysis of the discoloration problem. Some important processing trends and effects were identified. Based on these findings, a new, more focused program was formulated.

3.3.2 Second Stage Evaluation

The highlights of the second stage evaluation are summarized as follows:

A large slip batch (enough for casting 5 rotors) was prepared for each selected material/process combination. This is to ensure that all five castings are to be cast from the same material under the same conditions so that a more meaningful assessment can be made. A total of 7 material/process combinations were selected for evaluation.

- GTE SN502 (6 percent Y_2O_3 = 1 percent Al_2O_3 = 2 percent Avicel). The reduction of Al_2O_3 and the addition of Avicel (a binder) were found to reduce the discoloration.

  Result: Five presintered rotors showed no discoloration. However, due to high viscosity slip, the rotors had unfilled blade tips and cracks.

- Blended Si/Si_3N_4 (70/30). Conventional casting.

  Result: Nitrided parts exhibited 97-98 percent of theoretical weight gains. Discoloration on blades was present.

- Blended Si/Si_3N_4 (70/30). Pressure casting.

  Result: Same as above.

- Blended Si/Si_3N_4 (70/30). Inverted casting.

  Result: Same as above.

- Starck H-2 blended slip. This material showed low discoloration on rotor blades but was difficult to make into a consistent slip. A new procedure was recommended by Allied Corporate Labs. This involved preparing the slips of the Si_3N_4 and additives (Y_2O_3 and Al_2O_3) separately and then blending them together after adjusting them to a common pH.

  Result: Slip continued to be very viscous. pH adjustments and lower solids content did not show any improvement in slip viscosity. No castings were attempted.

- UBE (75 percent SN-E02/25 percent SN-E05) with conventional additives.

  Result: Rotors showed slight discoloration on blades. These rotors have a high presintered density (2.70 g/cc). Cracks on blades and dome occurred after presintering. Both conventional and very conservative presintering cycles were tried.

- UBE (75 percent SN-E02/25 percent SN-E05) with prereacted additives. Y_2O_3 and Al_2O_3 at 6:2 ratio was premilled then reacted at 1600C for 8 hours. Extensive reactions were observed as evidenced by a large amount of shrinkage (14 percent linear) and a significant color change. This prereacted material (billet) was crushed and milled and incorporated in UBE (75/25) by milling.

  Result: Rotors cast showed dark discoloration which turned light after presintering. One rotor which was cast with 50 psi pressure showed no discoloration on blades. Figure 103 shows rotors cast using conventional and pressure casting. Problems encountered were cracking on the dome and blades after presintering. Employing very conservative drying presintering cycles did not alleviate the problem. Figures 104 through 108 shows some typical particle size distribution and surface areas of some mill batches and raw materials.

In June 1986, studies were funded by IR&D in support of the rotor program in the area of development of high temperature materials. Test bar plates have been processed and ready for sinter/HIP. (1) Denka Si_3N_4 with 8 percent y_2O_3 + 3 percent ZrO_2; (2) UBE (75 E02/25 E05) + 8 percent Y_2O_3 + 3 percent MgO + 1.5 percent Ce hydrate; (3) Blended Si/Si_3N_4 (70/30) + 6 percent Y_2O_3 + 2 percent ZrO_2; (4) Si/Si_3N_4 (70/30) + 6 percent Y_2O_3 + 2 percent MgO.

Experiments were conducted to investigate techniques to enhance the casting rates in the bladed area. This was accomplished by coat-

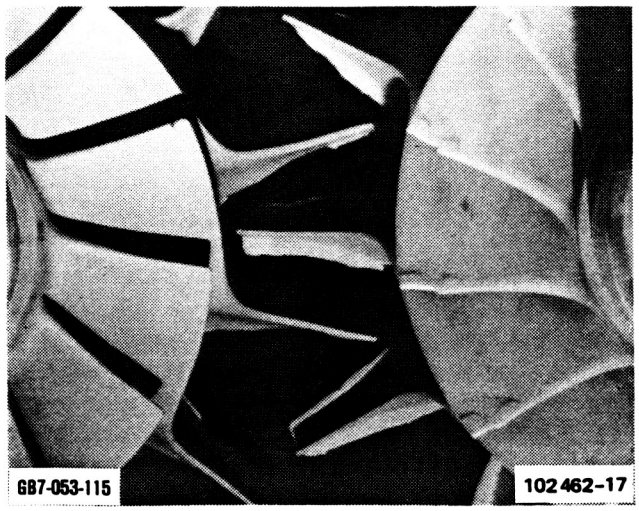

Figure 103. Rotor On Left Was Cast Using Conventional Techniques While Rotor on Right Was Cast With 50 psi Pressure.

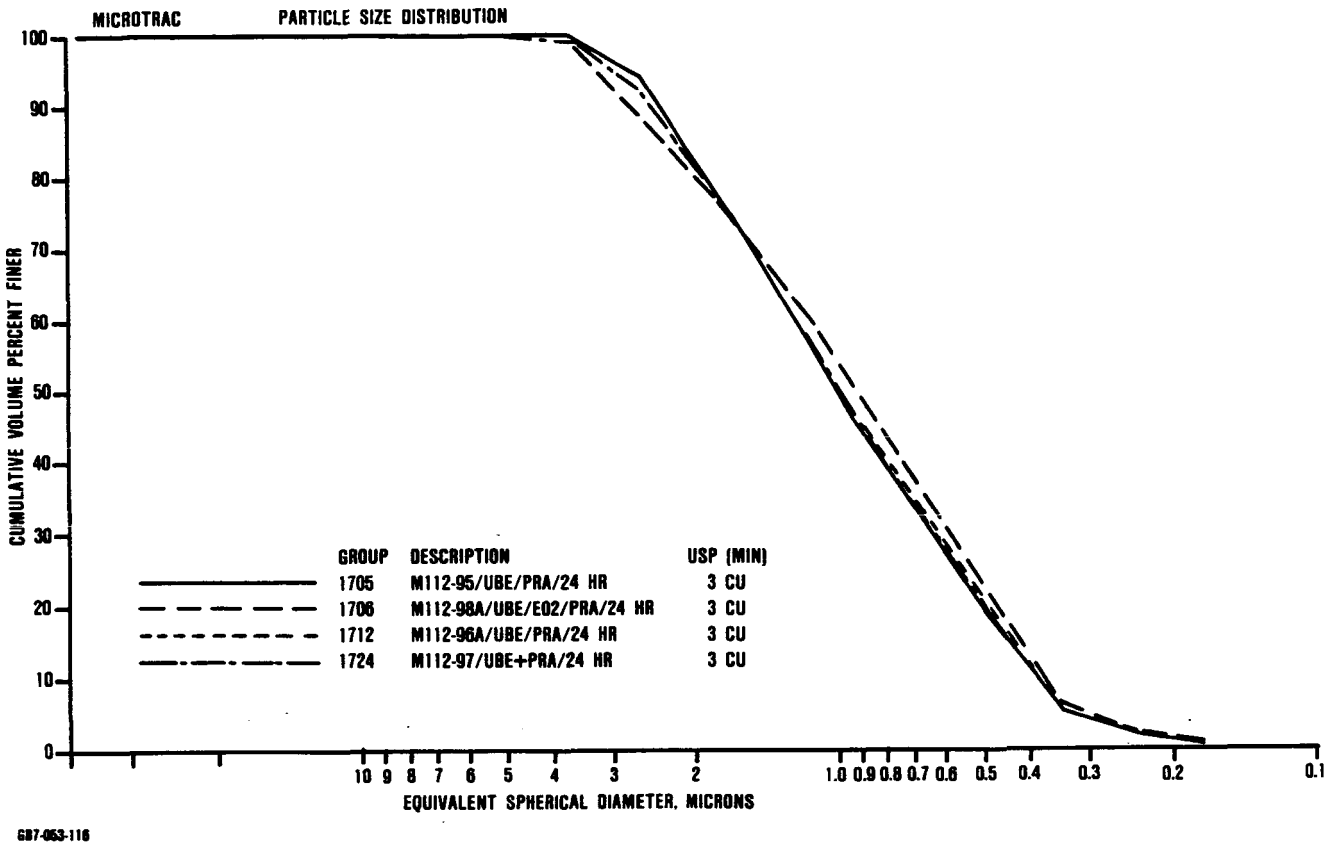

Figure 104. PSD Curves of Typical Mill Batches of UBE (75 E02/25 E05) + Prereacted Additives (6 Percent Y_2O_3:2 Percent Al_2O_3.

ing the inside surface of the wax mold with a layer of water absorbing material. One rotor was cast with a thin layer of boron nitride coating on the inside surface of the mold. After presintering, the coating appeared to be bonded to the cast rotor. Another was cast with a thin layer of plaster coating. After dewax, the blades had cracks although no discoloration was evident.

4.0 CERAMIC STRUCTURES

4.1 Turbine Shroud

Thirteen turbine shrouds were cast during the early months of this reporting period. Various casting, drying and prenitriding methods were evaluated in an effort to prevent cracking.

Casting 06036-01 was poured after soaking the plaster core in water for one hour prior to casting to prevent excessive thickness from forming in center before flanges were completely cast.

Casting 06136-01 maintained the use of the rubber top center core which was coated with petroleum jelly to prevent sticking and facilitate core removal. The rubber top center insert was sprayed with a coating of boron nitride for casting 06186-01. It was determined that sticking of slip to any nonabsorbent surface created a problem in removal of

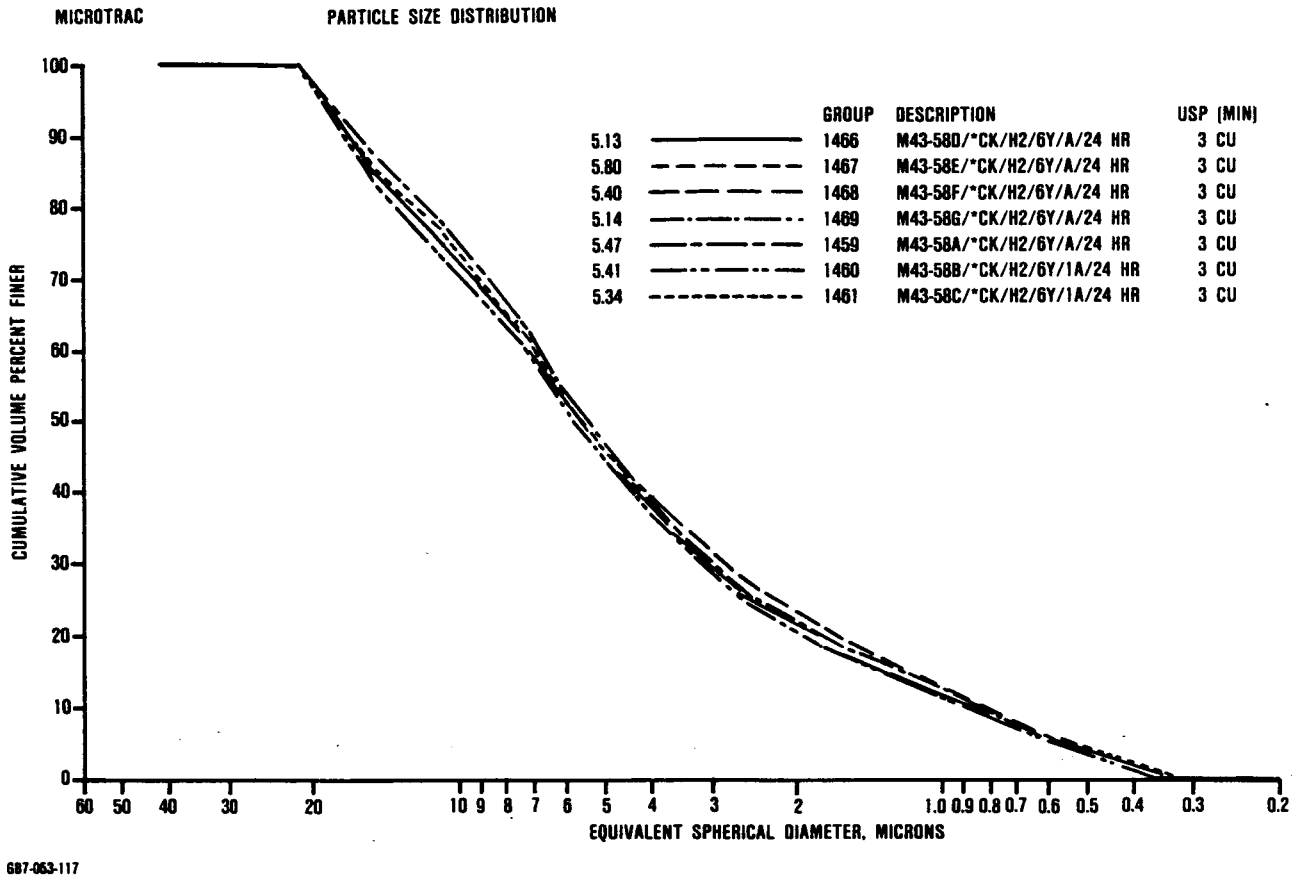

Figure 105. PSD Curves and Surface Area of Typical Mill Batches of Starck H-2 + 6 Percent Y_2O_3 2 Percent Al_2O_3.

inserts. Therefore, a plaster top center insert was made and used in place of the rubber coated mandrel.

Several castings of each of the above iterations were made to total eleven castings. Seven turbine shrouds cracked, three in mold, five in drying. Three shrouds were prenitrided and observed to have cracked during the prenitriding.

Two additional shrouds, S/Ns 826 and 826, were shipped to Garrett. All of the above shrouds were fabricated to the design in process prior to the start of this reporting period. Just prior to this, a design change was made which required new tooling for plaster molds. The new, near net shape plaster mold components and non-porous mold insert was received in April 1986. Additional modifications were required in the gating area and rubber liner. Initial castings revealed several problem areas such as flow lines and sticking to the rubber insert. Figure 109 shows the result of the adhesion to the insert which caused breaking of the shroud during insert removal. Other iterations with respect to casting technique were evaluated as listed below.

a. Top plaster ring replaced with wood ring with feed holes over each flange location.

b. Introduced registration plugs for alignment of bottom plaster insert with top rubber

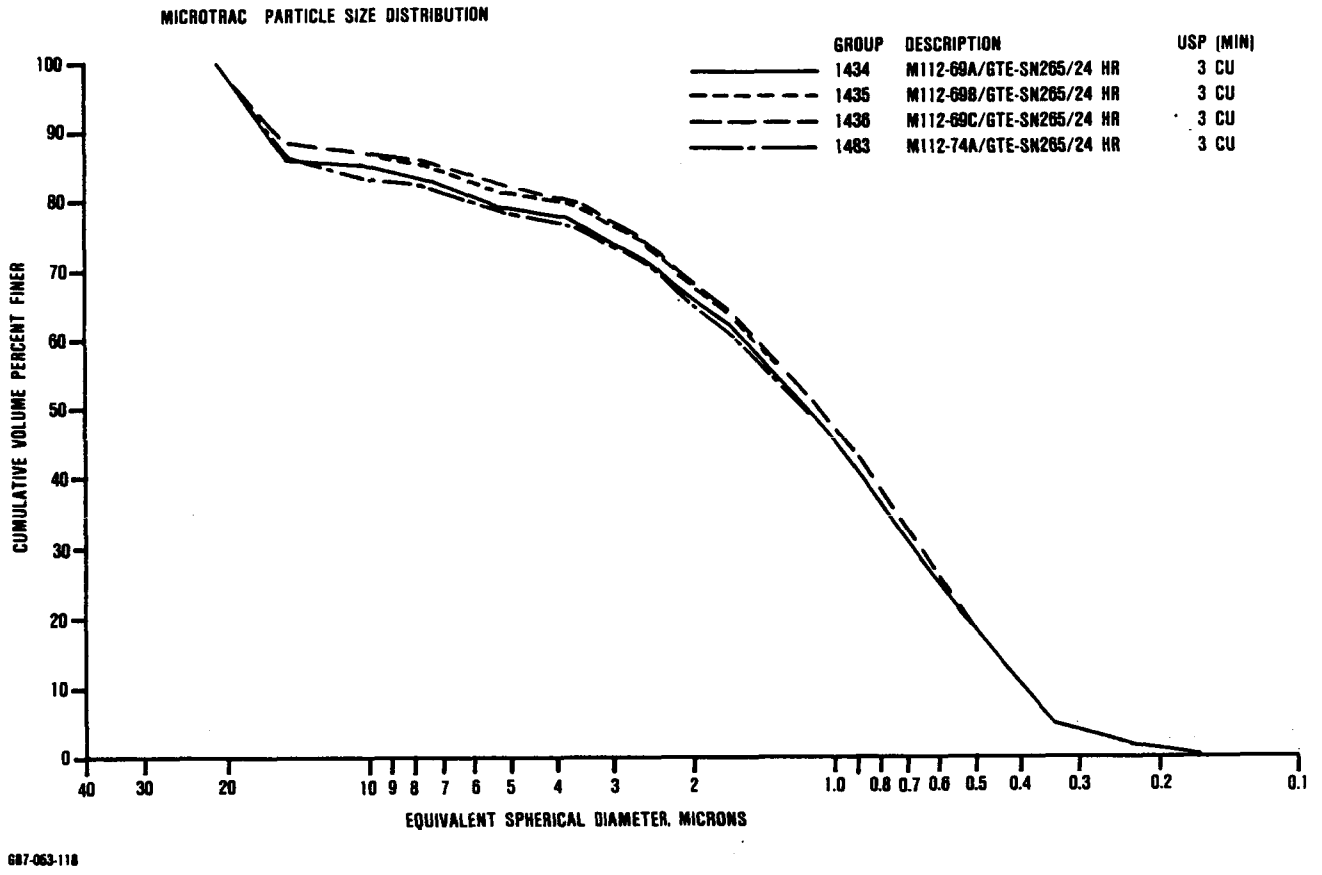

Figure 106. PSD Curves and Surface Area of Typical Mill Batches of GTE + 6 Percent Y_2O_3 + 1 Percent Al_2O_3.

coated mandrel made in both plaster and metal. Figure 110 shows a section of a casting with the metal plug in place. It can be seen that with the full plug air is entrapped beneath causing incomplete fill of the casting.

c. Metal registration plug sliced into rectangular shape with ends radiused to fit center hole in rubber mandrel. See Figure 111.

d. Bottom of insert plaster was machined in order to be centered. See Figure 112.

e. Top ring removed (not used during casting).

f. Casting normal[1] position feeding slips from flange area and through opening in center metal registration plug.

g. Mold filled with metal registration plate in place on plaster base insert with slip almost up to bottom of registration plate. Place rubber coated mandrel into position displacing slip, then topping off to desired flange level.

h. Drain cast mold without rubber coated top center mandrel. Addition to plaster base insert with plaster cylinder registered to insert to bring level up to flange height. See Figures 113 and 114.

Of all of the above, drain casting appeared to be the most promising technique since it

(1) Part cast with flange (large O.D.) up and small diameter down.

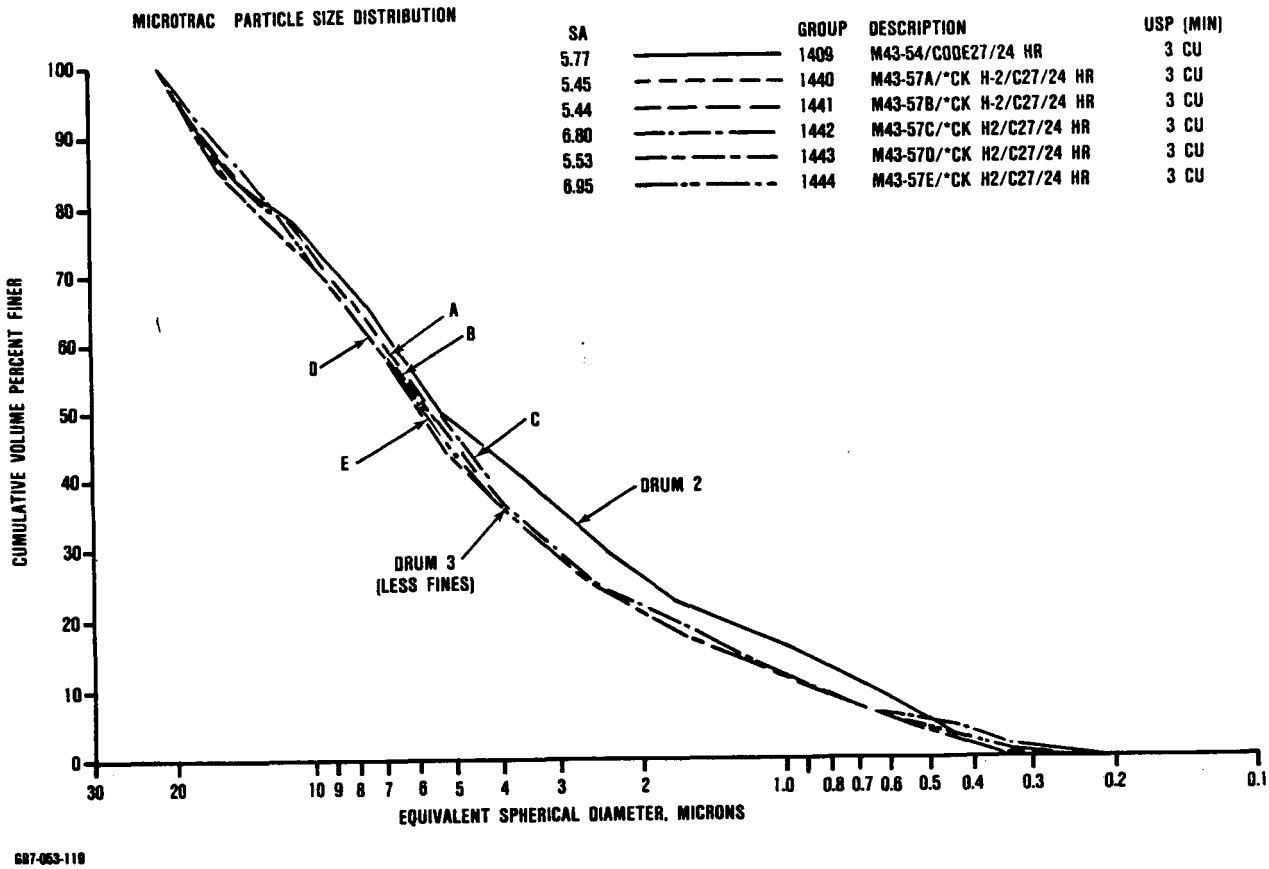

Figure 107. PSD Curves and Surface Area of Typical Mill Batches of Si/Si_3N_4 Blended Material.

eliminated the flow line and sticking of non-porous surfaces. However, the additional cross-sectional thickness which resulted with the elimination of the rubber coated center insert created other problems. Cracking of parts during drying and prenitriding, as well as added machine stock to be removed, became critical.

Drying of large, slip cast components, especially those with non-uniform wall thickness, proved to be one of the more crucial steps in processing. Extensive evaluation of drying and prenitriding cycles was conducted. It has become apparent that components such as the turbine shroud and transition duct must remain in the plaster mold after casting for a length of time sufficient to achieve good green strength. Subsequent to removal from the mold, it was essential that the casting be permitted to dry slowly and completely before attempting to prenitride. Several techniques have been used which include humidity oven drying, drying under an enclosure, subsequent exposure to air in a warmer, drier air, slowly heating in an oven over a long period of time to finally just exceed the boiling point of water and, also, allowing the part to remain in vacuum for several days just prior to prenitriding.

Although several other heavy wall components survived during drying and prenitriding, the turbine shroud continued to present cracking problems. Even shrouds that appeared to be crack free after drying, cracked during

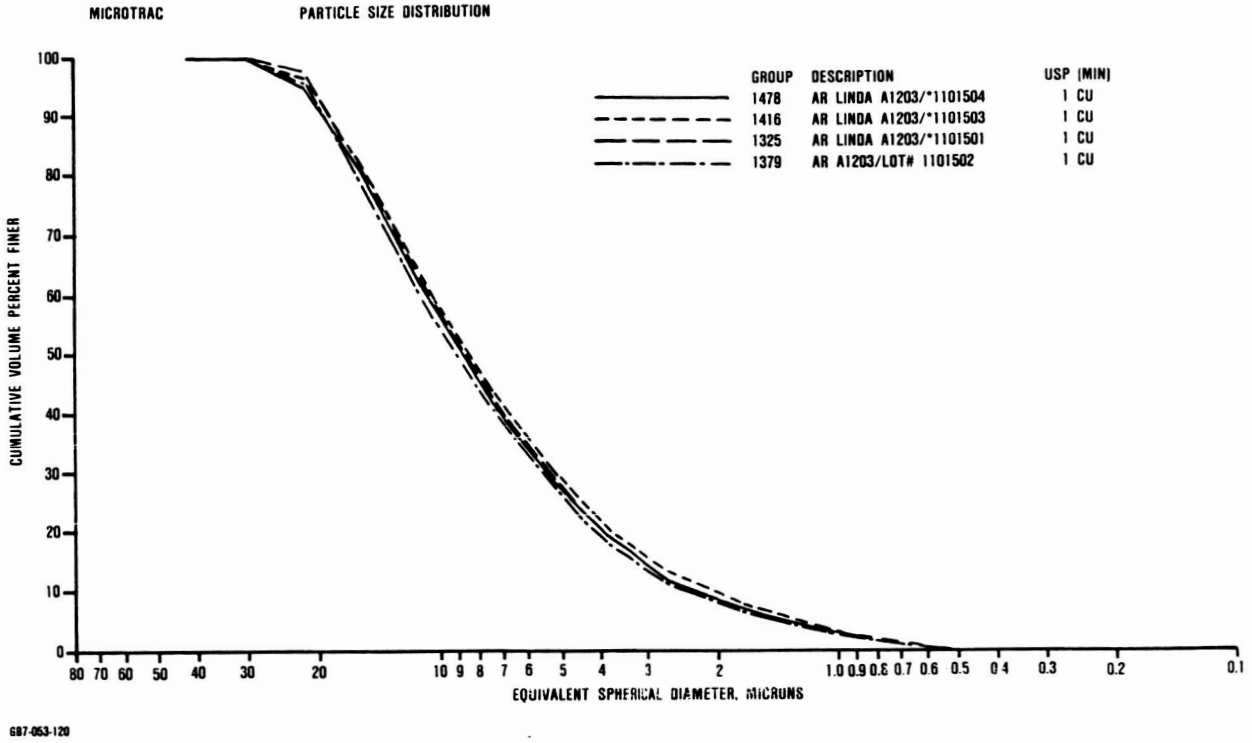

Figure 108. PSD Curves and Surface Area of Various Lots of Al_2O_3.

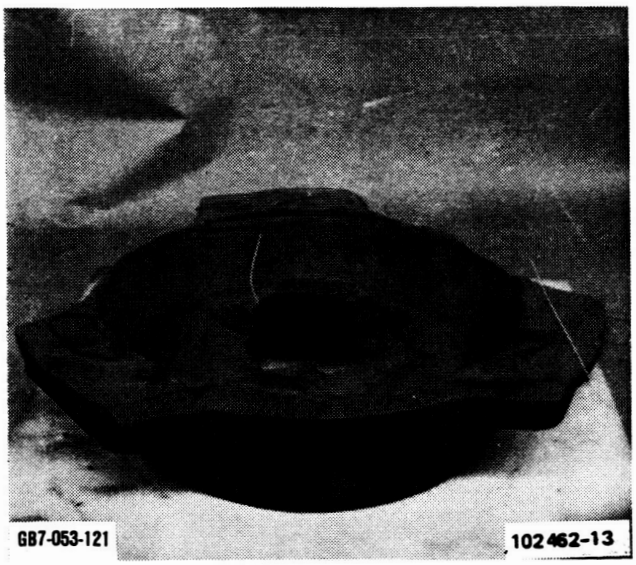

Figure 109. Breaking of Turbine Shroud Shown After Removal of Rubber Coated Mandrel.

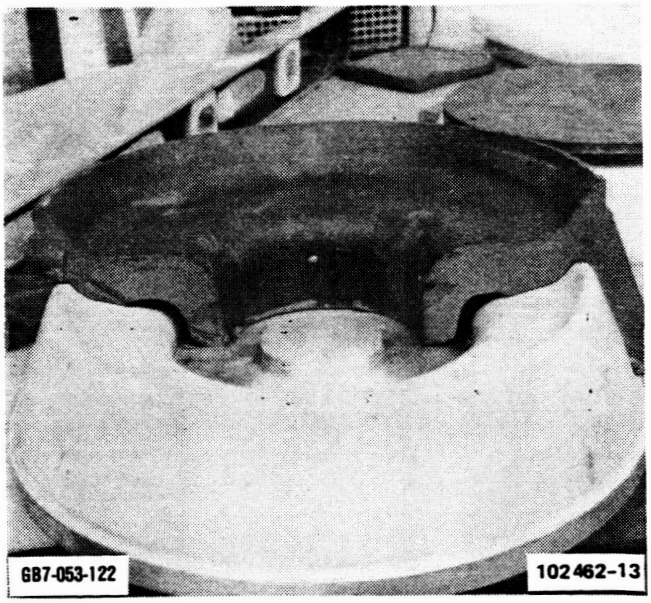

Figure 110. Section of Casting Showing Voids Due to Entrapped Air Caused By Full Registration Plug.

Figure 111. Metal Register Cut to Permit Air Escape and Additional Casting Into Center.

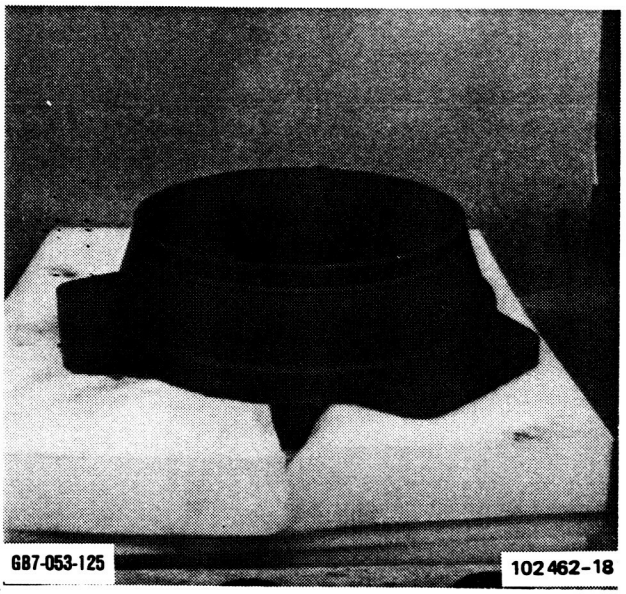

Figure 113. Plaster Contact Face of Turbine Shroud Casting.

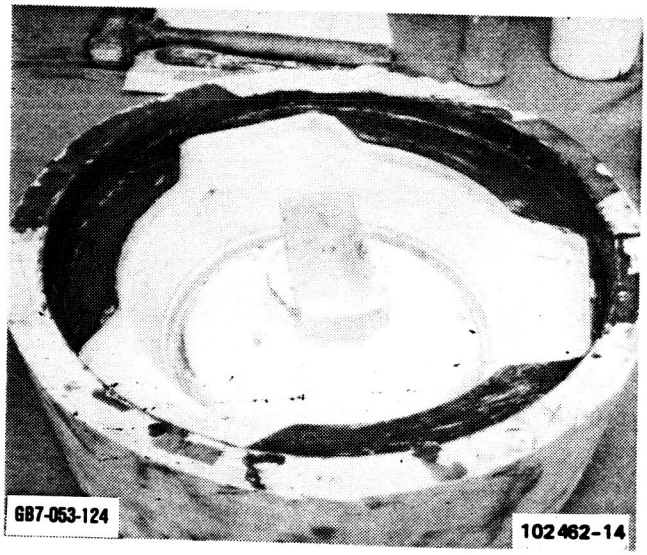

Figure 112. Plaster Mold With Metal Register In Place On Lower Plaster Insert.

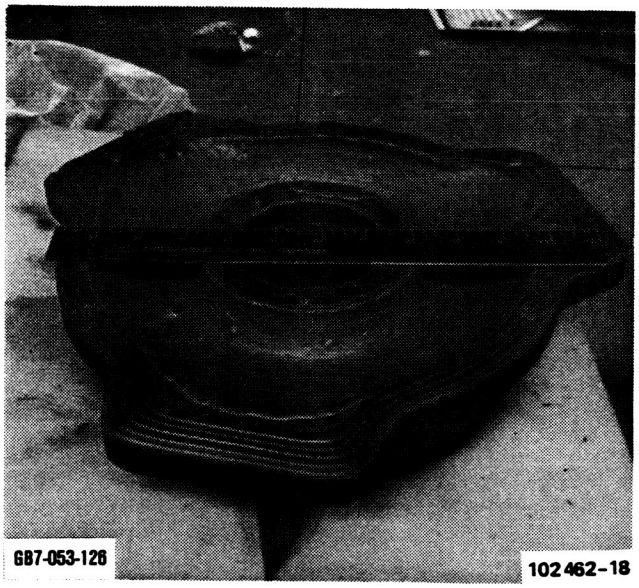

Figure 114. Drain Cast Surface Showing Excess Stock.

prenitriding. Consequently, alternate prenitriding cycles were evaluated. The prenitriding cycle, PN-15, which had worked successfully up to this time, was a ramp up to temperature in eight hours, held at temperature for eight hours and controlled cool down in eight hours. When drain casting was initiated, this cycle produced cracking in all components, i.e., turbine shroud, transition duct and backshroud.

The cycle which appeared to be optimum consists of maintaining the parts under vacuum for two days prior to heat-up to 250F, hold for six hours at 250F, 32-hour ramp to 1700F, and 32-hour controlled cool down to room temperature. In addition, it was found that setting the part in a bed of silicon powder eliminated the problem of point loading which occurred when placing the part on setter pins.

As work progressed, one turbine shroud survived flaw-free through prenitriding. However, further work was not authorized and this part was not machined or finally nitrided.

4.2 Transition Ducts

Approximately 30 transition ducts were cast during this reporting period. Six of these were fully processed and shipped to Garrett.

As with the turbine shroud the same problem areas were manifested with castings of the transition duct; flow lines, and sticking to the non-porous center insert. Iterations listed below ere evaluated.

a. Cast part in normal position with rubberized core and plaster core in place (large diameter in up position).

b. Casting poured in inverted position to allow slip to pour over rubber surface to eliminate flow lines. See Figure 115 and 116.

c. Vent slots cut into top of each vent port in plaster (inverted cast) to eliminate air entrapment on top of vent parts.

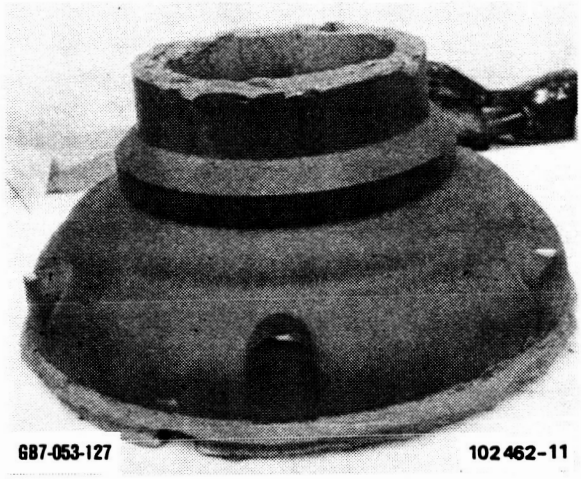

Figure 115. Plaster Contact Face of Inverted Casting.

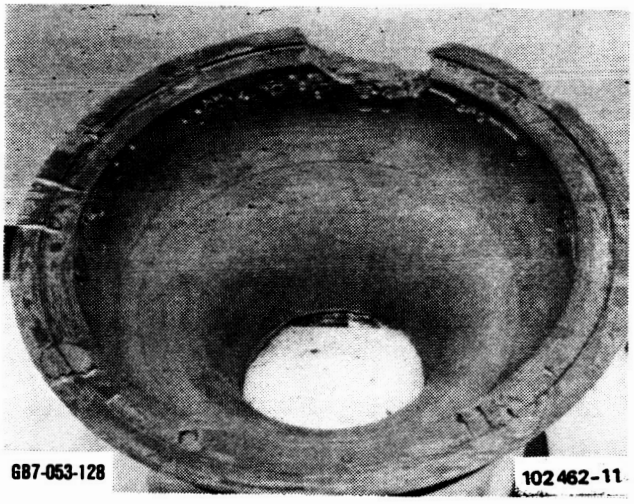

Figure 116. Inner Surface Showing Effects of Air Entrapment.

d. Plaster ring to fit within the I.D. of the plaster base to reduce the amount of casting surface of the normal 45 degrees wedge shape was fabricated.

e. Lubricate the rubber insert.

f. Drain casting was made without rubber insert. (Used 800 ml plastic beaker, coated

with vaseline, in bottom to reduce total slip use).

g. Extremely smooth plastic beaker surface locked in silicon casting in spite of vaseline coating of beaker at base.

Again, drain casting appears to be the most expeditious method for producing acceptable components. See Figures 117 and 118.

The duct shown in Figure 119 and 120 was successfully dried and prenitrided but has not been machined or nitrided.

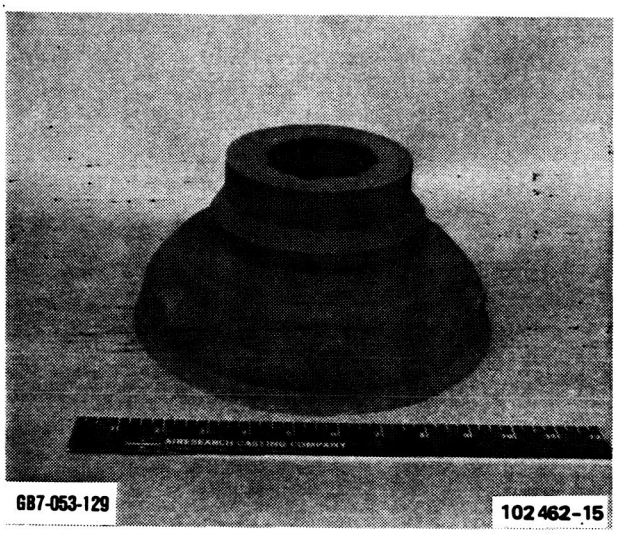

Figure 117. Drain Cast Transition Duct Showing Surface Cast Against Plaster Mold.

4.3 Turbine Backshroud

Although several backshrouds have been fully processed and shipped to Garrett, it was found that the primary difficulties encountered with backshroud castings have been flow lines and center line shrink. Efforts to eliminate these problem areas are listed below:

a. Bottom portion (drag) of one plaster mold coated with acrylic.

Figure 118. Drain Cast Transition Duct Showing Drained Interior Surface.

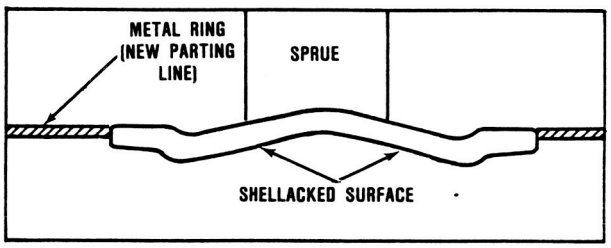

Figure 119. Gate In Cope-Drag Coated With Shellac.

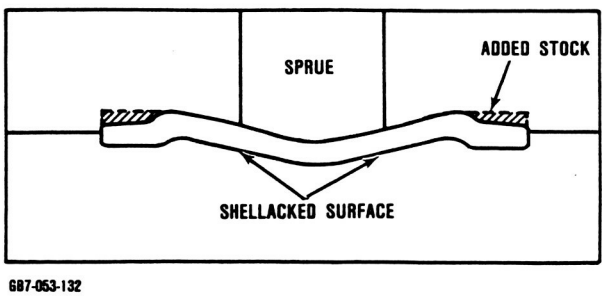

Figure 120. Gate In Drag Side (Mold Inverted) Cope Coated With Shellac. Increased Machine Stock On Outer Ring.

b. Bottom portion of second mold coated with enamel. (1 and 2) - molds were held at 45 degree angle and cast to permit slips to flow over coated surfaces.

c. Gravity feed mold from bottom (coated one side).

d. Remove ingate from plaster mold tool.

e. Cast mold with gate in top portion (cope) and drag coated with shellac. See sketch Figure 119.

f. Cast mold with gate in drag side (mold inverted) and cope shellacked. See sketch Figure 120.

g. Mold containing metal ring having a thickness which brings the top of the metal equal to the top of the O.D. of the casting to create new parting line for venting. See Figure 121.

h. Plaster cope machined at the outer ring portion to increase amount of machine stock in area normally machined to allow for air venting from critical face. See sketch Figure 120.

i. Cast solid flat round billet having sufficient diameter and thickness to machine entire backshroud.

j. Use insoluble wax for base of each mold to replace plaster. See Figure 122.

k. Scribe wider vent slots in plaster cope portions.

l. Use vaseline (petroleum jelly) to coat and seal drag surface.

m. Place circular cut green tape on center of drag directly under sprue to prevent direct impingement of slip onto plaster during pouring.

n. Use small pipette to pour slip into mold to better control rate of slip flow in effort to avoid air entrapment.

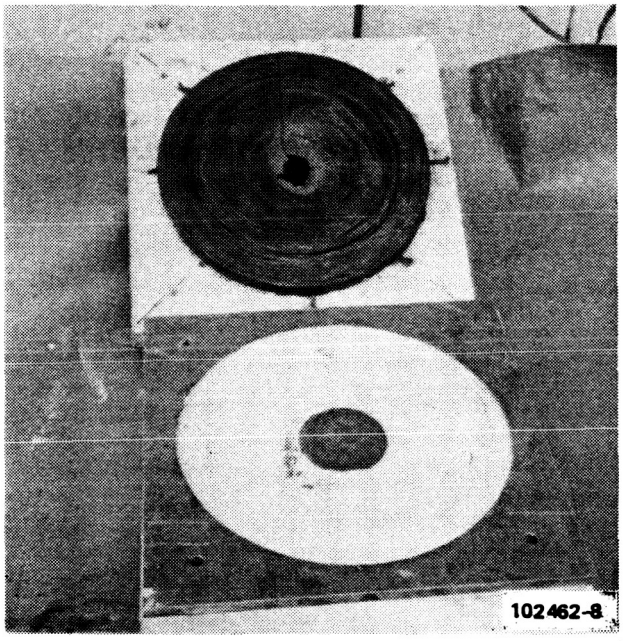

GB7-053-133

Figure 121. Drag Coated Mold Assembly Showing Metal Insert In Place.

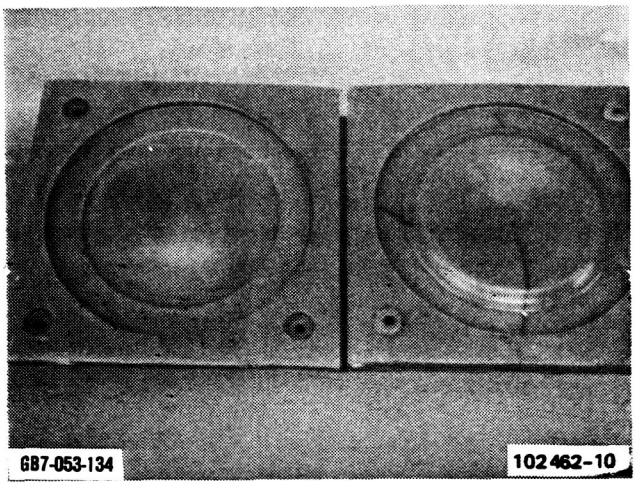

Figure 122. Wax Drag Sections.

An alternate to "i" above has shown the most promise, which is to cast an ingot where the base plaster is one of the net shape faces, and then completely machine the opposite face. This technique has virtually eliminated both flow lines and centerline shrink. Two shrouds were fabricated by this method and shipped to Garrett for further evaluation.

All other methods that involved coating of one plaster face to prevent casting to that surface, in an effort to eliminate center line shrink, resulted in sticking to the coated surface. The problem is identical to that learned in casting of the turbine shroud and transition duct where slip adhered tenaciously to all non-absorbent surfaces.

4.4 Flow Separator Housing

The tooling for the flow separator housing was extremely complex primarily due to the web areas. Several modifications were made such as increasing the web thickness. However, intact removal of the casting from the mold was never achieved as adhesion to the inserts caused several webs to break out. Further modification was anticipated but this component was placed on hold and no additional castings were attempted.

4.5 Combustor Baffle

Five combustor baffles were fully processed and shipped to Garrett which completed the order for this component.

4.6 Seal Rings and Wave Springs

Thirteen flow separator housing seal rings and eight wave springs were shipped to Garrett during this reporting period. In addition, three turbine shroud seal rings and one wave spring fabricated from a prior design were also fully processed and shipped to Garrett.

4.7 Stator Vanes

RBN-124 baseline as well as the low additive SRBSN materials were processed through nitriding (RBN-124) and sinter/HIP respectively.

The RBN-124 stators were inspected through X-ray and visual analysis. Five were rejected visually. Three were rejected by X-ray examination. Discussions with Garrett personnel indicated a problem with internal voids which were detected after thermal screening failure. The 19 remaining stators were re-X-rayed at a different angle of incidence. Only one additional stator was rejected. Destructive evaluation indicated no correlation between X-ray rejection and the presence of voids.

In an attempt to improve the high temperature strength, experimental evaluation of injection molding of stator vanes using the sintered-reaction bonded silicon nitride (SRBSN) approach was conducted. The sintering aid/levels in the SRBSN materials were as low as 0.5 percent Y_2O_3 and 0.5 percent Al_2O_3. The results were very encouraging in that the sinter/HIPped densities ranged from 3.22 to 3.24 g/cm^3 which are higher than 99 percent of theoretical. These efforts were conducted under ACC IR&D in support of the AGT program.

APPENDIX D

LIST OF SYMBOLS, ABBREVIATIONS, AND ACRONYMS

Acronym	Definition
ACC	AiResearch Casting Company
AE	Acoustic emissions
AGT	Advanced gas turbine
AGT101	AGT model being developed by Garrett/Ford
Al_2O_3	Aluminum oxide, brand name Sol Gel
AS	Aluminum silicate composition, regenerator core
ASEA	ASEA Pressure Systems, Inc., Los Angeles
ATS	Air turbine starter
Astroloy	High temperature superalloy
CBO	Standard Oil, formerly Carborundum Company, Niagara Falls, NY
CFDC	Combined Federal Driving Cycle
cfm	cubic feet per minute, ft^3/min
Corning	Corning Glass Works
dB	Decibel
DES-1000	Chrome-oxide coating from Kaman Sciences
DF	Diffusion flame (relates to combustor/nozzle)
DF-2	Diesel fuel grade 2
DOE	Department of Energy
ECU	Electronic control unit
EDX	Energy dispersive x-ray analysis technique
EPA	Environmental Protection Agency
F	Fahrenheit (degrees of)
FPI	Fluorescent-penetrant inspection
FSH	Flow separator housing
Ford	Ford Motor Company
Fuller's earth	fine, dust-like material for detecting flow paths
g	Gravity, 1-g = force equal to one gravity
g/cm^3	Grams per cubic centimeter
GE-Cordierite	Coating material made by General Electric
Garrett	Garrett Turbine Engine Company, Division of The Garrett Corporation
He	Helium (used for leak path detection)
HIP	Hot isostatic pressing
HP	High pressure
HPSN	Hot pressed silicon nitride
Hz, CPS	Hertz, cycles per second
IBM	International Business Machine, Inc.
ID	Inner diameter
IDH	Inner diffuser housing
inch	U.S. customary linear unit
in.HgA	Inches of mercury, absolute
in-lb	Inch-pounds (work)
I-85	Copper base coating material (regenerator seals)
I-112	Zine-oxide coating material, regenerator seals

APPENDIX D

LIST OF SYMBOLS, ABBREVIATIONS, AND ACRONYMS (Contd)

Acronym	Definition
JP-4	Kerosene base aviation jet fuel
k	Thousands of a unit, e.g., rpm, X1000
ksi	One-thousand pounds per square inch
Kyocera	Kyocera International, Inc., Kyoto, Japan
LAS	Lithium-aluminum-silicate composition-regenerator core
lb-in	Pound-inch (torque)
lb/min	Pounds per minute (flow)
LP	Low pressure
MAS	Magnesium-aluminum-silicate composition, regenerator core
MAR-M 247	Nickel based alloy, dual alloy turbine rotor
mil	One-thousandth of one inch
MOR	Modulus of rupture
N	Speed, rpm
NASA	National Aeronautics and Space Administration
NDE	Nondestructive evaluation
NGK	NGK - Locke, Inc.
NO_x	Nitric oxides
OD	Outer diameter
ODH	Outer diffuser housing
pH	Relative acidity to alkalinity balance
psia	pounds per square inch, absolute
psid ΔP	Differential pressure, pounds per square inch
psig	pounds per square inch, gage
pound, lb	U.S. customary weight measure 0.373 kilograms
p-p	Peak-to-peak
P_{rig}	Rig pressure psi
PV	Pressure-velocity value
RBSN	Reaction bonded silicon nitride
rpm	revolutions per minute
RM-20	Sintered reaction bonded silicon nitride ceramic material
SASC	Sintered alpha silicon carbide ceramic material
SC201 (SiC)	Silicon carbide ceramic material
Si_3N_4	Silicon nitride
S/N	Serial Number
S-77	Zinc-oxide based coating, regenerator seals
SN-71	NGK ceramic materials, sintered silicon nitride
SN-73	NGK ceramic materials, sintered silicon nitride
SN-81	NGK ceramic materials, sintered silicon nitride
SN-82	NGK ceramic materials, sintered silicon nitride
SN 220M	Kyocera ceramic materials, sintered silicon nitride
SN 250M	Kyocera ceramic materials, sintered silicon nitride
SN 270M	Kyocera ceramic materials, sintered silicon nitride
SSN	Sintered silicon nitride ceramic material

APPENDIX D

LIST OF SYMBOLS, ABBREVIATIONS, AND ACRONYMS (Contd)

Acronym	Definition
shp	Shaft horsepower
T	Temperature
Ti	Titanium
TIT	Turbine inlet temperature
$T_{3.5}$	Rating point - combustor inlet temperature
$T_{4.1}$	Rating point - turbine inlet temperature
UT	Ultrasonic techniques, inspection processes
W	Flow, rate as specified
Wayne-Kerr	Rotor dynamic measuring devices
watt	Electrical power - one volt x one ampere
Waspaloy	Heat resistant, high temperature superalloy
Y_2O_3	Yttrium oxide
Zyglo	Surface defect inspection process, brand name
2-D	Two-dimensional
3-D	Three-dimensional
μ	Micro, one millionth
$\mu\varepsilon$	Microstrain

This Page Intentionally Left Blank

APPENDIX E

REFERENCES

1) Garrett Turbine Engine Company, "Advanced Gas Turbine (AGT) Powertrain System Development for Automotive Applications," Semiannual Progress Report Number 1 (October 1979 through June 1980), NASA Report CR-165175, November 1980, Contract DEN3-167.

2) Garrett Turbine Engine Company, "Advanced Gas Turbine (AGT) Powertrain System Development for Automotive Applications," Semiannual Progress Report Number 2 (July 1980 through December 1980), NASA Report CR-165329, June 1981, Contract DEN3-167.

3) Garrett Turbine Engine Company, "Advanced Gas Turbine (AGT) Powertrain System Development for Automotive Applications," Semiannual Progress Report Number 3 (January 1981 through December 1981), NASA Report CR-167983, June 1982, Contract DEN3-167.

4) Garrett Turbine Engine Company, "Advanced Gas Turbine (AGT) Powertrain System Development for Automotive Applications," Semiannual Progress Report Number 4 (July 1981 through December 1981), NASA Report CR-167983, June 1982, Contract DEN3-167.

5) Garrett Turbine Engine Company, "Advanced Gas Turbine (AGT) Powertrain System Development for Automotive Applications," Semiannual Progress Report Number 5 (January through June 1982). Contract DEN3-167.

6) Garrett Turbine Engine Company, "Advanced Gas Turbine (AGT) Powertrain System Development for Automotive Applications," Semiannual Progress Report Number 6 (July 1982 through December 1982), NASA Report CR-168246, June 1983, Contract DEN3-167.

7) Garrett Turbine Engine Company, "Advanced Gas Turbine (AGT) Powertrain System Development for Automotive Applications," Semiannual Progress Report Number 7 (January 1983 through June 1983), NASA Report CR-174694, December 1983, Contract DEN3-167.

8) Garrett Turbine Engine Company, "Advanced Gas Turbine (AGT) Powertrain System for Automotive Applications," Semiannual Progress Report 8 (July 1983 through December 1983), NASA Report CR-174809, June 1984, Contract DEN3-167.

9) Garrett Turbine Engine Company, "Advanced Gas Turbine (AGT) Powertrain System for Automotive Applications," Semiannual Progress Report 9 (January 1984 through June 1984), NASA Report CR-174886 December 1984, Contract DEN3-167.

10) Garrett Turbine Engine Company "Advanced Gas Turbine (AGT) Technology Development Project" Technical Summary Report 10 (July 1984 through June 1985), NASA Report CR-179485 July 1986, Contract DEN3-167.

11) Garrett Turbine Engine Company "Brayton Cycle Solarized Advanced Gas Turbine" Final Report (February 1980 through March 1986) NASA Report CR-179559, December 1986, Contract DEN3-181.

12) Govila, R.K. "Strength Characterization of Yttria-Doped, Sintered, Reaction Bonded Silicon Nitride", Tech. Report SR-86-36, Ford Motor Co., 03-21-86.

PRECEDING PAGE BLANK NOT FILMED

1 Report No.	2. Government Accession No.	3. Recipient's Catalog No.
CR-180818		

4 Title and Subtitle	5. Report Date
Advanced Gas Turbine (AGT) Technology Development Project 1986 Annual Report (July 1, 1985 - June 30, 1986)	June 1987
	6. Performing Organization Code
7 Author(s)	8. Performing Organization Report No.
Engineering Staff of Garrett Turbine Engine Company, A Division of the Garrett Corporation	31-3725(11)
	10. Work Unit No.
9 Performing Organization Name and Address	11. Contract or Grant No.
Garrett Turbine Engine Company P.O. Box 5217 Phoenix, Arizona 85010	DEN3-167
	13. Type of Report and Period Covered
12. Sponsoring Agency Name and Address	Interim July 1985 - June 1986
Department of Energy Division of Transportation Energy Conservation Washington, DC 20545	14. Sponsoring Agency Code
	DOE/NASA/0167-11

15. Supplementary Notes
Interim Progress Report under Interagency Agreement
Project Manager T.N. Strom, Propulsion Systems Division,
NASA-Lewis Research Center, Cleveland, Ohio 44135

16. Abstract

This report is the eleventh in the series of Technical Summary reports for the Advanced Gas Turbine (AGT) Technology Development Project, authorized under NASA Contract DEN3-167, and sponsored by the Department of Energy (DOE). This report was prepared by Garrett Turbine Engine Company, A Division of the Garrett Corporation, and includes information provided by Ford Motor Company, the Standard Oil Company, and AiResearch Casting Company. The Project is administered by Mr. Thomas N. Strom, Project Manager, NASA-Lewis Research Center, Cleveland, Ohio. This report covers plans and progress for the period July 1, 1985 through June 30, 1986.

Technical progress during the reported period was highlighted by the 85-hour endurance run of an all-ceramic engine operating in the 2000-2250F temperature regime. Component development continued in the areas of the combustion/fuel injection system, regenerator and seals system, and ceramic turbine rotor attachment design. Component rig testing saw further refinements. Ceramic materials showed continued improvements in required properties for gas turbine applications, however, need continued development before performance and reliability goals can be met.

17 Key Words (Suggested by Author(s))	18. Distribution Statement
Advanced Gas Turbine Single Shaft Engine Ceramic Turbine Turbine Transmission	Unclassified - Unlimited Star Category 85 DOE Category UC-96

19 Security Classif. (of this report)	20. Security Classif. (of this page)	21. No. of Pages	22 Price*
Unclassified	Unclassified	123	

* For sale by the National Technical Information Service, Springfield Virginia 22161